Exploring adaptations of the carbon layer of the triple mesoscopic carbon perovskite solar cell.

Mark Cushworth

Thesis submitted to Swansea University in fulfilment of the requirements for the degree of MSc in Mechanical Engineering by Research.

Swansea University

2020

Abstract

This thesis explores possibilities for the improvement of the carbon layer within the triple mesoscopic carbon perovskite solar cell (mCPSC) architecture used in SPECIFIC labs at Swansea University. An increase in sheet resistance, resistivity and contact resistance is found in GEM carbon layers, within the mCPSC, as a result of annealing heat treatments and perovskite infiltration compared to carbon layers dried at 100°C. A unique application of a printed carbon capping layer, utilising the lower sheet resistance, contact resistance and higher mechanical robustness of the dried GEM carbon layer, is used in mCPSC devices. Devices with this capping layer are found to have increased fill factor, by 5-10%. Work function of the GEM carbon layer is enhanced with the addition of WO_3 particles with improvements up to 5% PCE seen in devices that contained WO_3 particles in the carbon layer. These devices have increased FF, V_{OC} and J_{SC} when compared to standard GEM devices. As well as possible enhancements of the carbon layer with GEM carbon ink, alternative carbon inks made in-house and sourced from commercial manufacturers are compared for use as the screen-printed carbon layer in the mCPSC. The comparisons are based on the following characterisation techniques: four-point probe measurements to calculate carbon layer sheet resistance and resistivity; profilometry to assess printed layer thickness and surface roughness; the Transmission Line Method (TLM) to find contact resistance at the interface between printed carbon layers and FTO substrate; Adhesion tape test is used to assess mechanical robustness of the carbon layer and Kelvin probe measurements are used to calculate the work-function of the carbon layer.

Declarations

This work has not previously been accepted in substance for any degree and is not being concurrently submitted in candidature for any degree.

Signed. [redacted] .....

Date.....29/09/2022.....

This thesis is the result of my own investigations, except where otherwise stated. Other sources are acknowledged by footnotes giving explicit references. A bibliography is appended.

Signed.. [redacted] .....

Date.....29/09/2022.....

I hereby give consent for my thesis, if accepted, to be available for photocopying and for inter-library loan, and for the title and summary to be made available to outside organisations.

Signed.. [redacted] .....

Date.....29/09/2022.....

The University's ethical procedures have been followed and, where appropriate, that ethical approval has been granted.

Signed... [redacted] .....

Date.....29/09/2022.....

Acknowledgements

Firstly, I would like to thank my supervisor professor Trystan Watson and his team: Dr Dave Beynon, Dr Rebecca Bolton, Dr Simone Meroni, Dr Sarah-Jane Potts, Dr Dimitrios Raptis and Carys Worsley for their continued support throughout this project. I am sincerely grateful to all members of the team for the guidance, knowledge and time made available to me. It has been a pleasure to work alongside this team and an invaluable experience. I would like to thank SPECIFIC and Swansea University for access to the labs and facilities which made this research possible. Finally, I want to extend thanks to my friends and family for their support and kindness throughout all of my time as a student.

Contents

List of Figures

List of Tables

List of Abbreviations

ASTM – American Society for Testing and Materials.

CPD – Contact Potential Difference

EIC – Elemental Inks & Chemicals

FF – Fill Factor

FTO – Fluorine-doped Tin Oxide

GEM – Gwent Electronic Materials

HT – High Temperature

mCPSC – Triple Mesoscopic Carbon Perovskite Solar Cell

PCE – Power Conversion Efficiency

PSC – Perovskite Solar Cell

PV – Photovoltaics

SWCNT – Single Walled Carbon Nano-Tube

TLM – Transmission Line Method

WF – Work Function

Chapter 1. Introduction

1.1 Background

In Q3 2021 Solar PV supplied 6.2 % of the UK's total electricity generation, while the capacity for Solar PV was increased by 269 MW from the previous year [1]. This growth for solar energy will continue along with all renewable energy to meet the demands created in the 2008 Climate Change Act's commitment to net zero greenhouse gas emissions by 2050 [2].

Along with the growing demand, research and development reveals promising new Solar PV technology for higher performance and lower cost commercial solar cells. The Perovskite Solar Cell (PSC) is a technology being developed with a variety of device architectures published, where efficiencies can reach 25.2 % [3][4]. PSCs typically make use of methylammonium lead iodide perovskite materials: crystal structures that can be composed for use as high efficiency photovoltaic materials with low processing costs [5].

The triple-mesoscopic carbon perovskite solar cell (mCPSC) is a Perovskite Solar Cell architecture, first published in 2013 [6] that has been recognised as having great potential for scale up and commercialisation due to the low cost, easy fabrication, and stability. As a result, mCPSC research is advancing internationally with aims of improved performance and scale up for commercial use. Review papers outlining advancements and opportunities for further development of the mCPSC have identified the carbon layer as an area that can be improved to boost overall performance, with Meroni et al. stating specifically that "compositional manipulation of the carbon layer was one effective route to performance enhancement" [4][7].

1.2 Aims and Objectives

The strengths of carbon compared to other counter electrodes directs the research towards optimising the material and continuing the development of the mCPSC architecture, rather than replacing it. As such, the purpose of this research is to explore avenues through which the carbon layer of the mCPSC can be adapted to improve overall device performance. This will be achieved by first reviewing the role of carbon in PSC devices and how it has been optimized in published research, characterizing the current carbon layer of the mCPSC architecture used in Swansea University SPECIFIC labs and then applying findings from literature to the carbon layer and evaluating their effects on the carbon layer and device performance. At the conclusion of this research will be an evaluation of the optimization techniques attempted throughout and proposals for further research.

Chapter 2. Literature Review

2.1 Perovskite Solar Cells (PSCs)

A methylammonium lead iodide perovskite and TiO_2 heterojunction solar cell with a gold electrode was reported in a 2012 paper displaying the use of perovskite as both a light harvester and hole conducting material [8]. This was made possible by the high hole mobility of the perovskite and allowed for the device to forgo the use of a separate hole transport layer which had been used in other PSCs alongside different perovskite materials that acted solely as charge generators[9]. The device had a PCE of 5.5 % at 1 sun and the simple design showed great promise for low-cost, high efficiency solar cells. Similar research has since developed perovskites low processing temperatures as a light harvester and hole conducting material within a solar cell, further promoting the technologies prospects for scale up [10]. These

developments in the creation of small scale PSC devices was soon translated into larger scale, high efficiency modules showing the scalability of the technology [11]. These device architectures use an expensive metal electrode requiring costly processing methods that involve preparation by thermal evaporation under a vacuum, with the processing of the Au counter electrode reported to cover 18.3 % of the total cell cost alone [12]. As an alternative to metal electrodes, carbon electrodes have been used in PV, selected for their low material and manufacturing costs whilst maintaining good conductivity and stability [13][14]. This was also seen in PSCs where early devices with carbon electrodes reported PCEs of 9 % making them a promising addition to the PSCs case as a low cost solar cell technology [15][16].

2.2 The triple-mesoscopic Carbon Perovskite Solar Cell (mCPSC)

The mCPSC, displayed in figures 1 and 2, are made up of three mesoporous layers, screen printed onto laser scribed FTO that has been spray coated with a compact TiO_2 layer. The laser scribe separates the FTO into two distinct electrodes. The first printed mesoporous layer is the TiO_2 electron transport layer that sits on one side of the laser scribe. This is followed by the ZrO_2 blocking layer separating the TiO_2 layer from the final carbon layer that extends over the scribe to make contact with the FTO therefore acting as a counter electrode. Perovskite solution is drop-cast onto the stack, permeating through the layers before crystallizing under heat treatment. The result of this is perovskite present throughout each layer as a light harvesting material and hole transport material rather than as a planar layer between electrodes as is the case in other PSC designs. As such the principle of the design dictates that under light, the perovskite will generate electron hole pairs, with the negatively charged electrons being collected by the positive TiO_2 layer and the positively charged holes by the negative carbon

layer. These layers remain separated by the ZrO_2 blocking layer and scribe in the FTO preventing electron hole recombination, where in the excited electrons fall back to the valence band recombining with holes before the opposite charge carriers are separated. As opposing charges build across the device by negatively charged electrons in the TiO_2 layer, and positively charged electron holes in the carbon layer a voltage is built across the device. The TiO_2 layer is in contact with FTO on one side of the scribe whilst the carbon layer is in contact with FTO on the other side of the scribe and so an electrode and counter electrode are formed either side of the scribe resulting in an electrical current once a device is connected to a circuit[6][17].

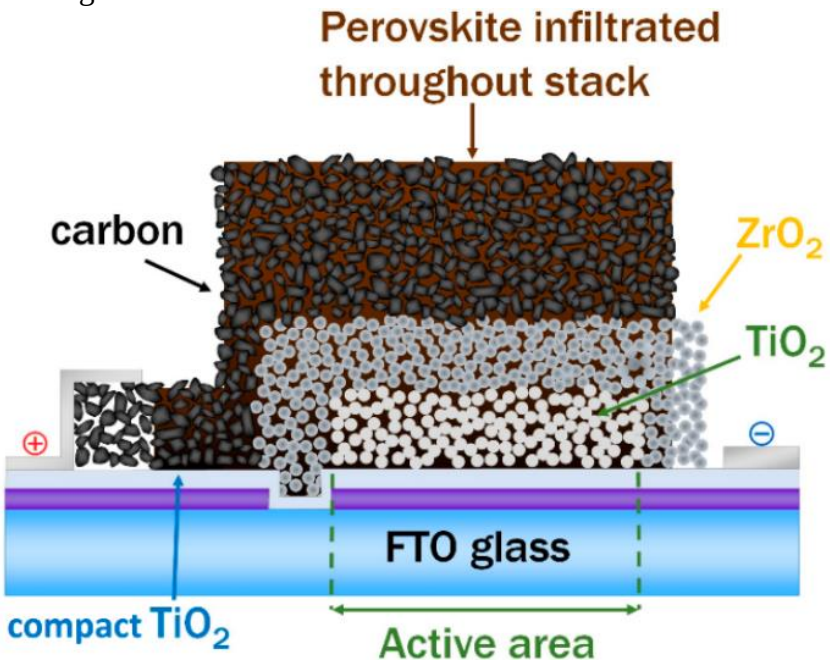

Figure 1 Cross section of mCPSC device [17].

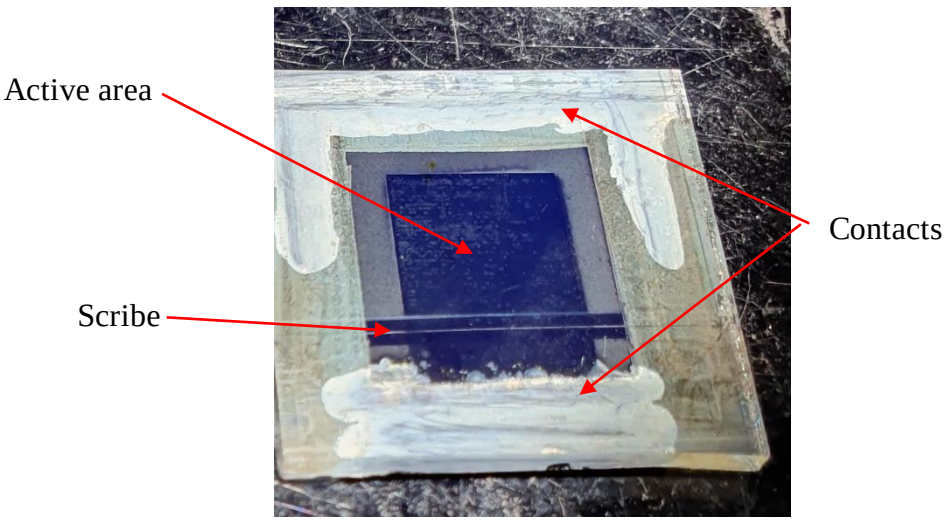

Figure 2 Underside of mCPSC device

2.3 Role of Carbon in mCPSC device performance

The key goals for a successful carbon layer are to host perovskite within the porous layer, collect electron holes generated in the perovskite and conduct electrical current. The structure of a typical carbon layer is an important in how these goals are met [6].

The carbon layer of the mCPSC is typically an ink made up of a resin containing carbon materials, screen printed onto a device and dried. The layer is porous as once the binding agent in the resin is burnt away, during the sintering process, there is space between the particles of carbon material which is important for infiltration of perovskite into the device. The porous carbon layer successfully hosts perovskite due to their chemical inertness preventing any interaction with the formation of perovskite [18]. The most common carbon materials used are graphite and carbon black. Graphite is a conductive crystalline carbon structure usually made up of many parallel layers oriented in a preferred direction resulting long flat particles, tens of microns in length, with good conductivity along this direction. Carbon black is conductive and paracrystalline, made up of many smaller crystal structures than graphite resulting in sub-micron scale, spherical particles with high surface area to volume ratio. In conductive carbon inks the high conductivity of graphite particles is supported by the increased interparticle contact provided by the high surface area carbon black particles. There are many types of graphite and carbon black, and these are not the only carbon materials used in carbon inks but these are the primary materials responsible for the carbon layers conductivity as an electrode [19][20][21].

The carbon layer collects the positively charged electron holes generated in the perovskite due to its alignment with the valence bands. Shown in the energy level diagram, figure 3, the typical energy level of carbon is -5 eV and the perovskite valence band is -5.4 eV. The difference in these energy levels determines the energy required for electron holes to move between the levels and so closer energy levels result in improved hole collection [22].

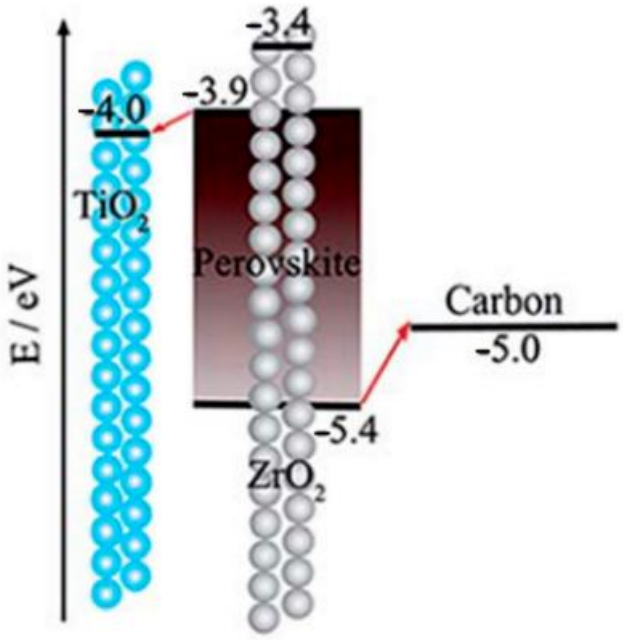

Figure 3 Energy level diagram of mCPSC [22].

The carbon layer has been identified as an area where improvements can be made to improve overall mCPSC device and large scale module performance [4][7]. As such there is previous work on enhancing carbon layer by targeting the roles described in this section and their effect on mCPSC device performance. Device performance is usually measured by power conversion efficiency (PCE) which is the output power of the device as a percentage of the power of light illuminating the device. The ratio of the maximum measured power of the device to the theoretical maximum power, fill factor (FF), maximum current density able to travel through the device, short circuit current density (J_{SC}) and maximum voltage able to build across the device when there is no current, open circuit voltage (V_{OC}) are used to evaluate performance

as these are closely linked to PCE. Reviewing the previous works surrounding the carbon layer will guide the research done in this thesis.

2.4 Previous Work on the Carbon Layer from Literature

In a previous study the conductivity of carbon layers was improved by increasing layer thickness resulting in greater device FF. However, increasing thickness also led to incomplete perovskite infiltration which was detrimental to device performance. Carbon layers between 5-15 μm were investigated finding 9 μm layers to be optimum for device performance. Device performance was also dependant on the size of graphite flakes in the carbon ink, with 8 μm found to be the optimum in 9 μm thick carbon layers when compared with 6 μm, 3 μm and 500 nm flakes. This was linked to the greater pore size and conductivity of the carbon layers with 8 μm graphite flakes [23]. Changing the carbon black content of the carbon layer also affects device performance. Carbon inks with graphite and carbon black material were made with a range of carbon black from 0-100 % of carbon material weight. Increasing the proportion of carbon black reduced conductivity but the optimum performance was seen in devices containing 20 % carbon black within the carbon layer. The success of the 20 % carbon black layer was attributed to the layer providing better uniformity for the infiltrated perovskite and greater conductivity than those layers with more carbon black improving device performance [24]. Different types of graphite have been employed within the carbon layer such as ultrathin graphite particles that provide more effective contact between the carbon and perovskite. This increased contact was due to greater specific surface area when compared with bulk graphite and improved device performance [25]. The effect of using different types of graphite particles on the carbon perovskite interface was observed again in a study comparing a range of six types of graphite from natural and synthetic sources. The highest performing devices were those including scaly graphite particles, which observed to have the largest crystallite dimensions.

Multiple devices saw improved FF over standard devices due to the improved conductivity of graphite particles. However, those devices with carbon layers containing a scaly graphite had the highest J_{SC} values, this indicates an increase in hole collection due to improved carbon/perovskite interface and set the performance of these devices above the rest [20].

Hole selection of the carbon layer has been improved by increasing the work function of carbon layers. Work function is increased with the use of additional materials such as single walled carbon nanotubes (SWCNT) [26]. Devices containing SWCNTs had improved PCE performance with an increase in FF, V_{OC} and J_{SC} as a result of improved work function and charge recombination lifetime, as a result of improved charge collection. Oxygen rich carbon black particles have also been used to improve carbon layer work function, again resulting in devices with improved PCE, FF, V_{OC} and J_{SC} compared to those with lower work function carbon layers [27]. Non-carbon materials have been implemented within the carbon layer to increase work function such as NiO, CuS, and WO_3 [28][29][30]. These materials act as a sort of stepping-stone between the carbon layer and perovskite valence band allowing for greater holes extraction and therefore improved device performance.

Additional carbon layers have been used to improve upon the standard mCPSC architecture. These carbon capping layers are printed onto infiltrated devices and cured at low temperatures so as not to interfere with the perovskite. The purpose of these layers is to provide an improved carbon electrode that can be tuned solely for conductivity whilst the original carbon layer below hosts perovskite and collects charge [31]. The use of metallic grids within the carbon capping layer is a unique application that takes advantage of the capping layer being processed after device infiltration [32]. Al and Cu metallic grids were placed on top of device before the additional carbon layer was printed securing the grids in place. These metallic grid layers had a sheet resistance much lower than the standard carbon layer, as well as the capping layer without grids. The result of these metallic grid carbon capping layers was an improvement in

device performance from ~11% to ~13%. This improvement is a result of the highly conductive capping layer increasing device FF. These capping layers also helped to improve device stability by providing a layer of protection to the perovskite hosting layers of the device.

The previous work done to improve mCPSC performance through enhancing the carbon layer highlights the importance of the carbon materials within the layer for conductivity, hole collection and porosity. However, it is evident that there is a balancing act between improvements to carbon layer conductivity and the carbon layer porosity, as seen in studies that altered the weight of carbon material and layer thickness. The importance of changes to carbon layer formulation makes carbon inks produced in-lab an attractive option. This is due to the formulation being more easily adaptable than from a commercial carbon ink which would be a less well-defined baseline for modification.

The use of additional materials to enhance hole collection is clearly a promising avenue for improving the carbon layer. Carbon layers with increased work function have been seen to have improved device performance in multiple areas; PCE, FF, V_{OC} and Jsc.

One area that has seen less innovation is the contact resistance between carbon and FTO. The contact resistance at this interface can result in large series resistance losses in larger scale devices and has perhaps been neglected due to the small impact on a device level [33]. Therefore, the effect previously implemented carbon layer improvements have on contact resistance between the carbon layer and FTO will be one focus of this work.

Chapter 3. Experimental Method

3.1 Characterisation of carbon ink.

Work on the carbon layer published in literature highlights its roles as a counter electrode and hole extraction layer as important factors in mCPSC device performance. The role of carbon layers as counter electrodes is evaluated though their conductivity, characterized by sheet resistance, resistivity and contact resistance in this work. These characteristics each describe different aspects of conductivity and are measured with specific methods outlined throughout this section. The hole extraction of the carbon layer is related to the energy level of the carbon layer and so work function measurements are used to characterize this aspect of the carbon layer. A solar simulator is used to measure mCPSC device data and evaluate the impact of changes in the carbon layer on device performance. The applications of these characterisation methods are described in this section.

3.1.1 Four-Point Probe

The counter electrode of the mCPSC and conductivity of the carbon layer is an important factor in device performance with the charge travelling laterally though the layer before being transferred to the conductive FTO substrate. Therefore, to evaluate the conductivity of carbon layers, sheet resistance is measured. Sheet resistance is used as it measures the lateral resistance along a theoretical square of a thin film, in units Ω/□ (Ohms per square). One drawback of sheet resistance as a method of evaluating conductivity is the influence of layer thickness. Resistivity of materials compares the innate conductivity of the material regardless of layer thickness and can be calculated using the sheet resistance and layer thickness of a sample.

To measure sheet resistance the four-point probe method uses four equally spaced probes, displayed in figure 4, to measure the resistance across a thin film between the two middle probes while the current flows through the two outer probes [34].

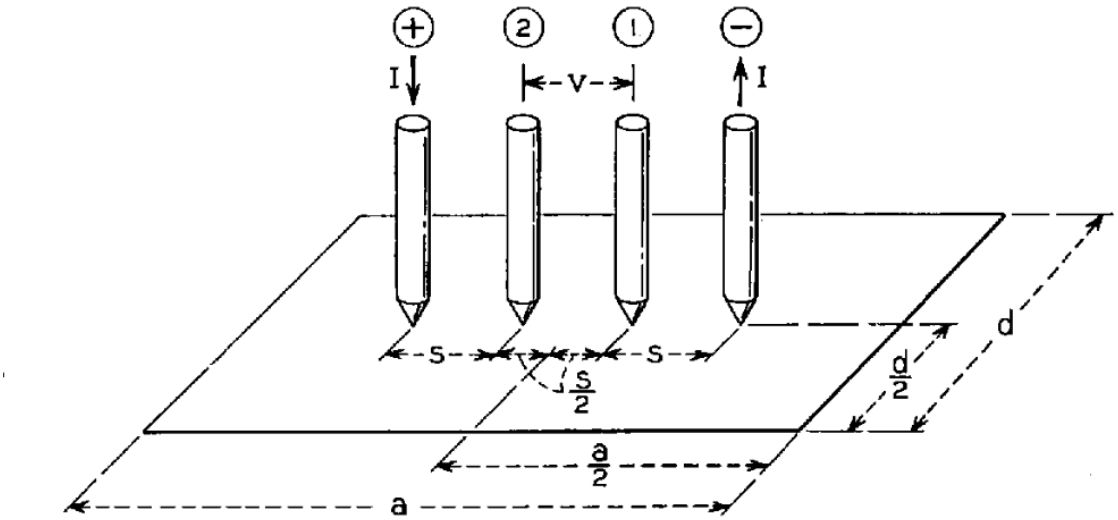

Figure 4 Four point probe arrangement taken from Smits et al. 1958 [34]

This allows for a resistance measurement of the substrate between the two inner probes without interference from the internal resistance of the wires and contact resistance. From this measured resistance R, the sheet resistance R_s can be calculated using (1):

$$R_s = \frac{\pi}{ln(2)} \frac{\Delta V}{I} = 4.53236R \qquad 1$$

This equation assumes that the film thickness is less than 40 % of the probe spacing and that the film area is sufficiently large and square. Samples created for sheet resistance measurements therefore need to adhere to these constraints. To accurately measure the

resistance of a thin film using the four-point probe method, the film must be deposited on a non-conductive substrate.

Sheet resistance (R_s) is measured in Ohms per square (Ω/□), as it is a measure of the resistance across opposite sides of a theoretical square, independent of size. Resistivity ρ (Ωμm) can be found from sheet resistance with (2):

$$\rho = \frac{R_s}{t} \qquad 2$$

Where t is the thickness (μm) of a sample. Thickness of printed samples would influence the sheet resistance and so resistivity can be used to compare conductivity regardless of volume. To measure the sheet resistance of screen-printed thin film samples with the four point probe the samples must be printed on a non-conductive substrate, glass was used in this thesis.

3.1.2 Transmission Line method

Contact resistance between the carbon layer and FTO substrate is responsible for current losses in mCPSC devices and so reducing the resistance at the carbon/FTO interface could improve performance. This is especially important in modules where there are many of these interfaces and so contact resistance contributes towards overall series resistance losses [33].

The Transmission Line Method (TLM) is used to find the Contact Resistance R_C between a semiconductor contact and the substrate it is deposited on. The TLM uses a set of resistance measurements between contacts at varying distances, L. From these measurements a plot of resistance as a function of distance can be formed. This plot represented in figure 5 where a trendline is used to extract different parameters of the contacts where R_T is the total measured resistance, R_s is the sheet resistance of the underlying substrate, W is the contact width, R_c is the contact resistance and L_T is the transfer length [35]. The version of TLM used in this study

is a recreation of the structure and method used Matteocci et al. in their investigation of Au contact resistance with and without blocking layers present [11]. The TLM structure shown in figures 6 and 7 was used to make the resistance measurements R_T as distances $L_{1\text{-}5}$ with contacts at each end of the structure used connected to a current creating the plot of R_T against L.

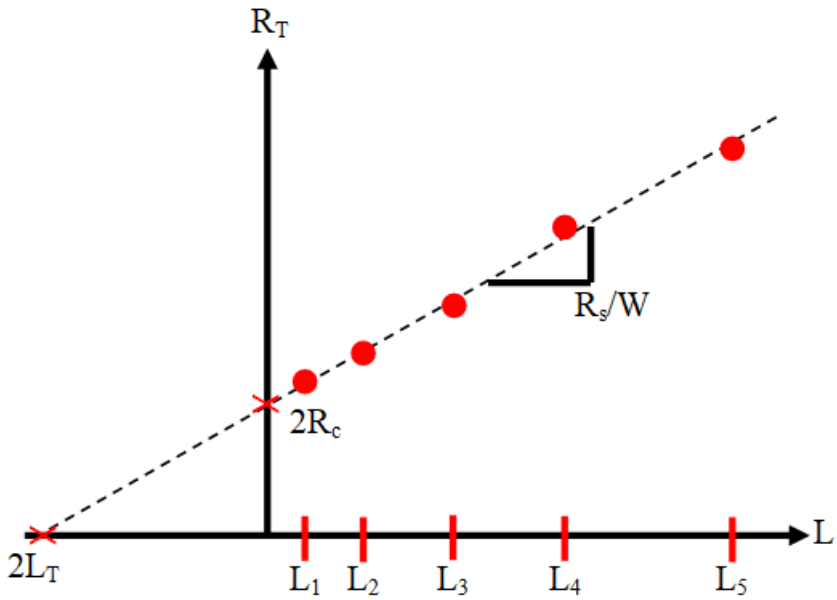

Figure 5 TLM plot of total resistance across different distances L.

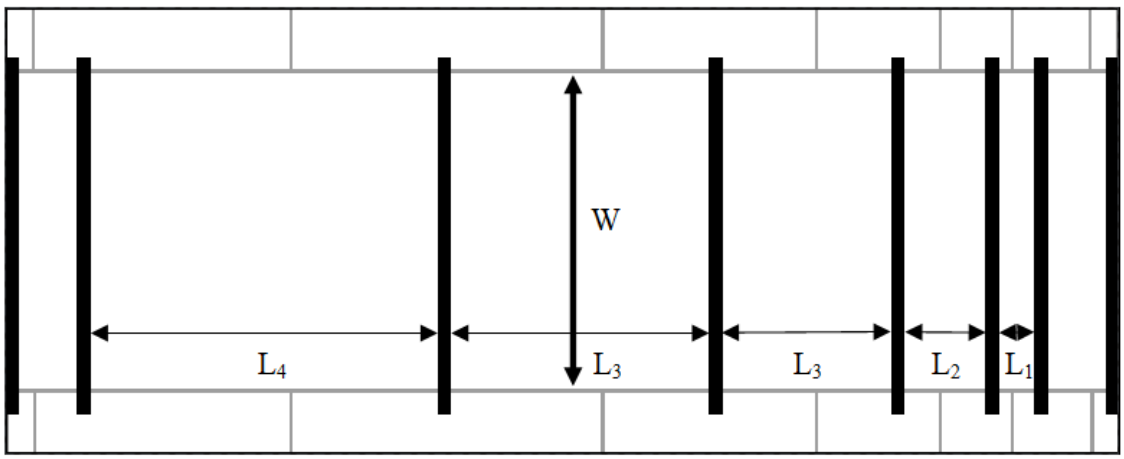

Figure 6 Diagram of the TLM structure.

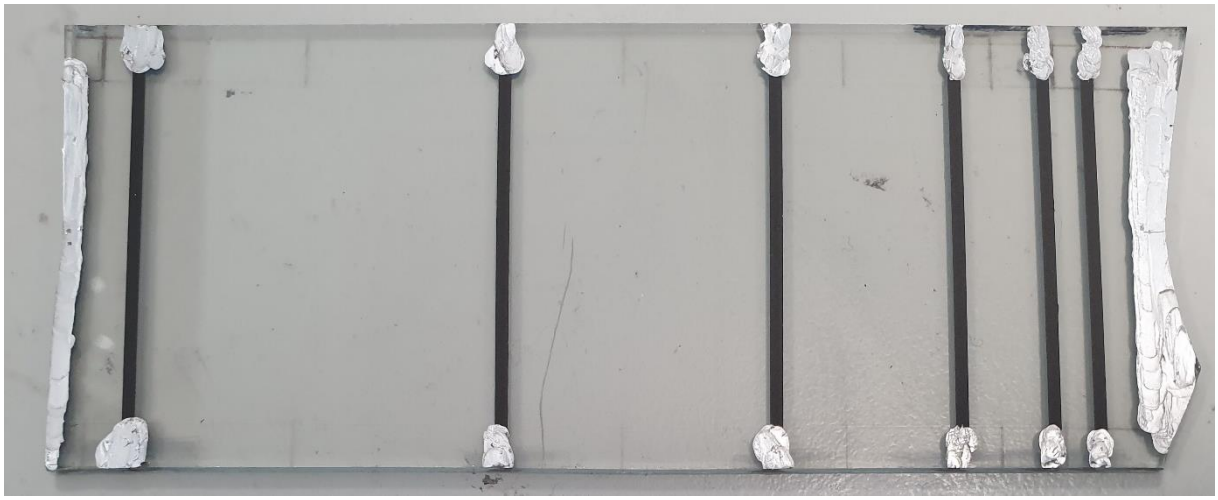

Figure 7Screen printed carbon on FTO TLM device with silver contacts.

The TLM plot can be used to extract these parameters however a shortcoming of this method that has been identified is the effect of modified substrates on the value of R_c. First identified by Reeves et al [36]. the sheet resistance directly below the semiconductor contacts may differ from the rest of the substrate surface and so alternative methods for extracting parameters that account for this potential modification of underlying substrate were devised. This method uses equations (3),(4) and (5):

$$L_T = \frac{R_{T,L=0}}{2\frac{\delta R_T}{\delta L}} \quad 3$$

$$\rho_c = R_S {L_T}^2 \quad 4$$

$$R_c = \frac{\rho_c}{A_c} \quad 5$$

Where L_T is transfer length, $R_{T,L=0}$ is the value of R_T when $L=0$, $\frac{\delta R_T}{\delta L}$ is the slope of the trendline fitted to the data, ρ_c is the specific contact resistivity, R_S is the sheet resistance of the substrate, A_C is the contact area, and finally R_C is the contact resistance.

Transfer length is described as a measure of the distance over an interface in which most of the current will transfer between a substrate and contact, represented by figure 8. As such where the transfer length is much less than the length of a contact, some of the contact will be inactive during current transfer [37].

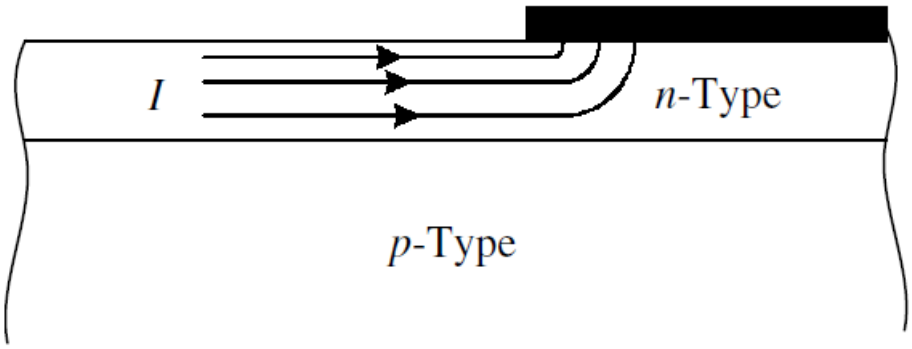

Figure 8 Example of current only transferring over part of an interface due to transfer length being much less than the length of an interface.

A shortcoming of the TLM measurement has been found in the observation of negative contact resistance results, as reported by Nouchi et al. in the contact resistance between graphene and Ag contacts in graphene field effect transistors [38]. These negative values were observed in work carried out for this thesis occurring when the line fitted to the measured resistance values would have a negative value for R_T at $L=0$ and as such a negative value for $2R_c$. As the results are so close to 0, any error due to a lack of data points in the trendline can give a negative result. The problem with these results is that the actual contact resistance must be positive, and a negative result would be a failure in the TLM measurement.

3.1.3 Profilometry

Surface roughness and thickness of carbon samples is measured using a Dektak profilometer. A needle is dragged across the surface of a sample producing a two-dimensional profile of the sample from the movement of the needle. This is useful data as it shows the average step height of a printed sample which is used as a measure of the sample's thickness. The surface roughness and skew are also given by the profilometry data. Surface roughness is represented as roughness average, Ra, an average of the deviations from the profile mean of a surface. Skew is a measure of the proportion of the deviations that are above or below the mean average, on a scale of 1 to -1. A skew above 0 indicates that there are more peaks than troughs contributing to the roughness average whereas below 0 means there are more troughs.

3.1.4 Mechanical Robustness of the carbon layer.

To investigate the influence of perovskite on the mechanical robustness of the carbon layer an adapted version of the ASTM Adhesion by Tape test (Method B) was used [39]. This test involves cutting a grid onto the film surface, applying adhesive tape for a set time, removing the tape and evaluating how much material from the area within the grid has been removed by the tape. The test is designed for more robust films than the printed carbon and so was adapted for more appropriate use here. For this investigation, as in the previous experiment, the following six sets of samples were created: carbon printed onto glass and dried; carbon on glass annealed; carbon on glass infiltrated; carbon and ZrO_2 on glass dried; carbon and ZrO_2 on glass annealed and carbon and ZrO_2 on glass perovskite-infiltrated. For each sample, six lines 2mm apart were cut horizontally and vertically into the carbon film to form a 10x10mm grid. Electrical tape was applied to the film and a pencil eraser used to ensure good contact between the tape and film. After 60 seconds the tape was removed by pulling the free end away at 180°. The results are determined using the classification of adhesion test results set out in the ASTM

Adhesion by Tape Test displayed in figure 9 [39]. There are six classifications which correspond to the percentage of area removed from within the grid starting from 5B at 0 % area removed and going to 0B with 65 % or more area removed. There is also a visual guide to help classify samples.

CLASSIFICATION	PERCENT AREA REMOVED	SURFACE OF CROSS-CUT AREA FROM WHICH FLAKING HAS OCCURRED FOR SIX PARALLEL CUTS AND ADHESION RANGE BY PERCENT
5B	0% None	
4B	Less than 5%	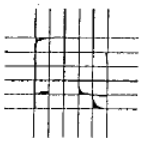
3B	5 - 15%	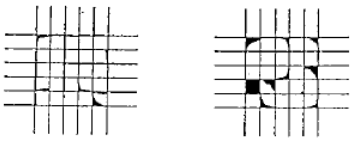
2B	15 - 35%	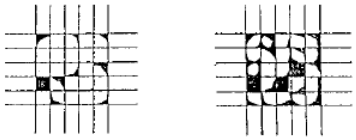
1B	35 - 65%	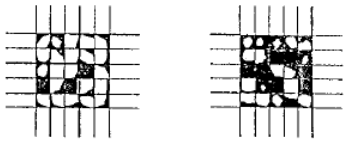
0B	Greater than 65%	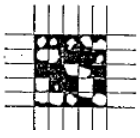

Figure 9 Classification of Adhesion Test Results from ASTM Standard Test for Measuring Adhesion by Tape Test.

3.1.5 Kelvin Probe

Work function of the carbon layer is a measure of the energy required for electron holes to move from the perovskite valence band to the carbon layer. The energy level diagram, figure 10, shows the energy levels of the different layers in the mCPSC. Increasing the energy level of the carbon layer to be closer to the perovskite valence band could improve device performance through improved hole collection in the carbon layer. The Kelvin probe uses an incredibly sensitive gold tip to measure the contact potential difference between the tip and conductive samples, as pictured in figure 11. The work function of a sample can be calculated with the work function of the probe tip and the CPD measured between the tip and sample. The work function of the probe tip is calculated with a CPD measurement between the tip and an Au test sample with a known work function value. These calculations are set out in (6) and (7):

$$Probe\ Tip\ WF = Test\ Sample\ WF - Measured\ Test\ Sample\ CPD \quad (6)$$

$$Sample\ WF = Probe\ Tip\ WF + Measured\ Sample\ CPD \quad (7)$$

Taking CPD measurements with the kelvin probe requires a sample to be set up under the probe tip attached to metal contacts. Due to its high sensitivity the probe is set up in a faraday cage blocking electromagnetic fields from interfering with measurements. Once the sample is set under the probe tip in the cage the tip is carefully lowered until the approach gradient, displayed on the kelvin probe software, reaches 300. At an approach gradient of 300 the distance between tip and sample is optimum for CPD measurements. When lowering the tip it is important not to make contact with the sample as this could damage the probe tip. The probe takes many CPD measurements over a selected time, creating a plot that will eventually stabilise to give a clear reading, example displayed in figure 12.

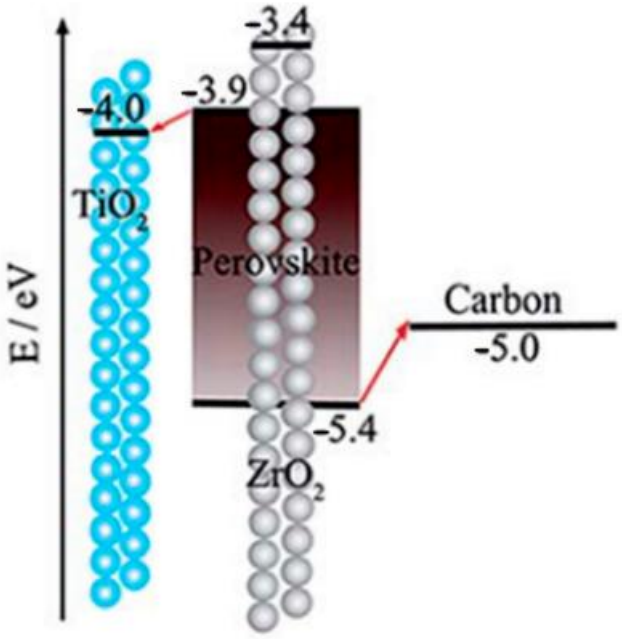

Figure 10 Energy level diagram for the mCPSC [22].

(Repeated from figure 3)

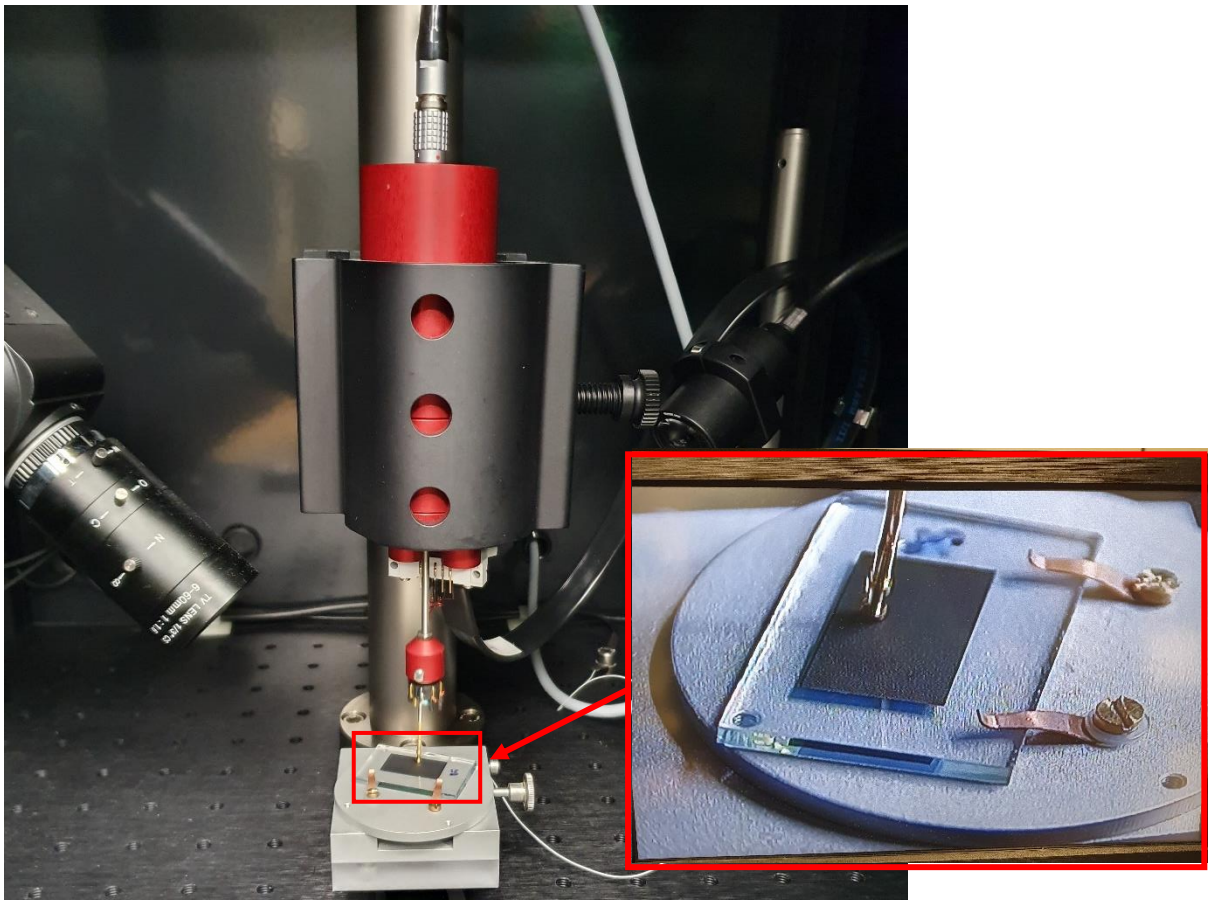

Figure 11 Kelvin Probe in the Faraday cage with gold tip at operating distance from the carbon sample.

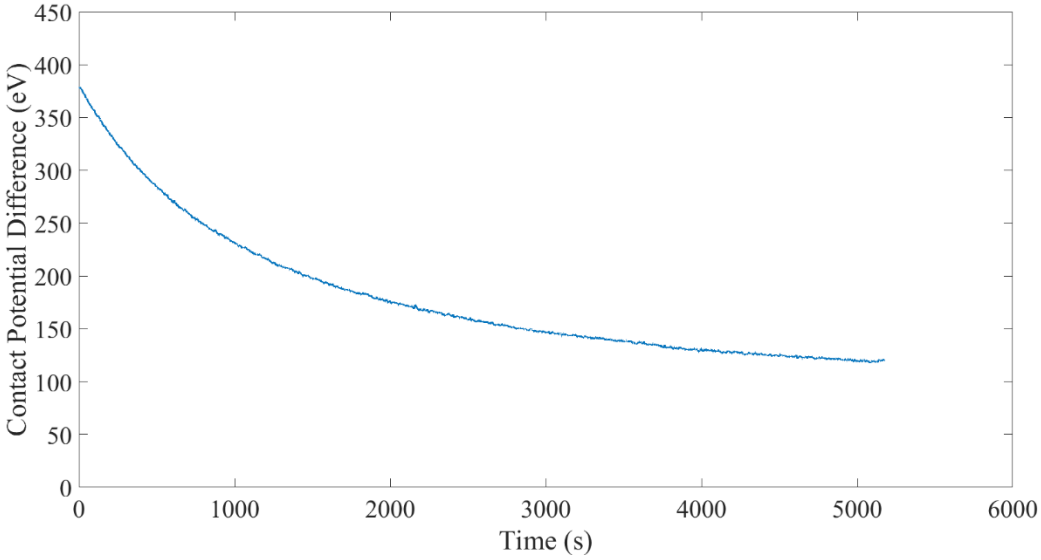

Figure 12 CPD measurement of Au test sample taken with the kelvin probe.

3.1.6 Solar Simulator

mCPSC device performance is measured using a solar simulator with light equal to 1 sun. Under illumination the devices are connected to a circuit with software measuring current density through the device and voltage across the device, plotting a J-V curve as shown in figure 13. Also, from these measurements the software calculates Power Conversion Efficiency (PCE) of the device, which is the power output of the cell as a percentage of the power of light illuminating the cell. PCE is the primary benchmark for solar cell device performance. The Fill Factor (FF) is also measured, and this is another efficiency measurement that is a ratio of the maximum measured power of the device to the theoretical maximum power. As power is a product of current density and voltage the maximum theoretical power is found with measurements of V_{OC} and J_{SC}. The V_{OC} is the open circuit voltage and occurs when there is no current and voltage is allowed to build to its maximum across the device. The J_{SC} is the short circuit current density which is the maximum current density able to travel through the device occurring when there is 0 voltage.

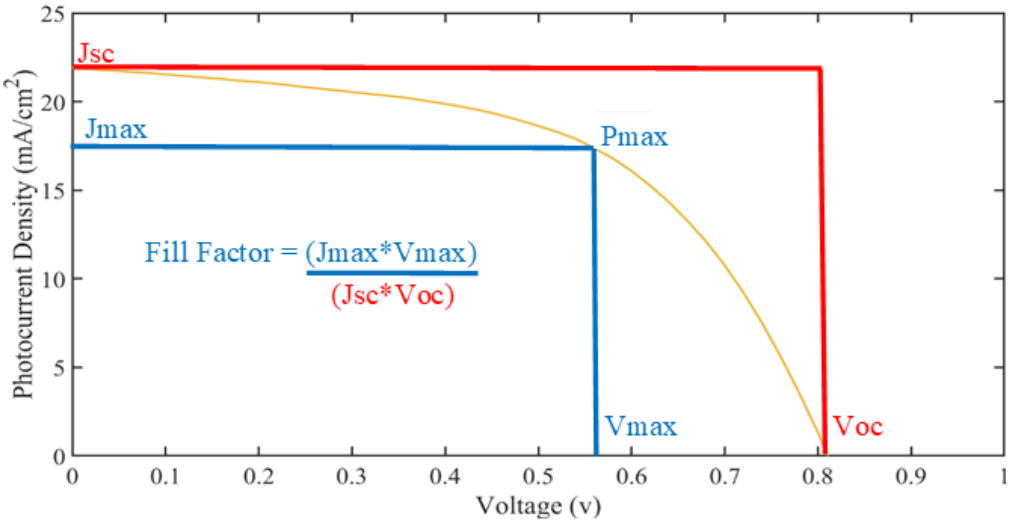

Figure 13 Example JV curve annotated to show FF,Voc and Jsc.

3.2 Experimental Fabrication Methods

3.2.1 Fabrication of Carbon Inks in-lab

Creating a carbon ink in-lab rather than using a commercial ink would provide a greater degree of control and a good baseline for future developments of the carbon layer. Published examples of carbon ink formulations and reported uses of commercial carbon inks were found to show that carbon content, solvents and binding materials influence ink morphology and electrical performance [40][41][13][19][21][31]. Based on these works two types of carbon inks were formulated with the guidance of SPECIFIC researchers with expertise in carbon inks. The low temperature inks were designed with solvents that would evaporate at temperatures ~100°C, similar to the commercial GEM ink that is used as standard. High temperature carbon inks were formulated with solvents that are removed at higher temperatures ~400°C.

The low temperature inks were created by first mixing 10g of resin made up of 12.5 % Tripolymer and 87.5 % Diacetone alcohol. These materials were selected to create low temperature resin with good viscosity for screen printing. All mixing was done in a speed mixer at 3500 rpm for 5 minutes, repeated twice with a 5 minute rest in between. After 24 hours the

carbon materials were added to the resin and the ink was mixed again. The ink resin before and after carbon materials were mixed in are displayed in figure 14, the colour change is evidence of the carbon material being distributed throughout the ink. After resting for another 24 hours the ink was mixed again for the final time. The carbon materials were Timrex SFG15 graphite, Imerys E360G carbon black and Imerys C65 carbon black. These carbon materials were selected for their good electrical conductivity as reported by the manufacturers. Initially two inks were made with the same proportions to find which of the carbon blacks would be most suitable in the printed carbon layers. Based on the work by Phillips et al. [21] inks were made with varying amounts of carbon material to investigate the optimum amounts for carbon layer conductivity. Different inks were made with the low temperature resin comparing total carbon material weights of 21.7 % and 29.4 % with varying ratios of graphite to carbon black: 1.8:1, 2.6:1 and 3.2:1. The amount of carbon black and graphite within carbon inks have been seen to affect printed layer conductivity and so finding an optimum formulation is important [23][21].

Figure 14 Ink resin (left) with clear yellow colour and carbon ink (right) with opaque black colour

The high temperature ink was made with a resin comprised of 4 g acetic acid and 4.73 g titanium isopropoxide with terpineol and carbon material added to the solution. A ratio of 1:4 terpineol to solution was used and for the carbon material a ratio of 3:20 carbon material to solution was used. The carbon material was made up of SFG15 graphite and E360G carbon black in a ratio of 7:3 graphite to carbon black. This formulation for the high temperature ink was based on work done by Jiang et al. [31].

3.2.2 WO_3 additives in carbon ink

To investigate the effect of a WO_3 additive in the carbon layer carbon inks were prepared with different amounts of WO_3 added. 0.3 g, 0.6 g and 0.9 g of WO_3 particles were added to three different 10 g pots of GEM carbon ink. Each pot was then mixed in a speed mixer at 3500 rpm for 5 minutes twice with 5 minutes rest in between. For four-point probe conductivity tests these inks were screen printed onto glass and for Kelvin probe work function measurements samples were screen printed onto FTO. All samples were dried at 100°C for 10 minutes. These inks were used to print carbon layer samples for conductivity measurements as well as in the fabrication of mCPSC devices.

3.2.3 Screen Printing

The TiO_2, ZrO_2, and carbon layers of the mCPSC are deposited by screen printing, a cost-effective technique that can be used for large scale manufacture [17]. Screen printing is a thin film deposition method that makes use of mesh patterned screen coated with ink above a substrate. The mesh pattern of a screen allows ink through depositing the pattern onto the substrate. The screen is coated with ink using a squeegee that simultaneously coats and pushes the screen down onto the underlying substrate, as displayed in figure 15. Important parameters

that determine the print quality for a given ink are the mesh thread, mesh gap snap off distance, flow speed of the squeegee and firmness of contact [42][43].

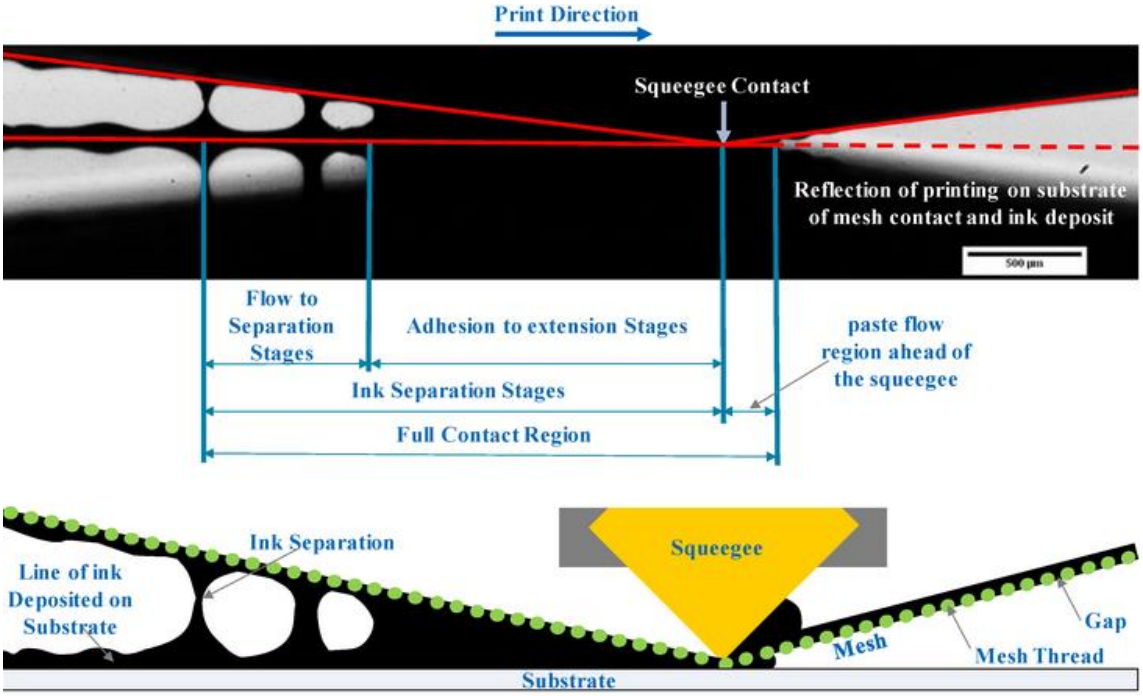

Figure 15 High speed image of squeegee forcing mesh into contact with substrate with labelled diagram, adapted from [42].

The screen printing of mCPSC layers in SPECIFIC labs at Swansea University is carried out using an ATMA electric flat screen printer, pictured in figure 16. This screen-printing machine allows screen parameters such as snap off distance, flow speed to be input digitally. The squeegee is held by a mechanical arm that can be adjusted with a dial for firmness with another adjustable mechanical arm holding a flood coater to collect ink allowing for constant prints at the push of a pedal. Using the ATMA screen printer allows for consistent printing conditions that can be reproduced, which is essential for the fabrication of mCPSC devices as any small difference in printed layers could affect device performance. Also, consistent printing conditions are achieved by having the ATMA screen printer located in a class 6 cleanroom which means there is limited dust particle count in the printing area. This limits the possibility of dust settling on substrates between prints potentially resulting in device faults.

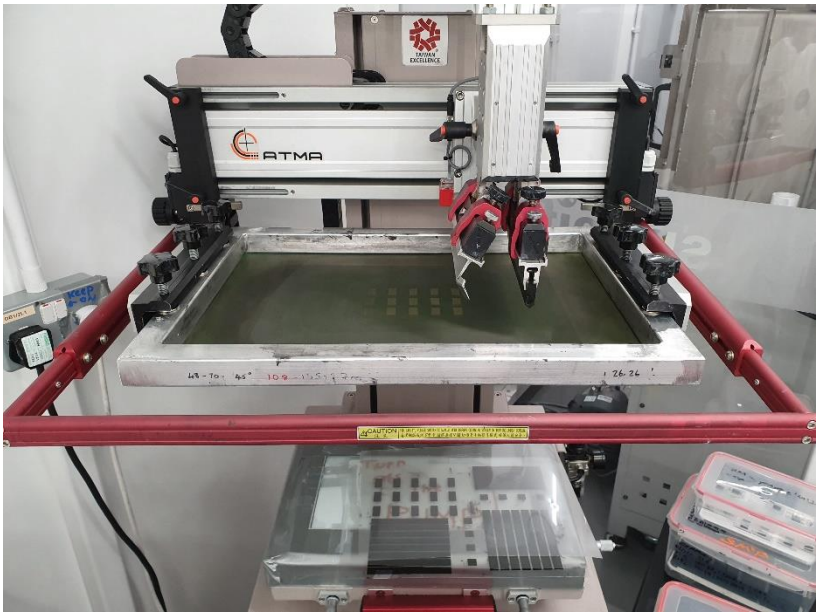

Figure 16 ATMA electric flat screen printer with squeegee, flow coater and screen set up.

3.2.4 Device Fabrication

mCPSC devices are comprised of an FTO substrate, compact TiO_2 layer, mesoporous TiO_2 layer, mesoporous ZrO_2 layer and porous carbon layer with perovskite throughout the porous layers as shown in figure 17.

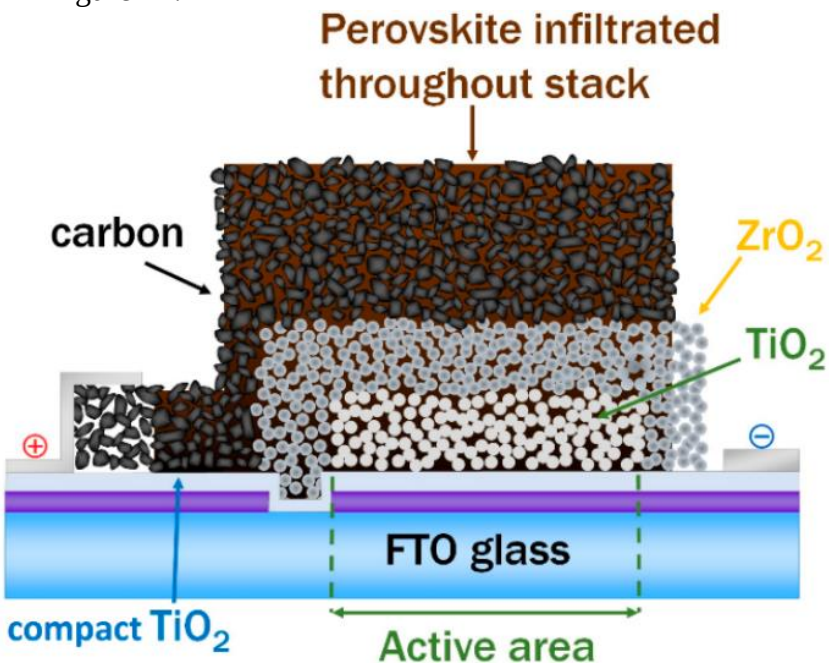

Figure 17 Cross section of the mCPSC adapted from [17].

(Repeated from figure 1)

Device fabrication begins with the preparation of the FTO substrate with laser scribing, followed by cleaning with acetone and deionized water before a final plasma clean in a vacuum chamber. The first layer, compact TiO_2, is deposited onto the FTO by spray pyrolysis. The mesoporous TiO_2 is printed using a screen with a mesh ruling of 130 threads/cm and thread diameter of 34 μm (presented as (130-34) screen), a2 double bevel squeegee at 0° and a flow coater at 10°. Once printed the mesoporous TiO_2 layer is annealed at 125°C, 250°C and 375°C for 10 mins at each temperature and finally 550°C for 30 mins with 5 mins in between each step. Once the annealed layer has cooled suitably the ZrO_2 is printed with a (130-34) screen, a double bevel squeegee at 0° and flow coater at 10°. The layer is then annealed at 100°C, 200°C, and 300°C for 10 mins at each temperature and finally 400°C for 30 mins with 5 mins between each step. The final layer, carbon is printed using a (48-70) screen, double bevel squeegee at 0° and flood coater at 30°. The carbon layer is annealed with the same heating sequence as the ZrO_2 layer. 18 μL of perovskite solution is drop cast onto the cell and allowing 20 mins for the solution to infiltrate the three mesoporous layers. The cells are then heated to 45°C for 1 hour for the perovskite to crystallize. During this time, and the previous 20 min wait, the cells are covered to prevent airflow over the cells affecting infiltration and crystallization. Once completed, the cells have silver contacts soldered onto the glass using an ultrasonic soldering system, one contact is added to the FTO surrounding the active area but does not touch the stack itself and the other contact is added to the section of the carbon layer that overhangs from the stack onto the FTO as described by Figure 18.

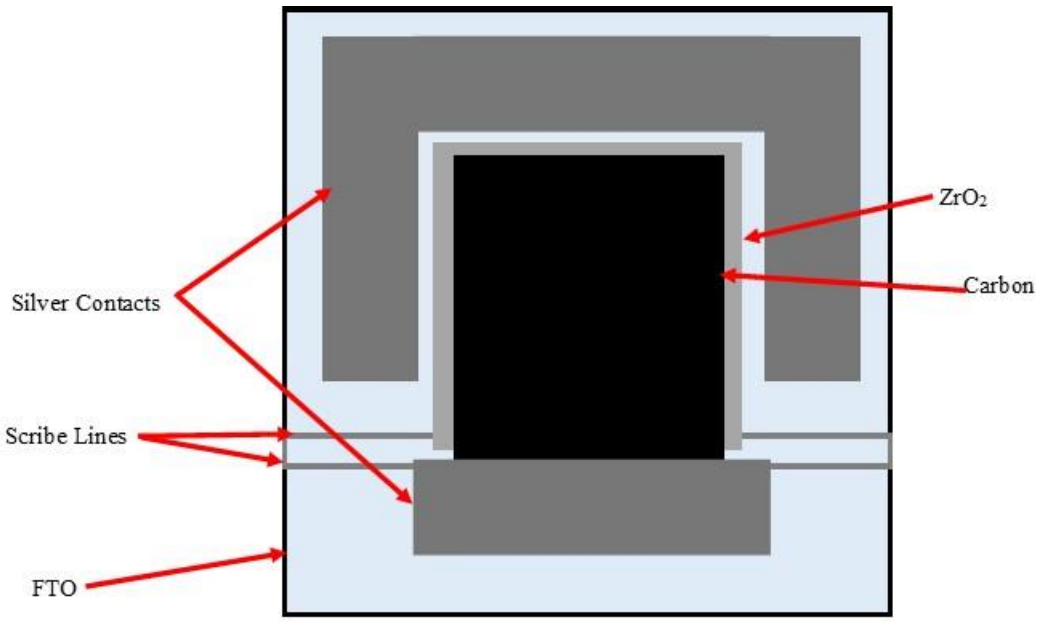

Figure 18 Top-down view of an mCPSC device.

3.2.4.1 Capping Layer

The carbon capping layer is an extra carbon layer screen printed on top of the original device structure after infiltration to act as the new carbon electrode. This is used to have a separate carbon layer for hole collection and carbon electrode layer so that each layer can be tuned to fit the different roles as it is often found that changes to the carbon layer improving conductivity can inhibit perovskite infiltration [31][32].

The effect of a carbon capping layer on device performance was investigated in this work. A schematic that shows how the capping layer was applied is shown in figure 19. Before printing the additional carbon layer, the section of the original carbon that is outside the active area, directly upon the FTO was removed using a razor blade. This allows the second carbon layer or capping layer to have a direct interface with the FTO. This is a unique application of the carbon capping layer that seeks to improve device conductivity through improved contact resistance provided by the interface between the capping layer and FTO. The carbon capping

layer was printed on to the standard mCPSC devices in alignment with the first carbon layer and immediately placed onto a pre heated hotplate to dry at 100°C for 10 minutes. This importance of having the cells quickly move to a hotplate after printing is to try and remove the solvents from the capping layer before they interfere with the perovskite in the layers below.

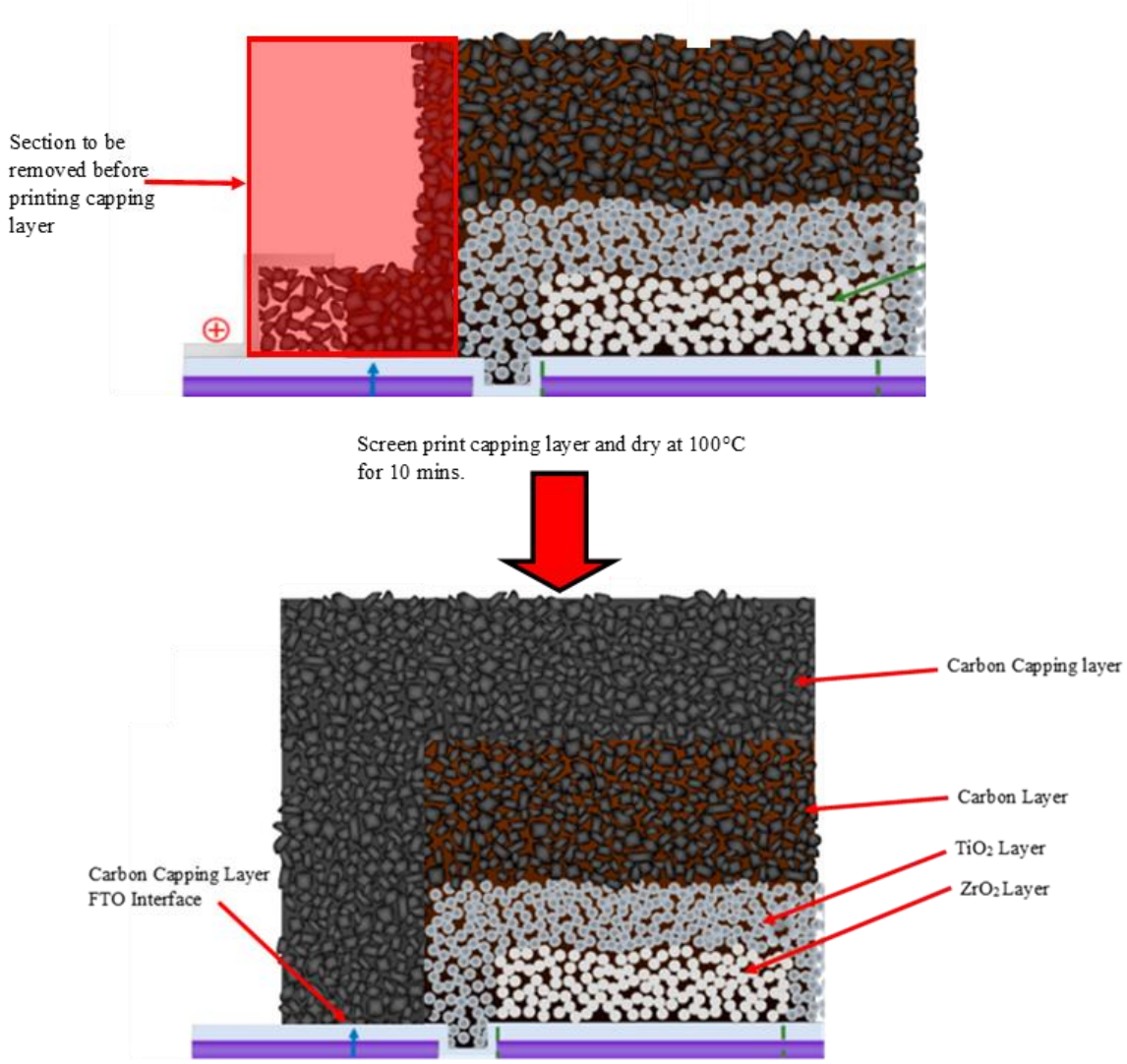

Figure 19 Fabrication process of the carbon capping layer for the mCPSC. Includes the removal of previous carbon/FTO interface before printing of carbon capping layer over the original carbon stack. Diagram of the carbon stack adapted from [17].

3.2.5 Preparation of Carbon Samples for Characterisation

The preparation the of carbon ink samples for Four-point probe, kelvin probe and adhesion test measurements was done in a way that replicates the fabrication of the carbon layer in mCPSC devices as closely as possible. To replicate the conditions of the carbon layer in the mCPSC, carbon samples were fabricated as screen printed with the same settings as used in device fabrication described above.

Investigations were carried out in this work to assess the effect of these replicated conditions on printed carbon samples. In these studies, carbon samples were created representing three different stages the layer undergoes during device fabrication. The three stages were dried, annealed, and infiltrated. Dried samples were heated to 100°C for 10 mins after printing producing a carbon layer with minimal post treatment as it would be before the annealing step in device fabrication. Annealed samples were heated up to 400°C following the sequential annealing program used for the carbon layer in device fabrication, producing a carbon layer as it would be after the annealing step in device fabrication. Finally, Infiltrated samples were created by annealing the printed samples after printing before drop casting perovskite 15µl solution into the carbon layer. The infiltrated samples were left to sit for 20 minutes before heating to 45°C for 1 hour, producing a carbon layer as it would be in a finished mCPSC device. Further studies were done investigating the effect of perovskite volume in carbon layers, with volumes ranging from 0-20 µl, and the effect of the underlying ZrO_2 layer on carbon conductivity. For the carbon layer samples printed on ZrO_2, the ZrO_2 was first printed following the parameters used in device fabrication, including annealing. The carbon samples were then printed on top of the ZrO_2 layer as they would be in an mCPSC device. Samples produced for four-point probe measurements were printed on plain glass rather than FTO as a conductive substrate would influence the resistance measurements. Alternatively, samples produced for

kelvin probe measurements were printed on FTO as a conductive substrate is required for samples to be properly grounded during work function measurements with the kelvin probe.

3.2.6 Fabrication of TLM samples for contact resistance.

The contact resistance of carbon layers on FTO were measured using TLM structures of carbon contacts screen printed onto scribed FTO substrates following the design in figure 18. Also, TLM structures of Au contacts on FTO were made using thermal evaporation deposition. These structures are used instead of the printed layers used for other measurements as the TLM requires a specific set of measurements as explained in the characterisations section.

The contact resistance between GEM ink carbon contacts was compared with the contact resistance between Au contacts and FTO as Au is one of the most common alternative materials used as an electrode within PSCs. For this comparison TLM structures were made, as shown in figure 18, using 6 contacts on FTO separated by 4,9,19,29 and 39 mm spacings sequentially. The FTO was etched with a pattern shown in faded lines in figure 20 to ensure the resistance is being measured across a known distance with the supplied current for each set of contacts.

For the carbon contact resistance three types of samples were created, dried, annealed and infiltrated. These samples were all screen printed onto the scribed FTO with the dried samples then being set onto a hotplate at 100°C for 10 mins. The annealed and infiltrated samples were set on a hotplate and heated to 100,200,300°C for 10 minutes before finally being heated at 400°C for 30 minutes. The infiltrated samples then had perovskite solution dropped into the contacts and were set onto the hotplate at 45°C for another hour for the perovskite to form [44]. Once the samples were printed and heat treatments were complete, silver contacts were soldered to the ends of each contact in order to protect the carbon contacts from the probe tips used to supply current and measure resistance. The Au sample was created with the same layout

in figure 20 but the Au contacts were deposited by thermal evaporation using a vacuum sealed bell jar. The measurements were taken and used to calculate Transfer length contact resistivity and contact resistance using the method outlined in the previous section. Limitations of this method for measuring the contact resistance exist in the use of a trendline in calculating results from the measured data. As a result of this, the most accurate results would require as many data points as possible over the greatest length possible however, the fabrication of the TLM structure determines that only a few data points are used over lengths less than 50 mm.

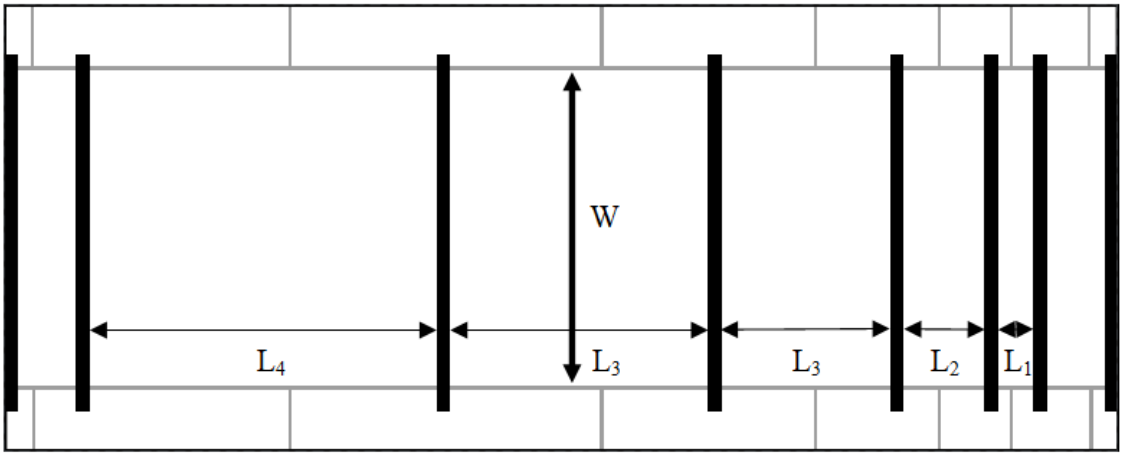

Figure 20 The TLM structure.

(Repeated from figure 6 for ease of reference)

Chapter 4. Results and Discussion

4.1 Lab-Formulated Fabricated Carbon Inks Conductivity

The carbon ink currently used for the mCPSC in SPECIFIC labs at Swansea University is the commercially supplied GEM carbon ink. In terms of manufacturing the mCPSC on a larger scale there are advantages to using commercially supplied inks for their larger supply but when looking to modify the carbon layer, an ink that was fabricated in the labs by researchers would be preferable. This is because knowledge of commercial inks is limited to the basic components, leaving the specific quantities and formulation techniques to be estimated. Inks made in the lab by researchers would therefore serve as a better baseline for modifications as the exact composition of these carbon inks would be known. Many researchers have published results of inks produced in labs, some of which will serve as reference points for the inks fabricated in this study [20][21][31][45].

The temperature of heat treatment for a carbon ink is dependent on the solvents and binders used to create the resin that the carbon material is mixed with. Different solvents and binders are evaporated and combusted at different temperatures. Carbon inks such as GEM only require heating to ~100°C for optimum conductivity but other carbon inks must be heated upwards of 300°C before their solvents are removed, and the carbon's optimum conductivity is reached [46].

In this work carbon inks designed for use after heat treatment ~100°C are referred to as Low Temperature Carbon Inks and those that are designed for use after heat treatment greater than this are referred to as High Temperature Carbon Inks.

Whilst the GEM ink is designed for use as a conductive carbon film after heat treatment of 100°C, the unique application of the carbon layer in the mCPSC requires the ink to be annealed

up to 400°C. This high temperature annealing is done to remove as much of the solvent and binding material as possible in the carbon ink to create a porous layer that can successfully host perovskite. As such, in the following sections low temperature and high temperature inks are fabricated and used to print carbon layer samples. The conductivity of these printed samples are compared with the GEM carbon layer to evaluate which carbon inks would be most suitable for use in the mCPSC.

4.1.1 Low heat treatment temperature inks

Low temperature carbon inks were created with a resin comprising of tripolymer and diacetone alcohol. This resin formulation was selected for a low solvent evaporation temperature and suitability for screen printing, based on recommendations of SPECIFIC researchers with ink formulation expertise. Formulations for the carbon component of the low temperature inks were based on work by C. Phillips et al. that investigated the effect of different weights of carbon black and graphite on carbon ink conductivity [21]. TIMREX SFG15 graphite was used as it is manufactured to have very high electrical conductivity applicable for use in conductive inks. Two carbon black options were compared: E360G carbon black and C65 carbon black, both manufactured by IMERYS.

4.1.1.1 Effect of Carbon Black on conductivity.

The carbon black powders E360G and C65 were compared by fabricating two carbon inks with the same proportional weight of graphite and carbon black in resin but using a different carbon black material in each. With these inks samples were printed on glass for sheet resistance and resistivity measurements using a four-point probe.

The sheet resistance of fabricated carbon inks containing E360G and C65 carbon black are higher than the GEM ink, as shown in figure 21. The E360G carbon black was found to have sheet resistance ranging from 25-45 Ω/□ whereas the C65 carbon black had significantly higher

sheet resistances ranging from 45-58 Ω/□. As the formulation and fabrication of these two inks was identical other than the carbon black used, this difference in sheet resistance is most likely a direct result of the difference in conductivity between the E360G and C65 carbon black. Figure 22 shows the resistivity of these inks compared with GEM and the same trend is visible, confirming the C65 ink's lower conductivity. The differences between these fabricated inks and the GEM ink, however, is more significant in the resistivity data. This is due to the difference in morphology of the inks resulting in a greater layer thickness for the formulated inks than the GEM. The morphology of these inks is largely dependent on the binder and solvents used in their formulation. The resistivity results indicate that the conductivity of the fabricated inks is much less than the GEM. Further work was done to fabricate carbon inks targeting increased conductivity by changing the amount of carbon material used in the formulation. Based on these results the E360G carbon black was used for this further work as the conductivity of layers with this carbon black was seen to be superior to those including the C65 carbon black.

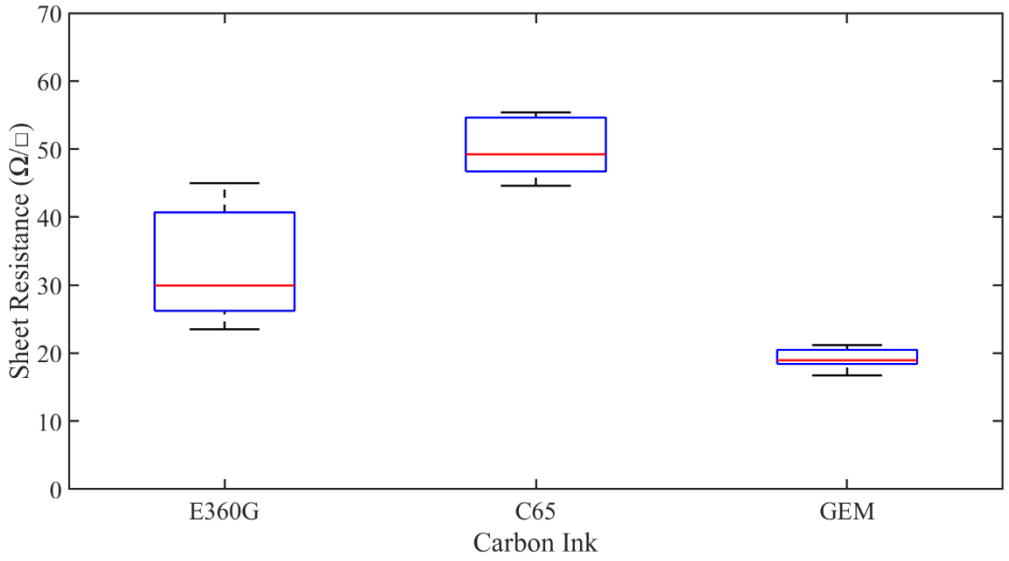

Figure 21 Sheet Resistance of fabricated inks containing different weights of carbon material with varying ratios of graphite to carbon black, from batches of five samples

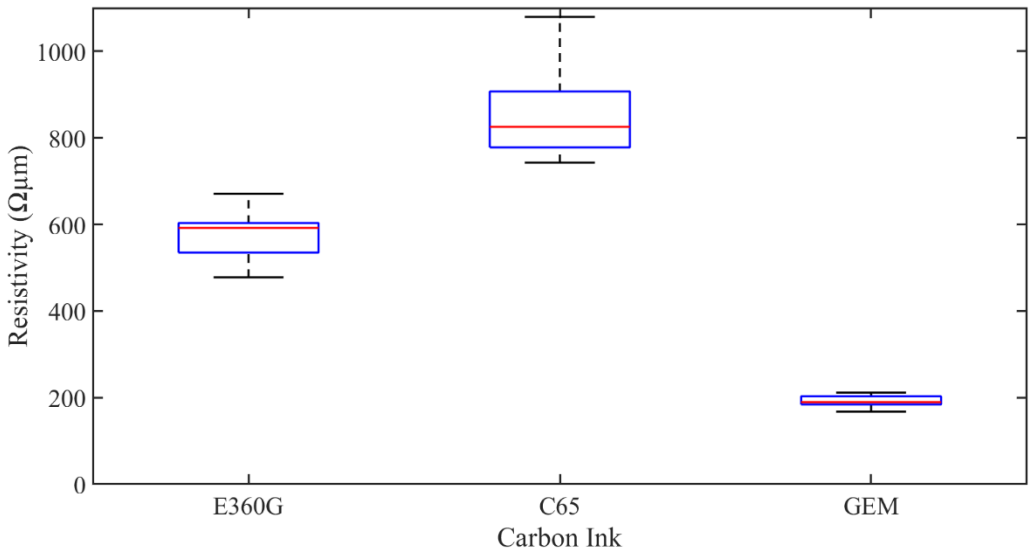

Figure 22 Resistivity of fabricated inks containing different weights of carbon material with varying ratios of graphite to carbon black, from batches of five samples

4.1.1.2 Effect of Carbon material weight and ratio of Graphite to Carbon Black on conductivity.

Inks were fabricated with varied weights of carbon material and with different ratios of graphite to carbon black. The proportion of carbon material used in carbon inks has been found to affect the conductivity and morphology of inks. As the carbon material is the conductive component of the carbon ink it is expected that a higher concentration of graphite and carbon black would improve conductivity, however this has to be balanced against any effects on the printability of the ink and its ability to host perovskite successfully. The ratio of graphite to carbon black is important as the larger graphite particles have higher conductivity but the smaller size of the carbon black particles can provide a greater surface area of contact between carbon material, all of which affects conductivity in the carbon ink [31][21][19].

The fabricated carbon inks containing different total weights of carbon material made up with different ratios of Graphite to Carbon Black have their sheet resistance compared on figure 23. The sheet resistance of the fabricated inks in order from highest to lowest was the High Carbon 2.6:1 ink (28-70 Ω/□), followed by the Low Carbon 1.8:1 (30-50 Ω/□), Low Carbon 2.6:1 ink (23-45 Ω/□) and High Carbon 3.2:1 (15-30 Ω/□). These results indicate that the sheet resistance is lower in inks with a higher concentration of graphite particles but the wide range of results for the fabricated inks, especially for the High Carbon 2.6:1, suggest that the formulated inks are inconsistent. This is evident when compared to the tight range of sheet resistance measured for the GEM (15-20 Ω/□). This inconsistency is likely due to the incomplete mixing of the carbon material during speed mixing leading to uneven distribution throughout the inks. The commercial GEM ink probably makes use of a more sophisticated and thorough process than the speed mixing process used for the fabricated inks resulting in a more uniform distribution of carbon material throughout the ink and therefore more consistent printed layers. As such the contents in each printed GEM layer are very similar whilst the fabricated ink layers have some variation. The most conductive samples measured of the High carbon 3.2:1 ink had a similar sheet resistance to the GEM, however the resistivity data, shown in figure 24, reveals that this is due to a thicker layer positively affecting the sheet resistance of the printed fabricated inks compared to the thinner GEM layer. From the resistivity data the conductivity of the GEM ink is far greater than the fabricated inks with the resistivity of the High carbon 3.2:1 ink being 400 Ωμm which is twice the GEM inks resistivity, 200 Ωμm. Furthermore, it should be noted that the resistivity data provides further clarity on the effect of higher concentrations of graphite improving the conductivity of carbon inks as well as showing that a higher concentration of all carbon material is preferable for lower conductivity. This is as expected as the carbon material is the conductive part of the ink, with the graphite particles in particular being the most

important factor in conductivity whilst the carbon black particles help to provide structure [19] [21][23][40].

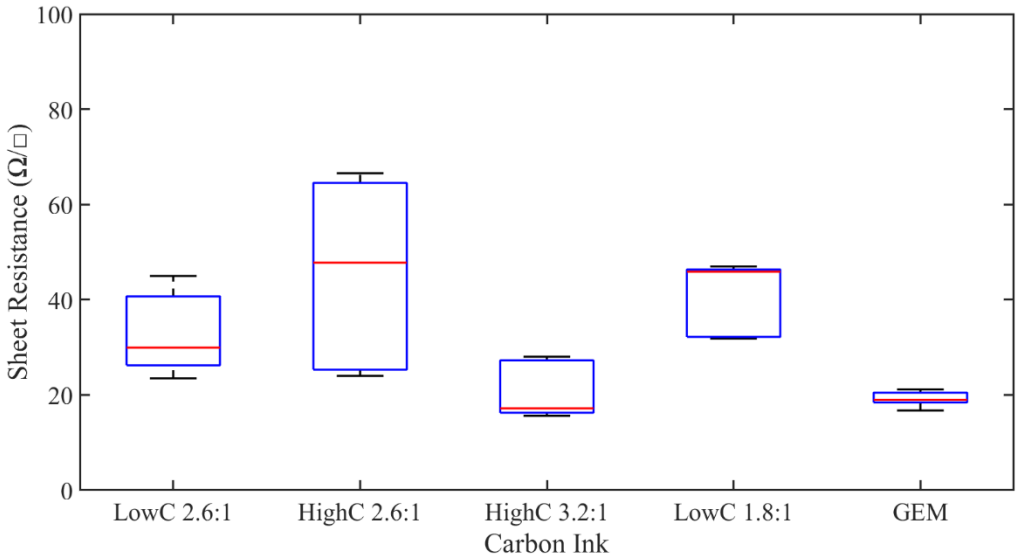

Figure 23 Sheet Resistance of fabricated inks containing different weights of carbon material with varying ratios of graphite to carbon black, from batches of five samples.

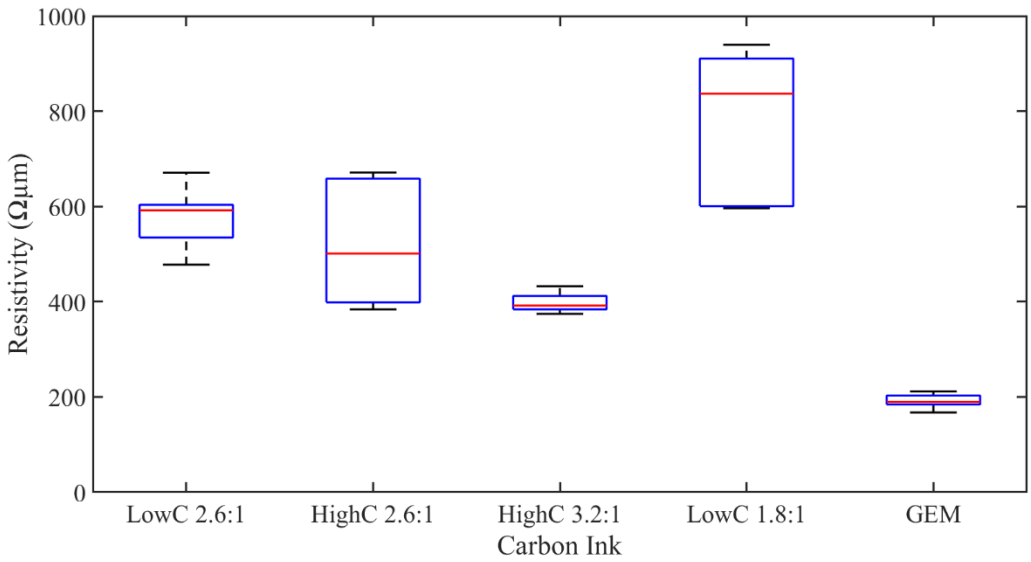

Figure 24 Resistivity of fabricated inks containing different weights of carbon material with varying ratios of graphite to carbon black, from batches of five samples.

The low temperature formulated inks were found to have much lower conductivity than the commercial GEM ink from these results. These ink formulations would also require further revisions to optimize printability and without conductivity at least comparable to the GEM ink this would be unjustified. The reasons for the lower conductivity of these formulated inks is likely a result of the formulation process as well as materials used. Commercial manufacturers have access to more sophisticated fabrication processes and so can produce carbon inks with excellent distribution of graphite and carbon black throughout the ink. The speed mixer suitably mixes carbon material through the ink resin as can be seen by the change in colour and consistency, but shear mixing cannot break down particles as thoroughly as a technique such as ball milling. The conductivity of carbon inks is dependent on graphite and carbon black and so whilst the materials used in the low temperature formulated inks are of a high standard there is no way of knowing how they compare to the GEM ink as the carbon contents of GEM are unknown.

4.1.2 High Temperature Ink

As the low temperature inks had failed to meet the standard of commercial carbon ink high temperature carbon ink was fabricated in-lab by a SPECIFC researcher with carbon ink expertise based on ink formulations published in literature [31]. The formulation used the SFG15 graphite and E360G carbon black with a ratio of 7:3 Graphite to carbon black. The carbon material was mixed in a solution comprising of acetic acid, titanium isopropoxide and terpineol. This fabricated ink is referred to as the HT ink hereafter. The conductivity of the HT ink was measured and compared to the GEM ink after drying at 100°C and annealing up to 400°C. This was done as there was expected to be a difference in the way the inks were affected by heat treatments as a result of the HT inks formulation being designed for high temperature use.

The sheet resistance of the fabricated high temperature carbon ink, HT ink is compared with the GEM ink after being dried at 100°C and Annealed up to 400°C in figure 25. The comparison shows that the HT ink has a much higher sheet resistance when dried but once the layers are annealed the HT ink has the lower sheet resistance of the two. The annealing process has an opposite effect on the two inks, increasing the sheet resistance of the GEM whilst decreasing the sheet resistance of the HT ink. The reason for this different response to annealing is the formulation of the ink's binding agents and solvents. The different solvents and binders in these inks are removed at different temperatures influencing the electrochemical properties of the layer [46][47][48][49]. As these inks are intended for use as a mesoporous carbon electrode layer in the mCPSC, they will be annealed to allow for optimum perovskite infiltration. Therefore, the HT ink's lower sheet resistance after annealing treatment makes it a promising candidate for use in the mCPSC. The resistivity data in figure 26 shows still shows the change in conductivity of each ink after annealing but the annealed resistivity of the GEM remains lower than the HT ink indicating that the HT ink's lower sheet resistance is a result of greater layer thickness, and that inherent conductivity of the GEM ink is greater. Overall, the HT ink's promising conductivity after high temperature annealing warrants further investigation.

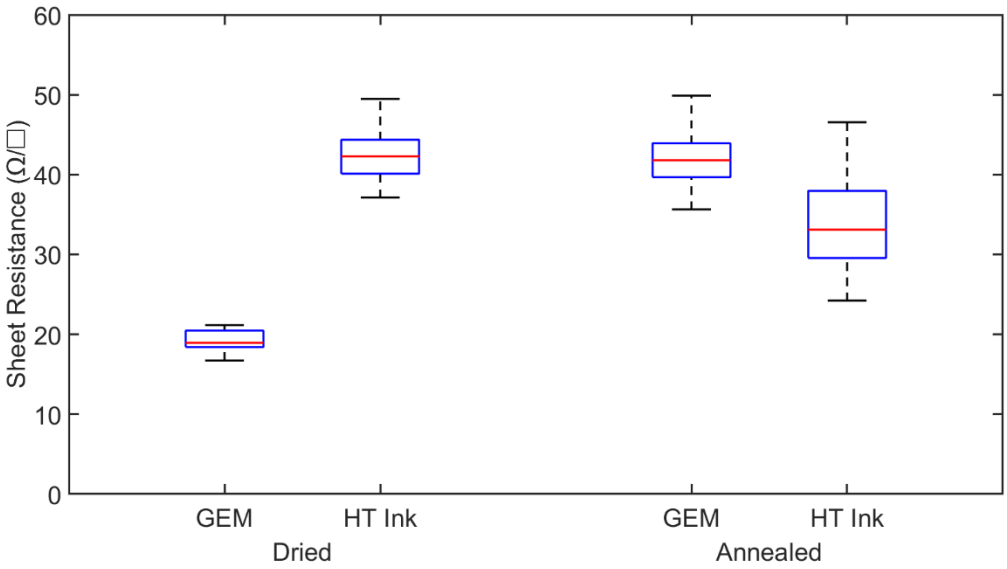

Figure 25 Sheet Resistance of fabricated HT ink compared with GEM, from batches of five samples.

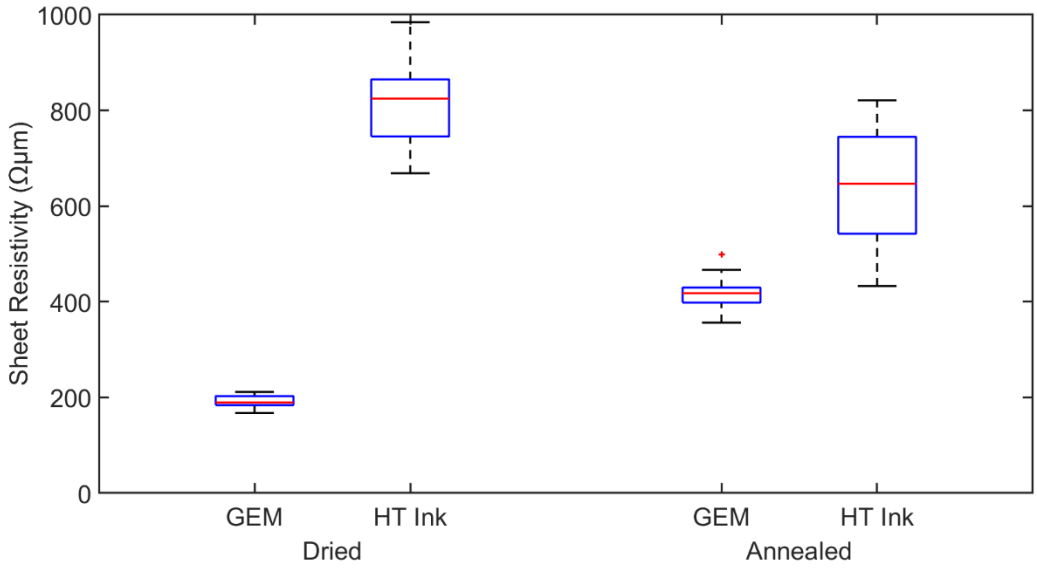

Figure 26 Resistivity of fabricated HT ink compared with GEM, from batches of five samples.

The improved sheet resistance and resistivity of the high temperature formulated ink show much more potential than the low temperature formulated inks. The conductivity is still behind that of the GEM ink but the different response to the heating process could be advantages in the mCPSC where the carbon layer is heated before infiltration.

4.2 Comparing Commercial Carbon Ink Conductivity

As no inks were formulated with clear conductivity improvements over the current commercial GEM carbon ink, it was determined that commercial carbon inks could be a more promising option for the improvement of carbon layer conductivity and device performance. There are many suppliers of printable conductive carbon inks which are advertised for use as thin film carbon electrodes. Identifying a carbon ink with similar or better conductivity than the GEM could result in device performance improvements or simply provide more options for larger scale manufacturing of mCPSC technology. A selection of five commercial carbon inks were compared to the current GEM ink used in devices and the most promising formulated carbon ink. The carbon inks being compared are listed in table 1. The information provided in table 1

was gathered from manufacturer websites where available with the exception of the Wondersolar ink. Wondersolar is a company with close links to a research group based in Huazhong University of Science and Technology, publishing work on the mCPSC and so the ink is presumably very similar to the ink used in that research [23].

To evaluate these inks as potential prospects for use in the carbon layer of the mCPSC their conductivity was compared. Conductivity comparison was made by measuring the sheet resistance, resistivity and contact resistance of the carbon inks on glass and FTO. Devices were made using the most promising carbon inks to compare with device performance of mCPSCs using the GEM carbon layer.

Table 1 Carbon Inks to be compared with manufacturers reported solids content, conductivity and recomendation for heat treatment.

Carbon Ink	**Manufacturer**	**Recommended Heating Temperature (°C)**	**Solids content**	**Reported sheet resistance**
Dycotec	Dycotec	100	43-46%	10Ω/□ at 25µm
Elocarb C/SP	Solaronix	450	~25%	15Ω/□ at 15µm
Wondersolar	Wondersolar	400	Likely similar to ink describe here [23].	
EIC03	Elemental Inks & Chemicals	100-140	38-42%	3Ω/□ at 25µm
Elocarb B/SP	Solaronix	400	unknown	7Ω/□ at 15µm
HT	Formulated in-lab	400		
GEM	Sun Chemical	100	38-42%	10Ω/□ at 25µm

4.2.1 Sheet Resistance and Resistivity

Sheet resistance and resistivity of samples were compared for printed layers dried at 100°C and annealed at 400°C. The different solvents and binding materials within the carbon inks can evaporate at different temperatures which changes the characteristics of a printed layer. Carbon inks with optimum conductivity after 100°C heat treatment are referred to as low temperature inks and those that perform best after being annealed at 400°C are referred to as high temperature inks. It is important to note that the carbon layer of the mCPSC is heated to 400°C to ensure removal of solvents and binders in preparation for perovskite infiltration regardless of the optimum heat treatment for carbon conductivity.

The sheet resistance of the carbon layers once dried are presented in figure 27 apart from the Elocarb G/SP which has been excluded for scaling up due to the sheet resistance being much higher than the other inks, at an average of 1260 Ω/□. The HT, GEM and EIC 03 inks had the lowest sheet resistance measured of the inks when dried, averaging 40, 20 and 10 Ω/□ respectively. The Wondersolar and Elocarb B/SP both had an average sheet resistance of 110 Ω/□, significantly higher than the most conductive inks, but lower than the Dycotec ink which had sheet resistances ranging from 110-160 Ω/□. The dried sheet resistance results show the conductivity of inks as a low temperature carbon electrode. The GEM and EIC 03 inks are described as low temperature inks and so there is an expectation that these inks will be highly conductive when dried at 100°C. The HT Ink is described as a high temperature carbon and was created with the intention of heating up to 400°C and so it would not be expected to perform as well as the GEM and EIC 03 inks when dried at 100°C, however its low resistance compared to the other high temperature inks is promising. The Dycotec, Wondersolar and Elocarb B/SP Inks are not suitable for use as low temperature carbon electrodes due the high sheet resistance displayed in this data, with the Elocarb C/SP (not included on the graph) being completely unusable at low temperature due to its extremely high sheet resistance. The EIC03

ink having the lowest sheet resistance when dried at 100°C makes it the best prospect for a carbon contact printed on top of an already infiltrated cell.

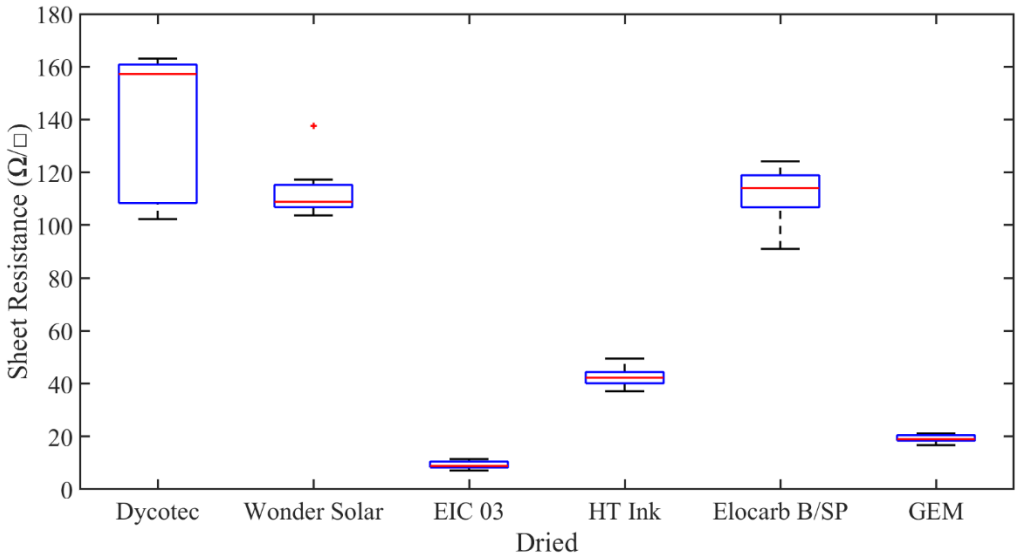

Figure 27 Comparing the Sheet Resistance of carbon inks when dried at 100°C after printing, from batches of five samples

The sheet resistance of these carbons gives a comparison of how they would perform as carbon contacts in a device when printed with the same parameters as GEM. The resistivity shows the inherent conductivity of a carbon ink. As such, the resistivity of these carbon inks can show the potential of carbon inks in cases where the printing parameters are changed to suit different morphologies of inks. Figure 28 shows the resistivity of the carbon inks when dried at 100°C, excluding the Elocarb C/SP and Dycotec due to high resistivity values. As previously mentioned, the Elocarb C/SP has high resistance at low temperatures likely as a result of the solvents and binders in the ink acting as insulation between conductive carbon material, causing high resistivity. The Dycotec ink printed in thick layers due to its high viscosity resulting in sheet resistance sometimes comparable to the Wondersolar and Elocarb B/SP but a resistivity that is much higher. The Dycotec has a higher solids content than the other inks which effects the viscosity and printability of the ink [43][21]. From the data displayed in figure 28 it can be seen that the EIC03 and GEM inks have the lowest resistivities when dried at

100°C, with a mean of 145 Ωμm and 190 Ωμm respectively. As was the case with the sheet resistance these inks were expected to have the lowest resistivity when dried as they are marketed as low temperature carbon inks whereas the others are designed for treatment at higher temperatures. The HT ink has resistivity ranging from 650-990Ωμm, which is far higher than the EIC03 and GEM inks. This gives a different view of the HT ink's conductivity when treated at 100°C than the sheet resistance data. An explanation for this difference is that the HT ink was prone to mesh marking due to its rheology which results in a very rough printed surface including variation in thickness in line with the pattern of the printing screens mesh[21][43]. As can be seen in the ink's profile in figure 29 these variations in thickness increase the average thickness of the print resulting in a greater sheet resistance measurement across the surface. The resistivity data therefore shows that without the mesh marking affect, this ink would probably perform similarly to the Elocarb B/SP when dreid at 100°C, which is more in line with the expectations for the HT ink due to it being reported as intended for high temperature use. The Elocarb B/SP ink resistivity ranges from 800-1050 Ωμm and the Wondersolar ink resistivity ranges from 1200-1500 Ωμm. This supports what was seen in the sheet resistance data for these inks when dried.

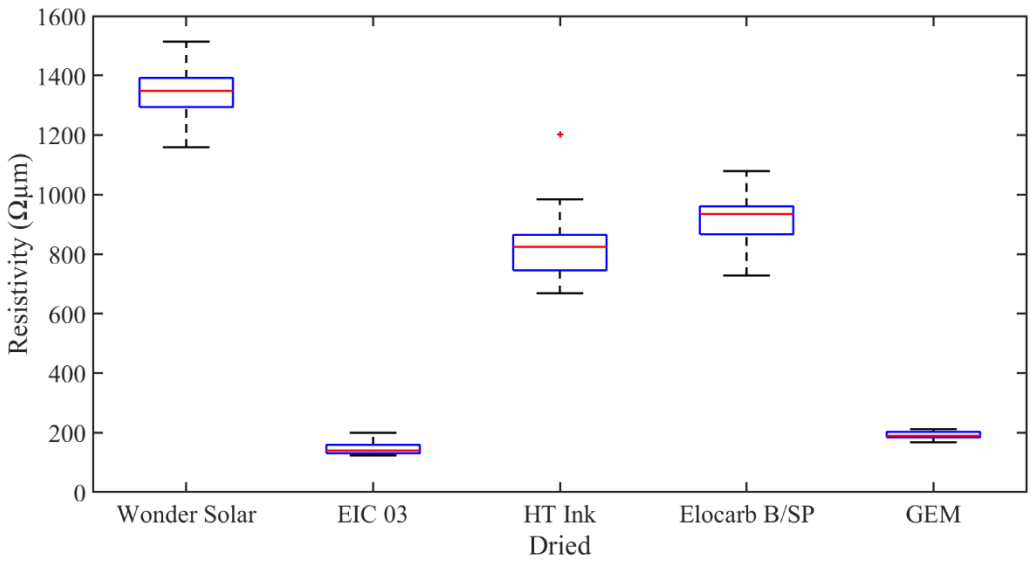

Figure 28 Resistivity of carbon inks when dried at 100°C, from batches of five samples.

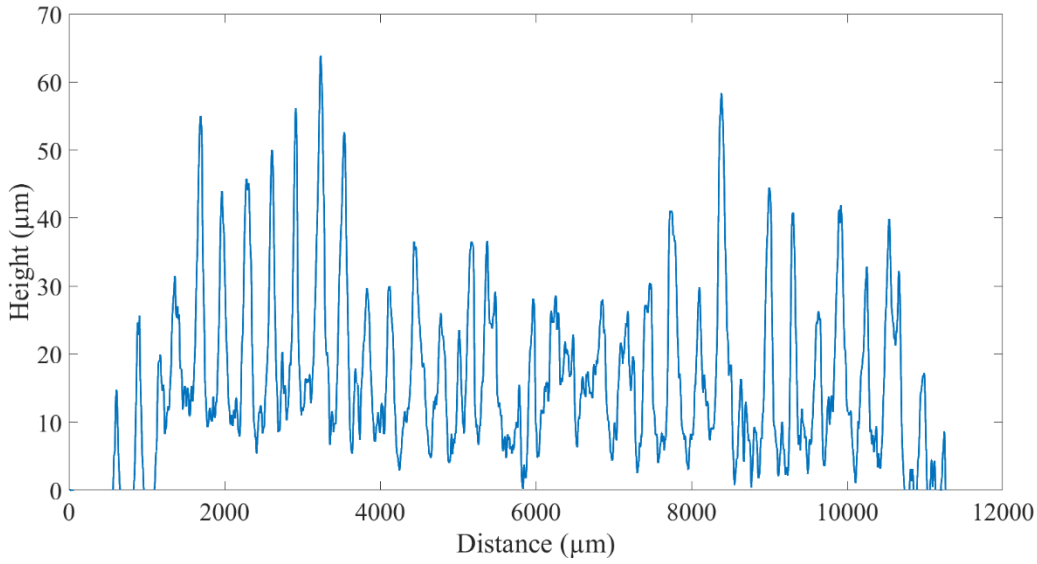

Figure 29 Profile of HT ink showing the effect of mesh marking on surface roughness.

The sheet resistances of the annealed inks displayed in figure 30 shows that the Elocarb C/SP, Wondersolar, EIC03 and HT inks had the lowest average sheet resistances ~30 Ω/□. The GEM ink had a greater average sheet resistance at ~40 Ω/□. Of these inks the lowest sheet resistance was seen with the EIC03 at 22 Ω/□ followed closely by the HT ink with a minimum of 24 Ω/□. The sheet resistances of the Elocarb B/SP ink measure in the range of 50-60 Ω/□ followed by the Dycotec ink in the range of 60-70 Ω/□. The low sheet resistance of the Elocarb C/SP, Wondersolar, EIC03 and HT ink after annealing would make them promising alternatives to GEM for use as carbon electrodes in mCPSC. Comparing these results to the sheet resistance of the dried samples from figure 27, it can be seen that the GEM and EIC03 inks have an increased sheet resistance once annealed by ~20Ω/□. The opposite effect is seen in the other inks which all show improved sheet resistance once annealed. This difference in response to heating treatment is what separates the GEM and EIC03 inks as low temperature inks whereas the others are reported as high temperature inks. Despite this the EIC03 ink still performs very well when annealed offering a lot of flexibility as to how it might be used.

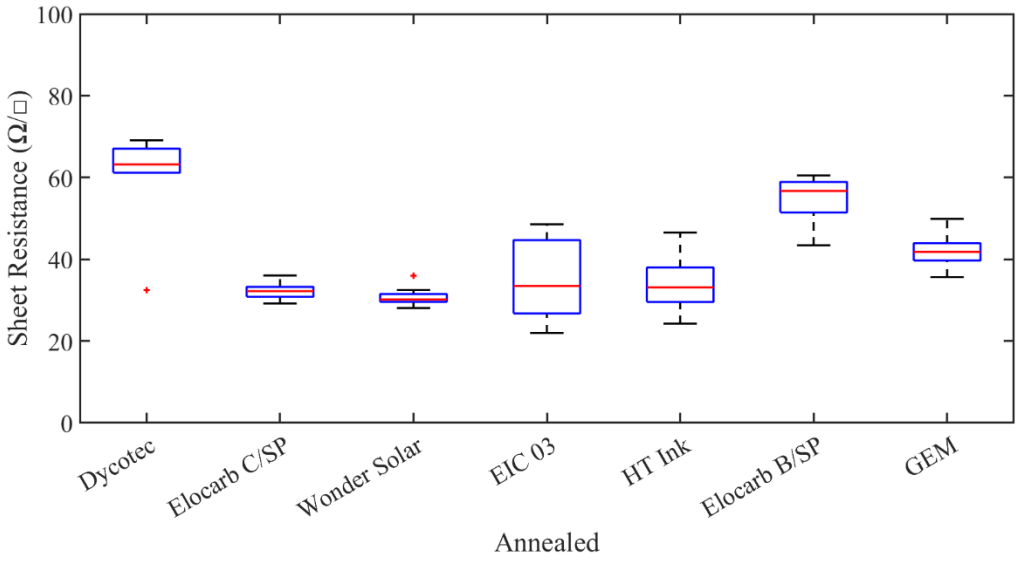

Figure 30 Sheet Resistance of Annealed Carbon Ink Samples, from batches of five samples.

The resistivity of the carbon inks when annealed is presented in figure 31, the Elocarb C/SP ink has by far the lowest resistivity at ~95Ω µm followed by Wondersolar at ~380 Ωµm, GEM at ~420 Ωµm, Elocarb B/SP at ~450 Ωµm, EIC03 at ~530 Ωµm. The HT ink had resistivity between 430-800 Ωµm and the Dycotec ink had resistivity between 660-950 Ωµm. These results show the inherent conductivity of the carbon inks when annealed disregarding print thickness and so if all the inks were printed into identical layers the Elocarb C/SP would be the most conductive. This is not reflected in the sheet resistance results due to the morphology of the ELocarb C/SP affecting the layer thickness when screen printed. The Elocarb C/SP samples were 2-3µm thick and so the sheet resistance of the printed layer is increased. The inks all have varying consistencies that affect a printed layer's thickness and roughness and so while the resistivity shows the materials conductivity, it is less useful for judging the specific application of a carbon layer in the mCPSC than the sheet resistance. As discussed with the sheet resistance results, comparing the resistivity of the samples when dried and annealed shows the difference between the low temperature GEM and EIC03 inks and the other high temperature inks. The

improved conductivity of these high temperature inks after heating up to 400°C has been observed in literature and described as improving the charge transfer across the carbon layer due to the removal of binding materials that would impede charge transfer [46][47][48][49]. The low temperature inks GEM and EIC03 experience an opposite effect with the conductivity decreasing after being annealed at 400°C. This could be the result of different binding materials having a different level of interference with conductivity across the carbon material in a carbon layer. It seems as though the binding material must be aiding conductivity in the low temperature inks and so the removal of binders after annealing reduces the conductivity of these inks unlike the high temperature inks which benefit from the removal of binding material.

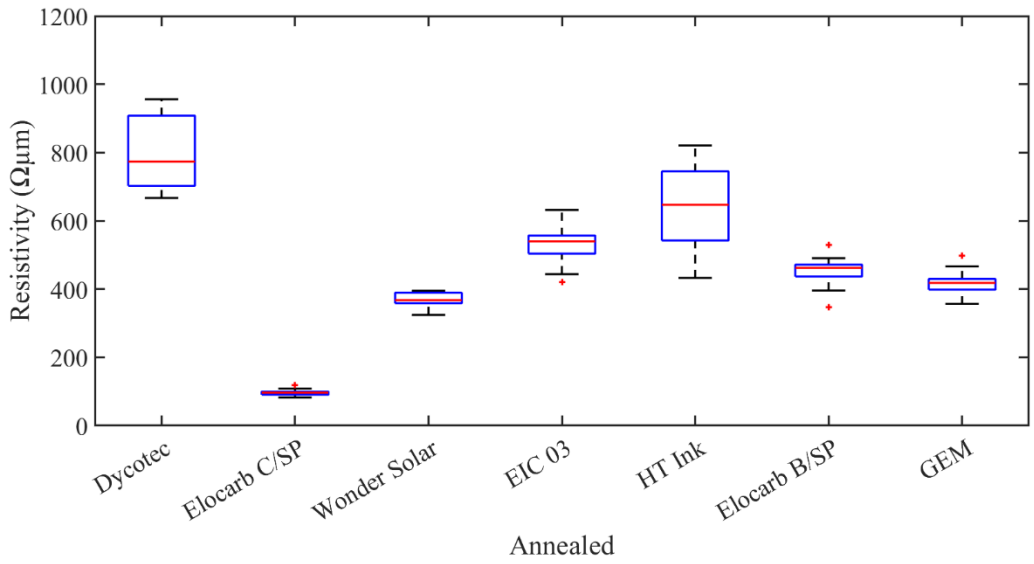

Figure 31 Resistivity of Carbon Inks After Annealing, from batches of five samples.

4.2.2 Commercial Inks Contact Resistance

Contact resistance is a measure of the electric at resistance present at the carbon/FTO interface and so a lower contact resistance will result in less current lost at the interface and higher overall device conductivity. The transfer length is proportional to contact resistance and indicates the average lateral distance current travels in one contact before crossing the interface. Transfer length can be a useful parameter in reducing the area needed for the carbon FTO interconnect, a reduction of which would free up area for the charge generating part of the mCPSC device.

The contact resistance and transfer length of carbon inks can be seen in figures 32 and 33. The Wondersolar, HT and GEM inks have similar contact resistance and transfer length around 0.01-0.02Ω with little difference seen between annealed and dried samples except for a slight increase in contact resistance for the GEM when annealed. The losses due to contact resistance in a device are negligible but in a module with many contacts in series the losses would be similar for these three inks. This is despite the difference in conductivity for these inks and so could appear to be an unexpected result. However, the conductivity of the inks in terms of sheet resistance is a measure of how easily current can travel laterally across a layer. The TLM method finds the resistance incurred when the distance travelled laterally is 0 and so it is only the resistance against current crossing from the carbon layer to the FTO. This means that contact resistance is influenced by the contact between carbon particles and the underlying FTO rather than sheet resistance which is dependent on contact between particles throughout the layer. As such it is possible for a less conductive layer to have lower contact resistance if there is a higher concentration of carbon material at the bottom of a printed layer, as could be the case with the HT and Wonder solar inks compared to GEM and EIC03. The EIC03 ink had a contact resistance of ~0.1Ω which whilst still too low to have an effect on a device could have an effect in modules. The contact resistance is 10x that of the GEM ink and so the losses

due to the series resistance in a module using EIC03 could be expected to be 10x as great than one with GEM. The Elocarb C/SP has by far the highest contact resistance when dried, likely as a result of the ink's extremely poor conductivity when dried. The annealed contact resistance is between the GEM and EIC03 inks making it less suitable than GEM for modules but potentially a better choice than EIC03 based on the contact resistance and transfer length alone. The transfer length of all these inks, apart from the dried Elocarb C/SP is below 1mm, so this is the average length of the carbon/FTO interface current is travelling along before moving between contacts. The length of the carbon/FTO interconnect should be higher than 1mm for these inks but probably no higher than 2mm in order to optimize the use of space in devices and especially modules. Previous studies have found that optimizing the amount of active cell area within modules, improving the geometric fill factor, will improve performance [33].

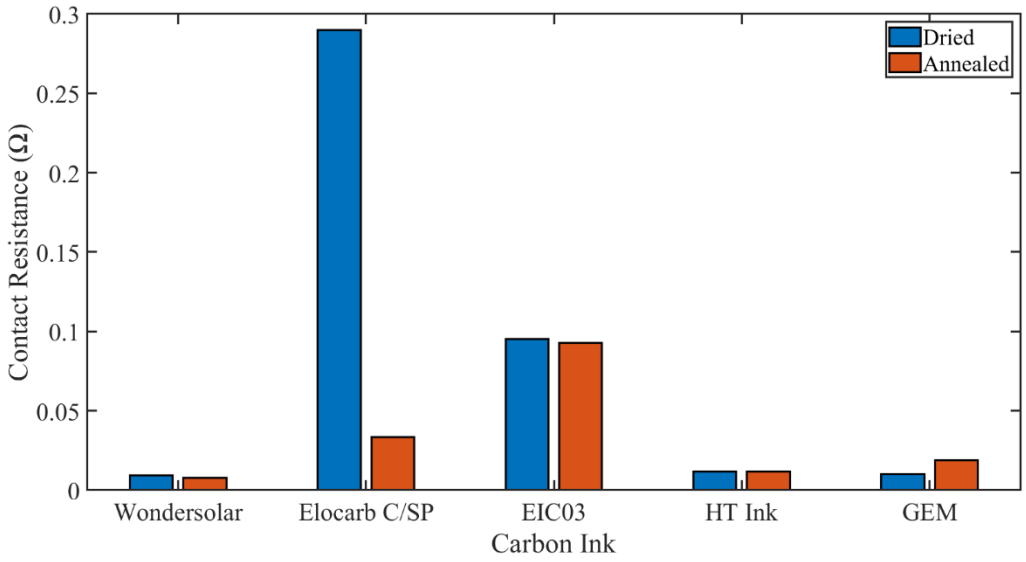

Figure 32 Contact resistance of carbon inks dried and annealed, from sets of two samples.

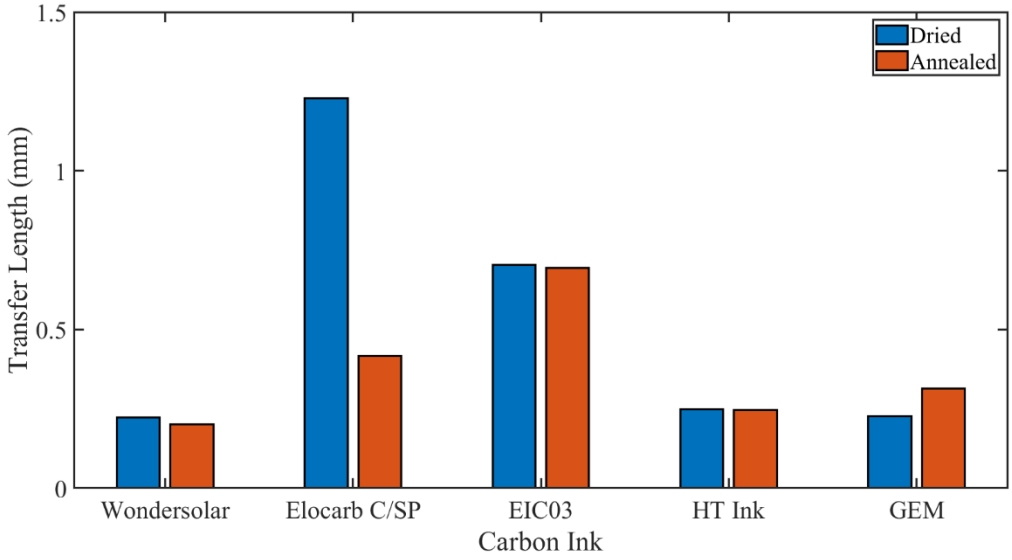

Figure 33 Transfer Length of carbon inks dried and annealed, from sets of two samples.

4.2.3 Commercial Carbon Inks Device Data

Three sets of devices were created using the GEM, EIC03 and HT ink as carbon layers. The device data is gathered using a solar simulator with a light intensity of 1 sun. The EIC03 and HT inks were selected primarily for the low sheet resistance measured of annealed layers printed with these inks. The GEM devices serve as a benchmark as this is the ink currently being used for devices in SPECIFIC labs at Swansea University.

Figures 34a, b, c and d show the device data for mCPSCs made using GEM, HT, and EIC03 ink for the carbon layer. The PCE results for these devices, figure 31a, show that the HT devices had a lower efficiency than the GEM and EIC03 devices. The GEM devices had the greatest efficiency on average but the EIC03 had the single highest device efficiency of 7.0 %. The reason for the poor performance of the HT devices can be seen in figure 31d that shows the J_{SC} of these devices was less than half that of the GEM and EIC03 devices. The low J_{SC} indicates low charge extraction in these devices and so it is possible that the HT carbon layer does not host the perovskite as well as the GEM and EIC03 layers. This could be a result of poor infiltration in the layer or the solvents and binder of the HT interacting negatively with the

perovskite. The Fill Factor for the devices, seen in figure 31b, are all comparable as would be expected from the similarly low sheet resistances measured for these carbon inks. This makes the lower PCE of the HT devices unlikely to be a result of poor resistance within the device. The average V_{OC} is also similar for these devices which indicates the energy levels of the electrodes are similar resulting in similar band gaps. However, the EIC03 devices have a greater range of V_{OC} results which indicates some inconsistency in the devices and is likely responsible for the greater range of PCE results for the EIC03 devices. The average PCE of the GEM devices is 5.0 % and for the EIC03 devices 4.0 %. This difference in average performance is reflected in the average FF, V_{OC} and J_{SC} of the GEM devices being slightly greater than in the EIC03 devices. However, these are very similarly performing devices compared to the HT devices.

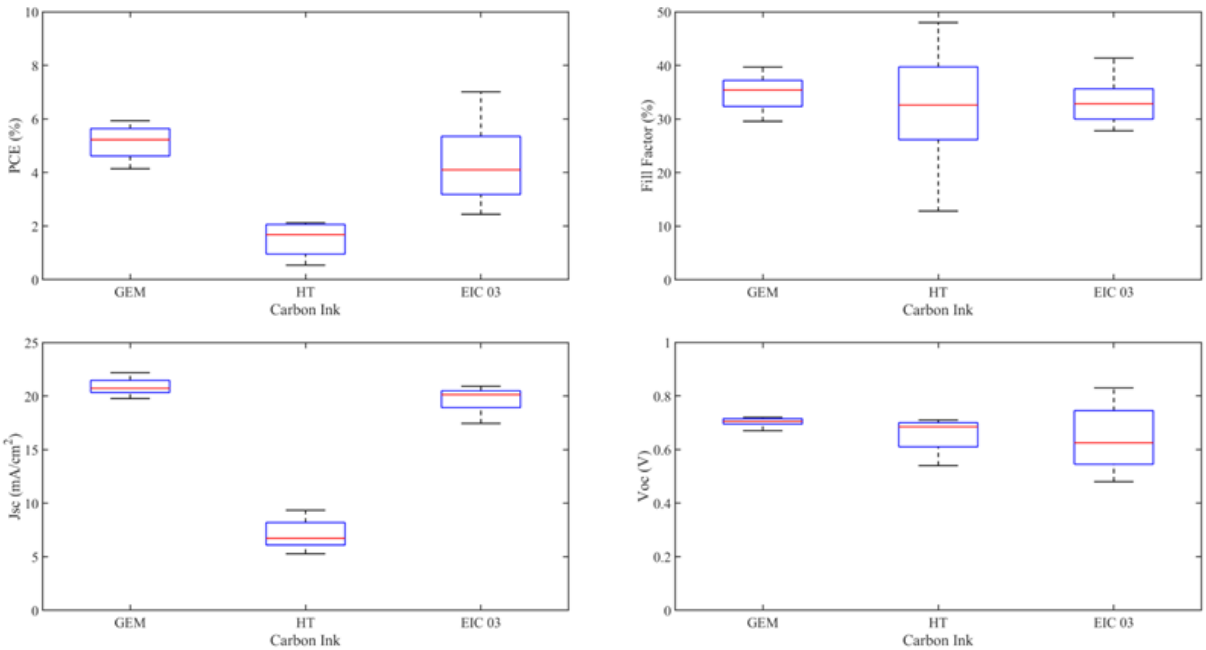

Figure 34a (top left) PCE, b (top right) Fill Factor, c (bottom left) Jsc, d (bottom right) V_{OC} data for devices with GEM, HH and EIC03 carbon layers, from sets of four cells.

JV curves for the champion cell of each set of devices, GEM, HT and EIC03 is shown in figure 35 and the data in table 2 When comparing these cells, the low J_{SC} of the HT cell can be seen

very clearly compared to the others which is what results in the low PCE and FF for this cell. The EIC03 cell had the highest PCE, 7.0 % with the best GEM cell having a PCE of 5.9 %. Comparing the other characteristics of these two cells it can be seen that the J_{SC} values are similar and the FF of the EIC03 cell is a little greater than the GEM. The biggest difference is in the V_{OC} with the GEM being 0.70 V and the EIC03 0.83 V. This suggests that the carbon layer in the EIC03 device had a more optimum energy level compared to the GEM carbon layer resulting in a greater band gap for the cell. Considering the results for these champion cells alongside the results for all of the devices, the GEM and EIC03 carbon layers have similar behaviour, outperforming the HT ink as a carbon layer in the mCPSC.

Table 2 Cell data for GEM, HT and EIC03 champions.

	PCE (%)	FF (%)	Voc (V)	Jsc (mA/cm^2)
GEM	5.9	38.0	0.70	22.18
HT	2.1	35.2	0.69	8.72
EIC03	7.0	41.4	0.83	20.39

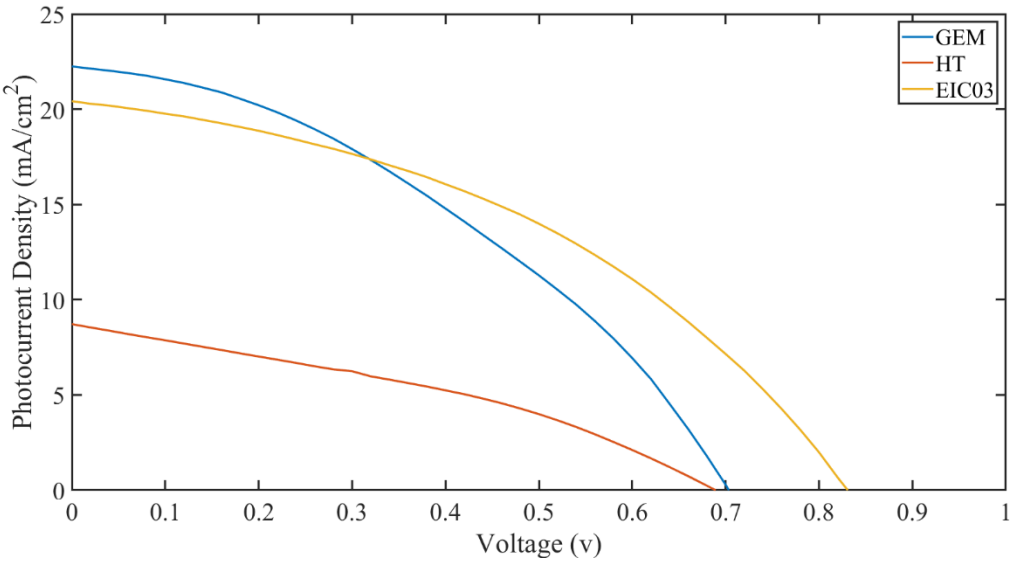

Figure 35 JV curve for GEM, HT and EIC03 champion cells.

The device data shows that the EIC03 carbon ink is a suitable alternative to GEM ink but not an improvement. This is reflected in the similar sheet resistance and resistivity data for these inks but does not reflect the higher contact resistance of the EIC03 ink. The contact resistance of the EIC03 could therefore be an issue in modules. The HT ink that was formulated in lab was found to unsuitable in device when compare with the GEM and EIC03 inks. The low PCE of the HT devices caused by poor J_{SC} was likely an issue caused during printing as it has been seen that the HT layers are affected by mesh marking.

4.3 Benchmarking Of Existing Carbon Layer Technology

4.3.1 Carbon conductivity.

As the counter electrode of the mCPSC, once electron holes are collected, the electrical current flows laterally through the carbon layer to the carbon FTO interface. As such carbon conductivity is important, especially sheet resistance as this is a measure of the thin carbon film's lateral resistance. In this section the conductivity of the carbon layer is evaluated in terms of sheet resistance and resistivity and the conditions within the mCPSC are replicated to evaluate the effect on carbon layer conductivity. These conditions include the heat treatment and perovskite infiltration of the carbon layer, and the influence of the ZrO_2 surface that the carbon is printed on top of in the mCPSC.

The sheet resistance of carbon layers dried at 100°C, fully annealed and infiltrated with perovskite were compared both printed on glass and ZrO_2. Figure 36 shows the dried samples had the lowest sheet resistance, ranging from 10-25Ω/□. Of the dried samples those on ZrO_2 were found to have greater sheet resistance, around 23-25Ω/□, whereas the samples printed on glass were measured at 10-20Ω/□. All of the annealed samples had sheet resistance between 30-35Ω/□, with similar ranges for both glass and ZrO_2 samples. It was found that the sheet

resistance was greatest for the infiltrated samples as well as the greatest range of measurements 15-50Ω/□. There was a comparable range of sheet resistances for the infiltrated samples on glass as on ZrO_2. These results show a clear trend of increasing sheet resistance from annealed samples compared to dried, as well as some further increase for the samples that have been infiltrated. However, the effect of the underlying substrate on carbon layer conductivity is not clear from the sheet resistance measurements. Figure 37 compares the resistivity of each set of samples. This graph gives a clear understanding of the effect of the underlying ZrO_2 on carbon layer conductivity. For dried, annealed and infiltrated samples those that were printed on a ZrO_2 layer had greater resistivity than those printed straight onto glass. Also, there is a much larger variation in measurements for the infiltrated samples indicating that the addition of perovskite and crystallization process can have varying outcomes within the structure of the carbon layer, or the perovskite is forming a capping layer above the carbons surface which would influence sheet resistance. The diagram, figure 38, shows how a perovskite capping layer sitting above the carbon layer would interfere with four-point probe resistance measurements. Due to perovskite being less conductive than carbon this interference would result in increased sheet resistance and resistivity measurements. The resistivities of the annealed samples on glass were ~350Ωμm compared to the dried samples which were ~230Ωμm. The greater conductivity of the dried samples is likely due to the presence of the binding materials of the carbon ink that are still present after the solvents are removed when samples are heated at 100°C. These binders are removed during the annealing process and so the lower conductivity of the annealed samples suggests that without the binding agents the contact between carbon materials in the layer is diminished [31]. As previously mentioned, the infiltrated samples have a much greater range of resistivity from 350-600Ωμm. The lower end of these results is similar to the resistivity of the annealed samples and so it seems that the addition of perovskite does not help to make up for the lack of binding agent when filling in

the pores left by the annealing process. Instead, it appears that the best case for infiltration is that the carbon layer remains as conductive as when the annealed layer is infiltrated but in worse cases the addition of perovskite decreases the conductivity of the carbon layer significantly.

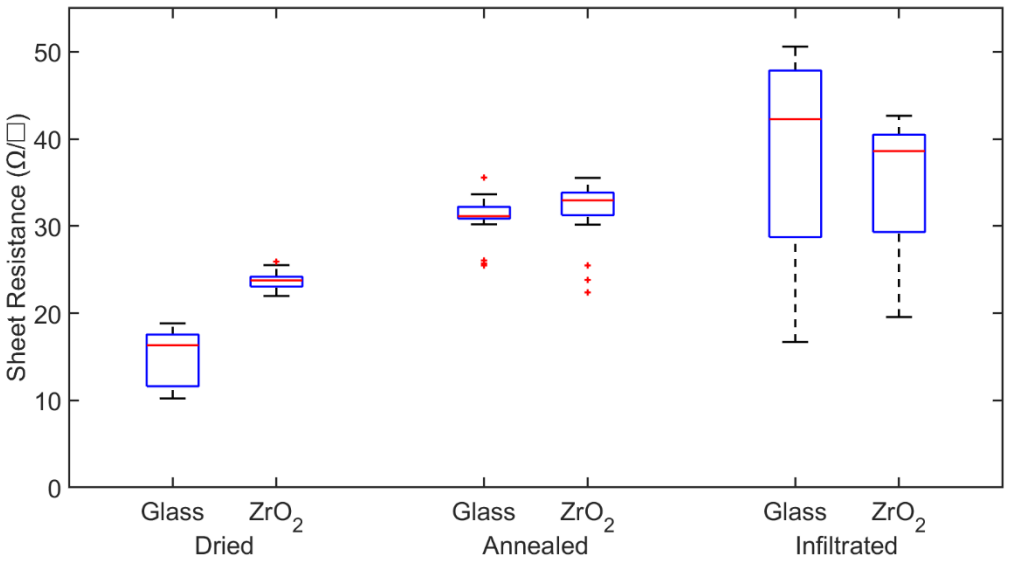

Figure 36 Sheet Resistance for carbon layer (GEM) printed on glass and ZrO2. Compared for dried, annealed and

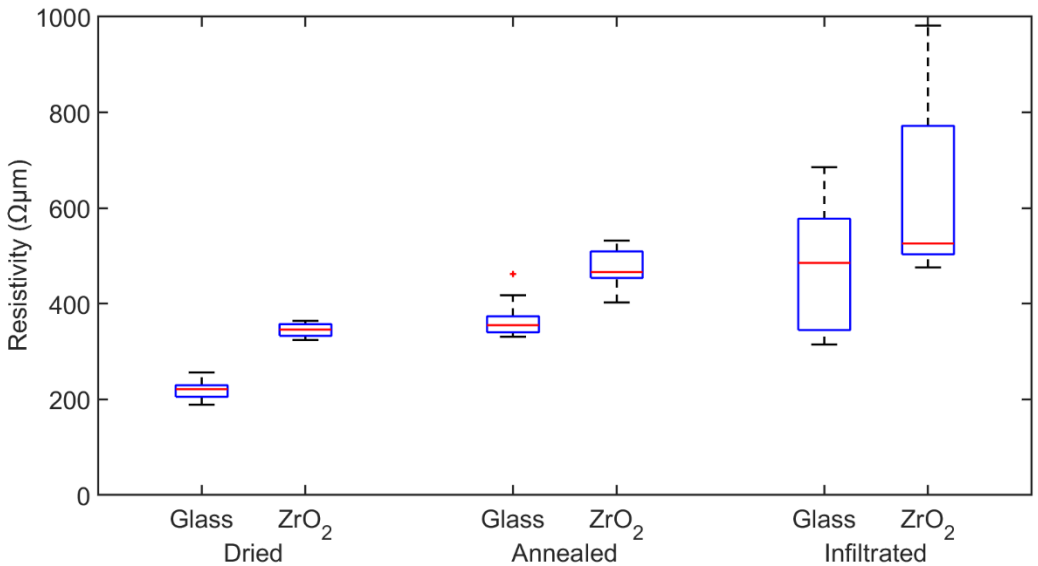

Figure 37 Resistivity for carbon layer (GEM) printed on glass and ZrO2. Compared for dried, annealed and infiltrated

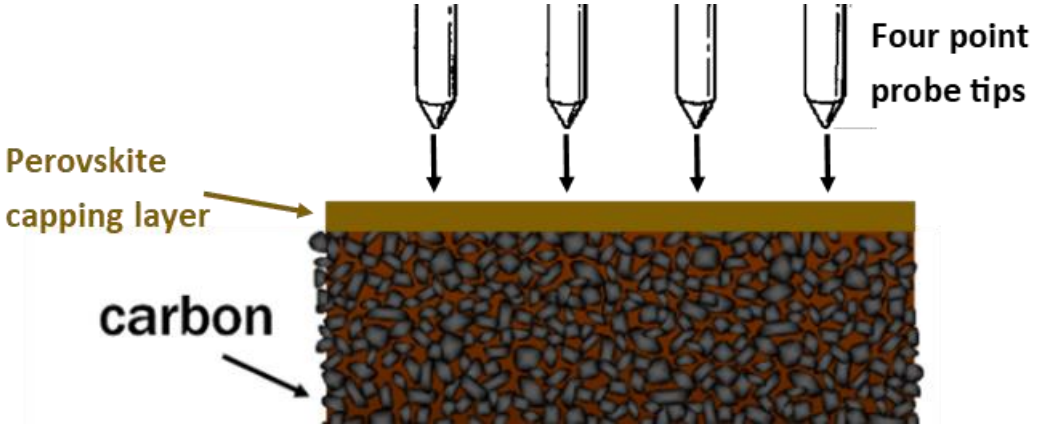

Figure 38 Diagram showing perovskite capping layer between probe tips and carbon layer.

These results show that printing the carbon layer onto ZrO_2 has a negative impact on the conductivity of the carbon layer compared to a glass substrate. Also, both the annealing and perovskite infiltration of the carbon layer have a negative effect on conductivity. These conditions are important steps in the creation of mCPSC devices and so by understanding how they inhibit conductivity efforts can be made to minimize their impact on the carbon layer. In this section it was proposed that perovskite infiltration was causing increases in conductivity due to the formation of a capping layer and diminishing the interparticle contact within the carbon layer. In the following sections the effects of the ZrO_2 layer, annealing and perovskite infiltration on the carbon layer will be explored further.

4.3.1.1 Impact of ZrO_2 and Surface Roughness analysis

In the previous section it was found that carbon layers printed onto ZrO_2 had decreased conductivity compared to those printed straight onto glass. In this section the reasons for this effect are explored through the analysis of surface roughness. This analysis was done using profilometry to assess the average surface roughness (Ra) and skew of printed layers. Ra is the deviation of a surface from its mean height and skew shows whether these deviations are mostly

positive or negative. A positive skew means roughness is caused mostly by raised bumps in the layer and a negative skew means that it is mostly troughs.

The surface roughness of carbon layers printed on ZrO_2 was much greater for all cases than those printed on glass, as shown in figure 39. This increased surface roughness could be a key factor in the increased resistivity seen in carbon layers printed on ZrO_2, shown in figure 34. This link between increased surface roughness and increased resistivity has been found in thin ITO films by Tang et al. where it was proposed that the increased surface roughness would cause electron scattering reducing the mean free path length of the electrons and therefore increasing resistivity [50]. The relationship between carbon layers surface roughness and resistivity in the data presented in this study suggest a similar relationship to that found in the ITO thin films.

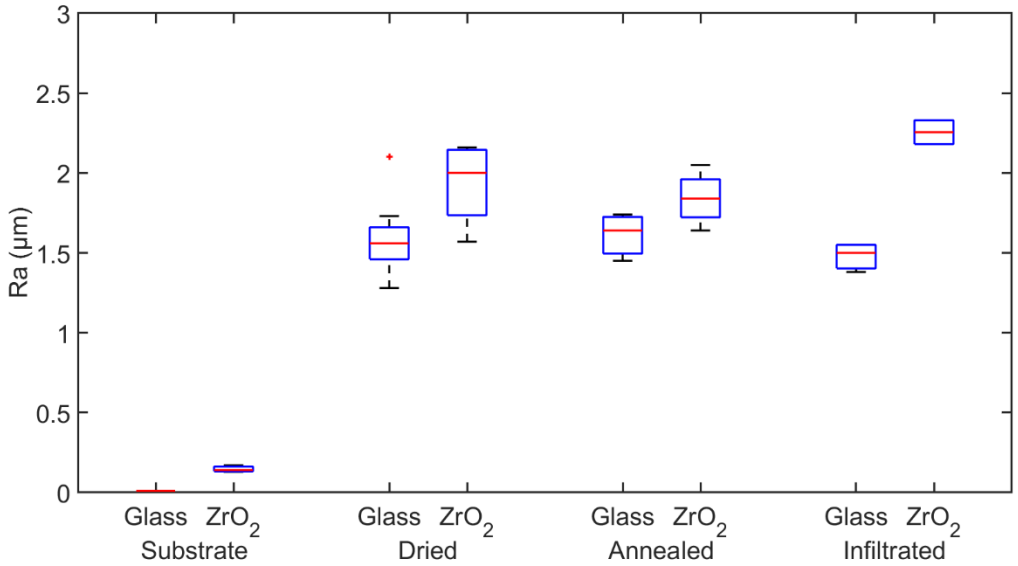

Figure 39 Surface Roughness, Ra (um) of ZrO_2 and glass substrates and carbon layers printed on substrates dried, annealed, and infiltrated, from sets of five samples.

The relationship between surface roughness and resistivity for these carbon layers is shown in figure 40. Here it can be seen that for each group of samples, dried, annealed and infiltrated, there is generally increased resistivity in samples with greater surface roughness. There is however some variation from the trend and so it is clear that surface roughness is far from the only factor affecting the resistivity, but it does have some influence.

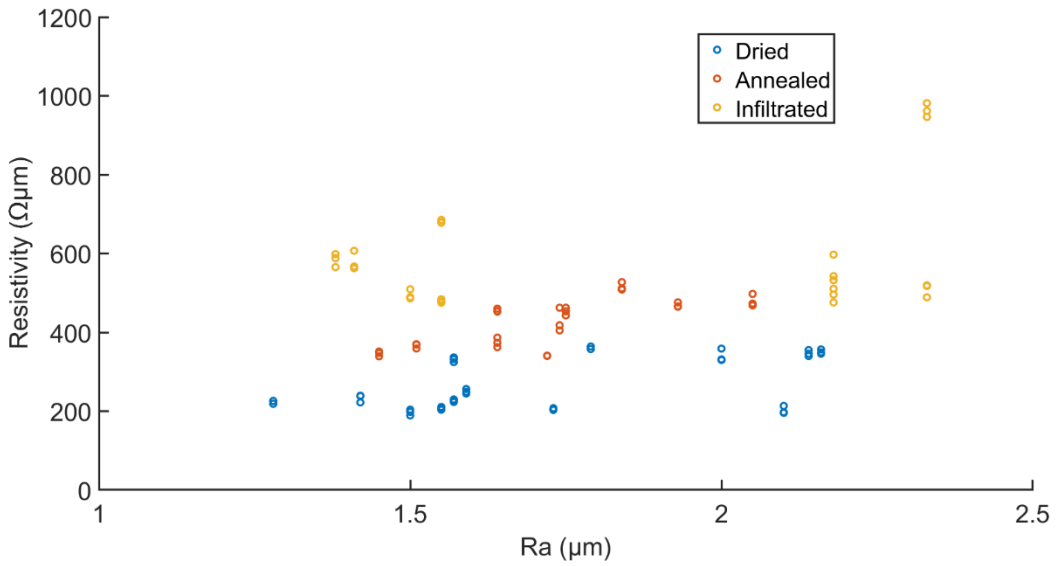

Figure 40 Relationship between surface roughness and resistivity for dried, annealed and screen-printed carbon layers on glass and ZrO_2

The Skew of the profilometry data for the dried annealed and infiltrated carbon layers printed on ZrO_2 and glass shown in figure 41 reveals a trend of lower skew for carbon layers on ZrO_2. This skew for all samples is positive showing that there are more peaks than troughs in the surface contributing to the roughness. The lower skew seen in the ZrO_2 samples shows that there are more troughs in the surfaces of these carbon layers than those printed on glass, this indicates that the increased roughness of carbon layers on ZrO_2 is a result of material from the carbon layer sinking into the dips of the ZrO_2 substrate leaving dips on the surface of the carbon. This wouldn't occur with a glass substrate due to the smoothness of glass. The skew is lower for the annealed and infiltrated samples on ZrO_2 than the dried samples. This is

unlike the samples on glass which are consistently skewed around 0.5 for all cases. The lower skew could be the result of troughs in the surface of annealed carbon sinking further after the further removal of binding agents, however there is little change between the overall roughness of dried and annealed layers so it could be the entire layer sinks slightly lower into the ZrO_2 below when annealed.

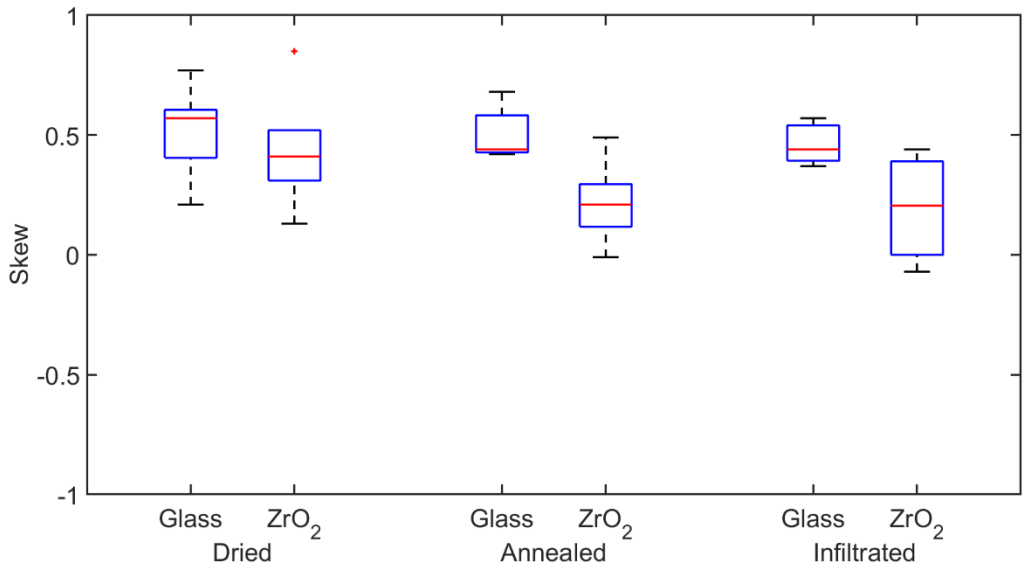

Figure 41 Skew of profilometry data for dried, annealed and infiltrated carbon layers on ZrO2 and glass substrates, from sets of five samples.

The profile of a carbon layer printed on ZrO_2 is compared with the profile of a carbon layer on glass in figure 42. This plot gives a visual representation of the surface roughness of the carbon layers on each substrate as well as the height of the ZrO_2 substrate layer which can be seen in the first 2000 µm. This visualization shows the increased roughness of the carbon layer on ZrO_2 supporting the Ra data given previously. This is most notable when looking at the troughs of the carbon layer on ZrO_2 which go down to a similar level as the lowest troughs of the carbon layer on glass, below 10 µm away from the glass surface (0 µm). This is significant as the carbon layer on ZrO_2 is around 3µm higher than the layer on glass due to the thickness of the underlying substrate.

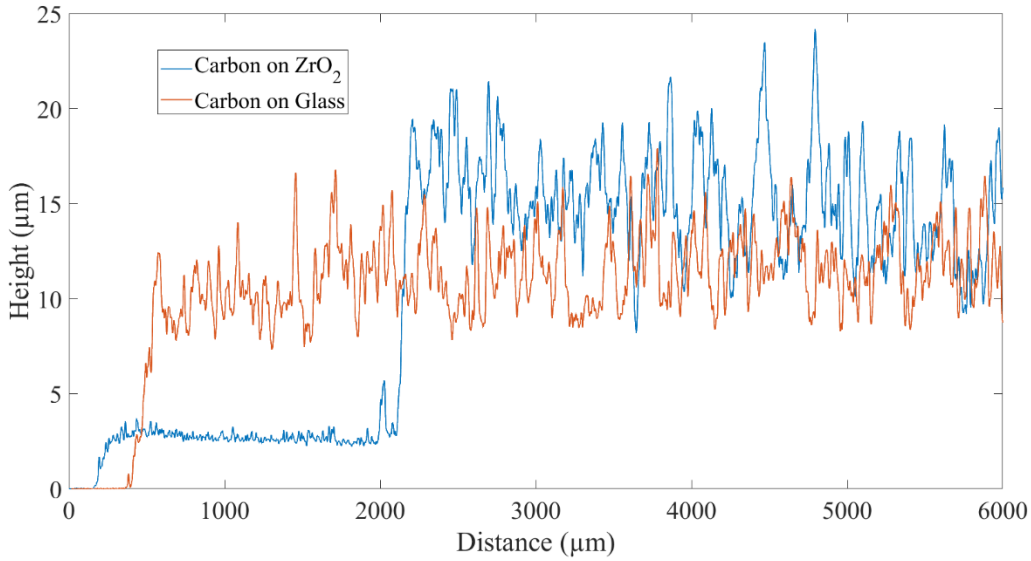

Figure 42 Profilometry of a GEM carbon layer screen printed on ZrO2 compared to a layer on glass.

These findings show that the lower resistivity of carbon layers printed on ZrO_2 compared to glass, seen in figure 36, are closely linked to increased surface roughness in the carbon. Furthermore, the increased surface roughness of carbon layer on ZrO_2 are the result of the ZrO_2 layer being considerably rougher than glass. The conductivity of the carbon layer is heavily dependent on the contact between the carbon materials within the layer, consequently the surface roughness may reflect disorder throughout the entire layer reducing contact between carbon material. It is reasonable to propose that decreasing the surface roughness of the underlying ZrO_2 and therefore the carbon layer, would improve conductivity. As such there is an opportunity for an investigation into how reducing the surface roughness of these layers would affect overall performance in an mCPSC device.

4.3.2 Influence of perovskite volume on carbon conductivity

The conductivity of perovskite infiltrated carbon layers was found to be reduced compared to annealed and dried layers. As the charge generator and hole transport material present throughout mCPSC devices the carbon layers conductivity is highly important. In this section the influence of varying volumes of perovskite within the carbon layer is investigated to better understand the effect of infiltration on the carbon layer and so that an optimum amount of perovskite solution for the carbon layer in the mCPSC may be found.

The sheet resistance of samples, seen in figure 43, with 0 µl perovskite have the smallest range compared to those that were infiltrated. This was seen in the previous study and is likely due to the varying success of the infiltration and crystallization process, the infiltration step has the greatest room for error and so this is reflected in the wider range of results. The increasing volume of perovskite seems to decrease the sheet resistance of samples in volumes up to 12 µl, however the samples with 15 µl and 20 µl have increased sheet resistance, these being the only samples with sheet resistance over 40 Ω/□. These results are consistent for sheet resistance of carbon on glass and on a ZrO_2 layer. As previously mentioned, this could be a result of larger volumes of perovskite inhibiting the contact between graphite and carbon black particles within the carbon layer therefore reducing conductivity. However, it is also possible that the 15 µl and 20 µl samples had a capping layer of perovskite form above the surface of the carbon. This capping layer would give increased resistance measurements with the four-point probe as the probes would not be in contact with the carbon itself but the perovskite that had risen above the carbon layer as described previously in figure 38. The sheet resistivity of the samples, shown in figure 44 reveals that the range of results were much greater in samples with an underlying ZrO_2 layer, and the resistivity of these samples is greater than the carbon layers printed onto glass. As the perovskite infiltrates both the carbon and ZrO_2 layers it is possible that where the perovskite crosses the boundary between these layers charge is being led away

from the carbon layer decreasing overall conductivity. A key difference shown in the resistivity measurements that is not seen in the sheet resistance is that the resistivity of the 15 µl and 20 µl samples on ZrO_2 are less than those with lower perovskite volumes. It could be that the 3µm ZrO_2 layer below the carbon results in less perovskite being present in the carbon layer for these samples, than those on glass, and as such the negative effects of high volumes of perovskite are avoided here.

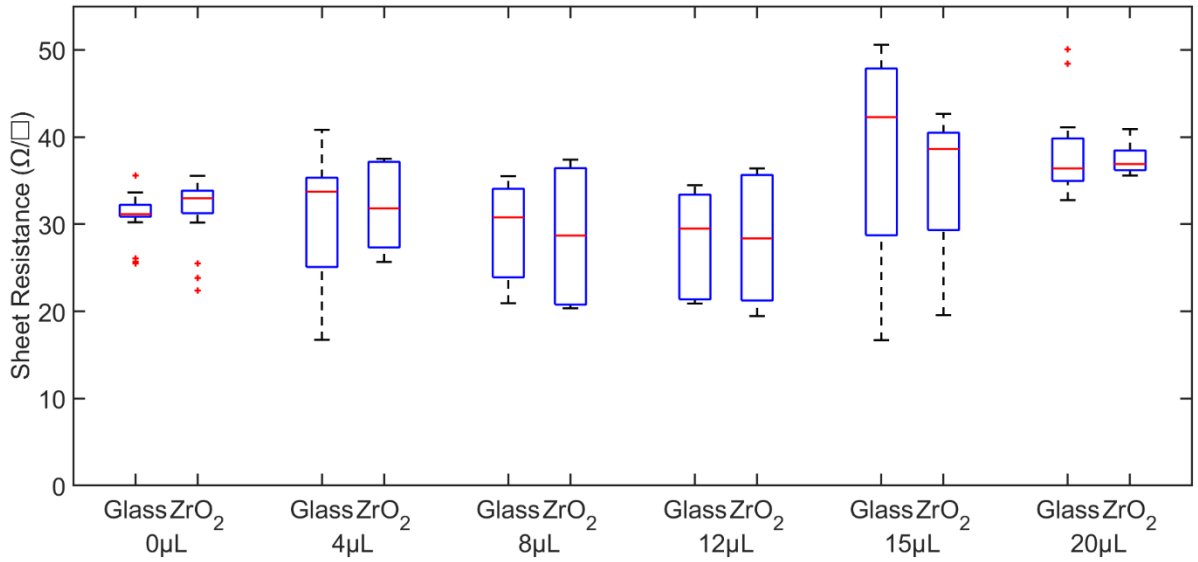

Figure 44 Graph of Sheet Resistance for Gem Carbon with different amounts of perovskite added, from batches of five samples.

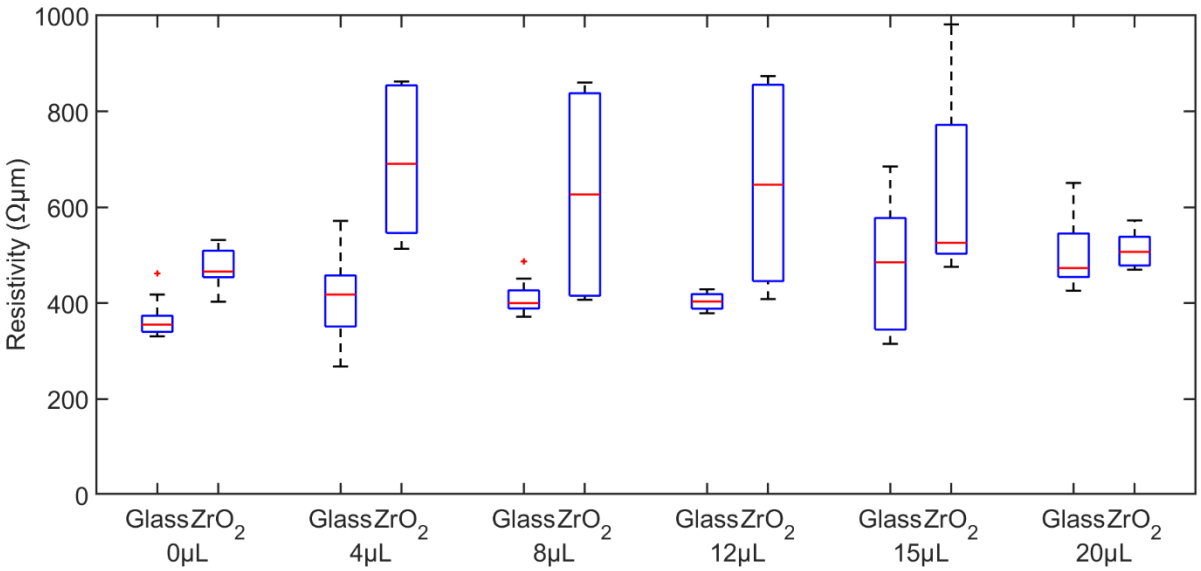

Figure 43 Graph of Resistivity for GEM carbon with different amounts of perovskite added, from batches of five samples

Whilst the crystallization of perovskite can be identified visually by a darkening of colour in the layers and lack of patches on the undersurface these results show the resulting conductivity of these layers can vary for a given volume of perovskite solution. However, for conductivity of the carbon layer, these results suggest that a volume of perovskite between 12-15µl is most suitable. As the carbon layer is roughly 75 % of the overall mCPSC thickness this correlates to between 15-20 µl of perovskite solution for an entire device. With regards to the carbon layer the risk of using a greater amount of perovskite solution is the reduction in conductivity through the inhibition of interparticle contact or the formation of a capping layer. These carbon conductivity drawbacks must be weighed against the effects of lowering perovskite volume in a device as the role of perovskite is crucial to performance.

4.3.3 Influence of Annealing and Perovskite Infiltration on Mechanical Robustness of Carbon

In previous sections, carbon layers that were annealed up to 400°C have been found to have greater sheet resistance than those dried at 100°C. It was observed in the measurement of these samples with the four-point probe that annealed carbon layers were more easily damaged by contact with the probe tips with material being visibly removed where the probe tips made contact. This indicates that the mechanical robustness of the carbon changes during the annealing process and could be linked to the conductivity of the carbon layer. To measure and classify the extent of these changes the ASTM adhesion by tape test was used. This is a standard test usually applied to thin film coatings. Dried, annealed and infiltrated carbon layers were compared, both on glass and ZrO_2. The ASTM adhesion by tape test (Method B) classifies results by assessing the percentage of the material removed from the surface of the substrate as can be seen in the right-hand side for each of the images in figure 45. For further clarity the left-hand side of each image includes the tape to show material that was removed. The figures

are as follows; 45a carbon layer dried on glass, 45b carbon annealed on glass, 45c carbon infiltrated on glass, 45d carbon dried on ZrO2, 45e carbon annealed on ZrO_2 and 45f carbon infiltrated on ZrO_2. The images 45a and 45d show that <5% of material was removed from the carbon dried on glass and carbon dried on Z_rO_2. 45b, 45c, 45e, and 45f show >80% of material was removed from the surface of the annealed and infiltrated carbons on both glass and Z_rO_2. These results indicate that the dried carbon is most robust most likely due to the presence of binding agents within the carbon ink. After the annealing process has removed the binding agents the carbons are left much less robust and so much more material is removed by the tape test. The addition of perovskite solution to the carbon does little to improve the robustness of the carbon layer as there is a comparable amount of material removed for the annealed and

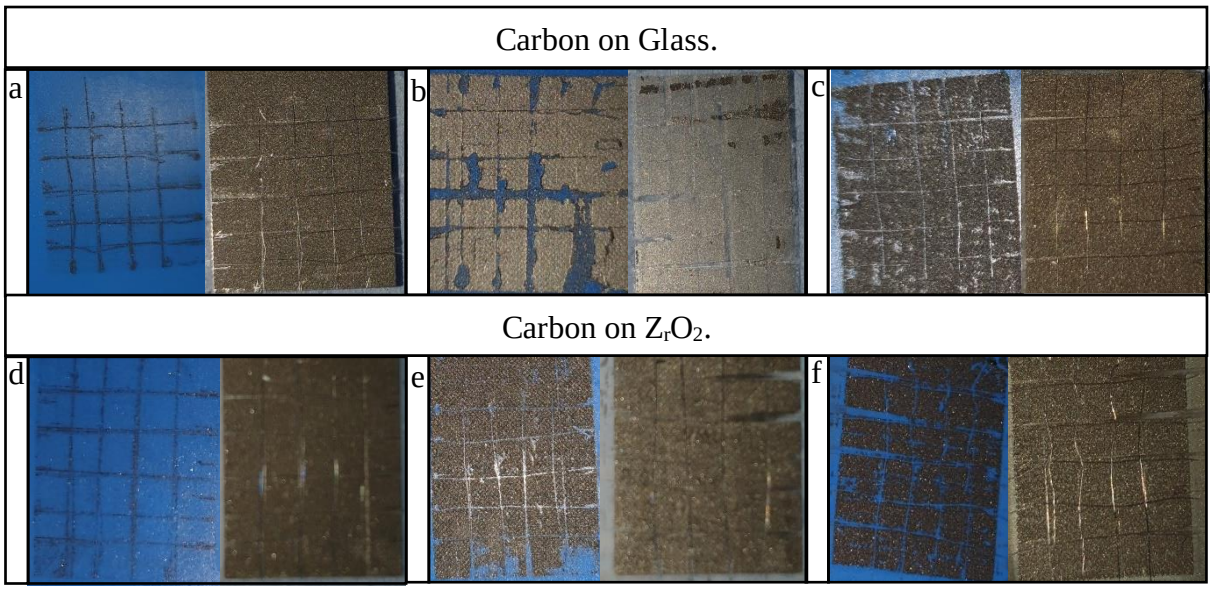

infiltrated samples. The samples on Z_rO_2 appear to have less volume of material removed with tape in each case despite the percentage of the surface removed being very similar. This indicates that the carbon at the bottom of the layer in contact with the substrate has a stronger bond to the Z_rO_2 substrate than with the glass substrate.

Figure 45 Adhesion by Tape Test results, tape left and substrate right for a) Carbon Dried on Glass b) Carbon Annealed on Glass c) Carbon Infiltrated on Glass d) Carbon Dried on ZrO_2 e) Carbon Annealed on ZrO2 f) Carbon Infiltrated on ZrO_2

Before considering conductivity, these results show that proper care and storage of mCPSC device is important as the carbon layer becomes fragile during fabrication and is most susceptible to damage sitting exposed on the top of the stack. Considering how these results relate to the performance of the carbon layer it follows expectation that when the layer is physically held together with the most strength there would be more contact between the carbon particles within the layer. This reflects what has been seen in conductivity measurements that show the dried layers, which are the most robust and have the lowest resistance. Alternatively, when the layer is less robust after the annealing process has removed the binding agents, there is less interparticle contact and this causes the higher resistance for these layers. This process is a key part of the mCPSC fabrication as the removal of solvents and binders from the carbon layer make it suitably porous for perovskite infiltration. The similarity between the robustness of the infiltrated and annealed layers suggests that whilst the perovskite fills the space in the annealed carbon layer it does little to strengthen it. As such there is no increase in contact between carbon materials in the layer and the conductivity is not improved. The effect of annealing and perovskite infiltration on the mechanical robustness of the carbon layer help demonstrate why these processes decrease the layer's conductivity. A dense carbon electrode will be more conductive than a porous carbon electrode containing similar materials, but it is necessary for the carbon layer to be porous in order to host perovskite. The use of carbon capping layers has targeted this issue by using a separate carbon layer, on top of the original device, that does not need to host perovskite.

4.3.4 Contact Resistance of Carbon compared to Au

The contact resistance and transfer length of GEM and Au were found using the TLM method. The contact resistance is the resistance at the interface between the electrode and FTO substrate which in devices is a very small area. As such the contact resistance has a negligible role in single devices but in modules there are many of these interfaces in series and so the contact resistance can contribute to the overall series resistance of modules. This makes contact resistance an important factor in the scalability of devices. The transfer length is the average distance the charge travels laterally before crossing the interface and is directly proportional to the contact resistance. A decreased transfer length allows the area of contact between carbon and FTO to be reduced without increasing contact resistance, the carbon/FTO interface is not an active part of the cell meaning that no charge is generated here. Decreasing the area of the carbon/FTO interface allows more space to be dedicated to the active area of cells increasing geometrical fill factor and overall module performance [33].

The contact resistance found from GEM ink contacts on FTO, when dried at 100°C, annealed up to 400°C and with the addition of perovskite are compared to Au (gold) contacts in figure 46a. The Au on FTO had the least contact resistance at 0.05Ω followed by dried GEM at 0.1Ω, annealed GEM at 0.19Ω and the infiltrated GEM at 0.51Ω. These resistances are all low enough to be negligible compared to the sheet resistance of an electrode within a single mCPSC device, but within a module these resistances become significant. A similar pattern is seen here as with the sheet resistance of the GEM ink where the resistance is greatest in infiltrated samples and lowest in dried samples. This shows that when the charge transfer within the GEM ink is decreased the charge transfer between the GEM ink and the underlying substrate is also decreased. The greater presence of binding material in the dried samples compared to the annealed samples may be the reason for the higher rate of charge transfer by providing more

contact between the carbon materials and the FTO substrate below. Figure 46b shows the transfer length for each contact which is proportional to the contact resistance, as explained by equation 3. The transfer length of a given contact can be used to minimize the size of a contact in order to decrease the geometric fill factor of a module [33], however the transfer length is below 1mm for all the GEM samples and Au and so it could become impractical to use such small contacts.

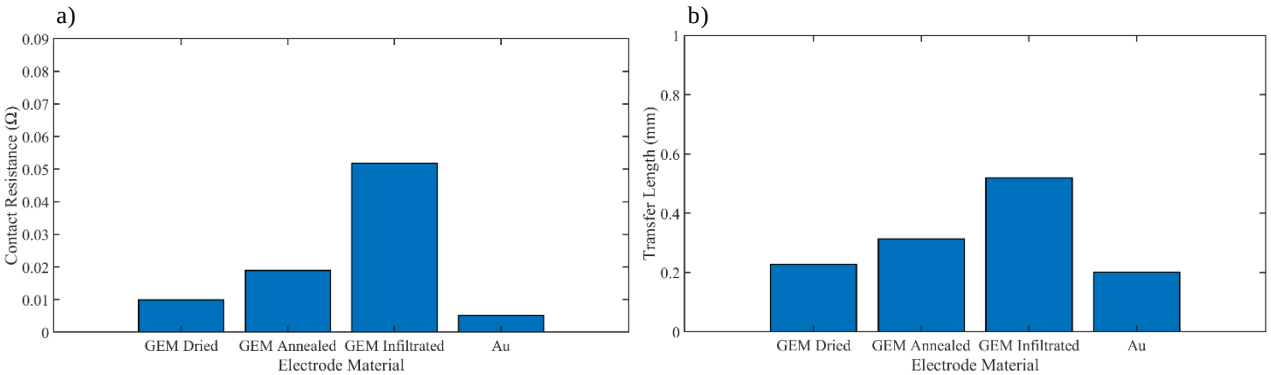

Figure 46 Contact resistance of GEM ink dried, annealed, infiltrated and Au on FTO. b) Transfer Length GEM ink dried, annealed, infiltrated and Au on FTO. From sets of two samples.

As the results show that the contact resistance between infiltrated carbon layers and FTO is significant this is likely to cause current losses due to series resistance in modules. As it is outside the active area of the cell, perovskite is not necessary at the carbon/FTO interface but is a consequence of the fabrication process of the mCPSC. The lower contact resistance between dried carbon and FTO would make this a preferable interface and as perovskite is not necessary at this part of the cell a dried carbon/FTO contact is possible. At the small scale this could be achieved in devices by removing the carbon layer in contact with FTO and replacing it with a printed dried carbon capping layer.

4.3.5 Existing carbon layer technology summary.

In this section the conductivity of the carbon layer has been investigated with conditions present in the mCPSC recreated to evaluate how the carbon layer is affected. It has been found that the removal of binders during annealing and addition of perovskite during infiltration increase sheet resistance, resistivity and contact resistance of the carbon layer on FTO whilst also decreasing the layer's mechanical robustness. This is most likely a result of reduced interparticle contact between carbon materials graphite and carbon black within the carbon layer when compared to the dried carbon. It is proposed that a carbon capping layer would address these issues by taking advantage of the higher conductivity and low contact resistance of the dried carbon layer that is separate from the perovskite infiltrated layer so as not to inhibit infiltration. The application of a capping layer is explored in the next section with the creation of mCPSC devices.

Furthermore, it has been seen that the surface roughness of carbon printed on ZrO_2 is increased compared to carbon layers printed onto glass and that there is an increase in resistivity associated with this increased surface roughness. The surface roughness of these layers is dependent on the morphology of the ink being printed and so targeting this area for improvement would have to be done during formulation of ZrO_2 and carbon inks. This avenue for potential improvement would be more complex than applying a carbon capping layer and would probably involve many iterations of inks before reaching any improvements, as such this was not taken further in this research.

4.4 Capping Layer

Printing an additional carbon layer on top of the mCPSC structure after infiltration has previously been found to improve device performance [31]. The use of a carbon capping layer in this way separates the roles of the carbon between the two layers with the original layer focusing on hole collection and the capping layer being the counter electrode. As a result, the capping layer can be processed in a way that prioritizes conductivity without having to compromise its ability to host perovskite. This has been applied here by using a dried carbon layer as a capping layer as it has been found in previous sections that dried carbon layers have lower sheet resistance and resistivity than infiltrated layers and so this lower resistance counter electrode layer should improve device conductivity. In this study the capping layer is also being used to improve contact resistance at the carbon FTO interface as described in figure 47.

The diagram displayed in figure 47 shows that before printing the capping layer, the section of carbon that overhangs the ZrO_2 layer is removed, this is the section is highlighted in red. The carbon capping layer is then printed onto the stack becoming the new counter electrode layer as well as filling in the space left by the removed section forming a new interface with the FTO. Using this design, the capping layer should not only improve device conductivity through lowered sheet resistance in the counter electrode as has been seen previously but also through a reduction in contact resistance between the carbon electrode and FTO as it was seen in previous sections that contact resistance is lower between dried carbon layers and FTO than infiltrated layers.

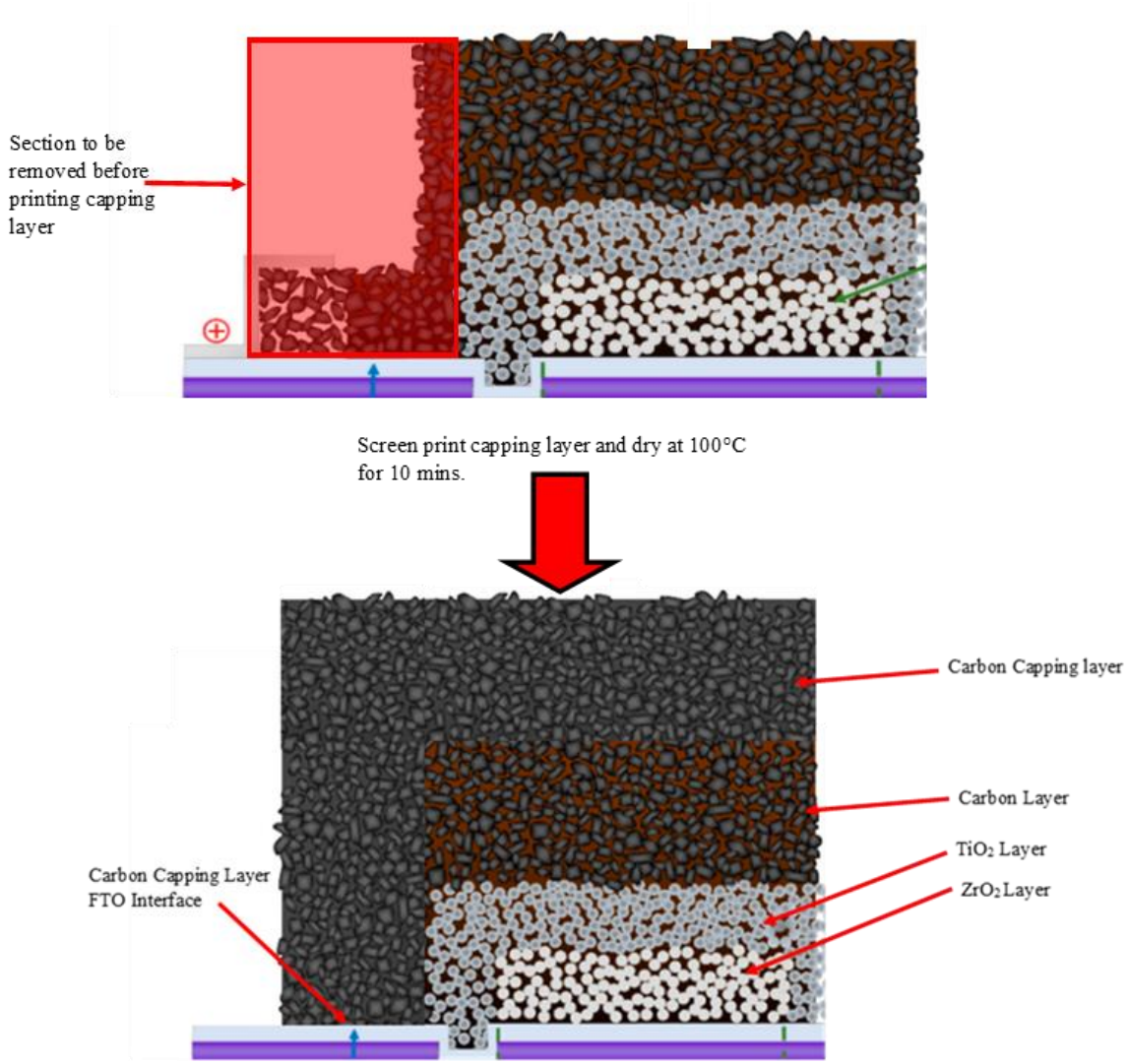

Figure 47 Fabrication process of the carbon capping layer for the mCPSC. Includes the removal of previous carbon/FTO interface before printing of carbon capping layer over the original carbon stack. Diagram of the carbon stack adapted from [17].

The results for devices with a carbon capping layer are compared to standard mCPSC devices in figures 48a, b, c and d. The PCE results show that the devices were largely similar in performance with average PCEs ~5%. Whilst the J_{SC} values of the cells are also similar there is a noticeable difference in both the FF and Voc. The V_{OC} of the capping layer devices are generally lower (with some cells having much lower Voc, that may be considered outliers). Conversely the FF of the capping layer cells are higher than the single layer cells. The low PCE seen in some of the capping layer cells can be attributed to those with exceptionally low V_{OC} and likely a result of a fault. Whilst this fault could be something caused by the additional printing and heating steps required to deposit the capping layer it could have been the standard fabrication process before the capping layer was introduced. However, as there are possibilities for error with every stage of creating devices the additional steps required for the capping layer increase the chances of error and so the more complex fabrication process can be considered a drawback of adding a capping layer.

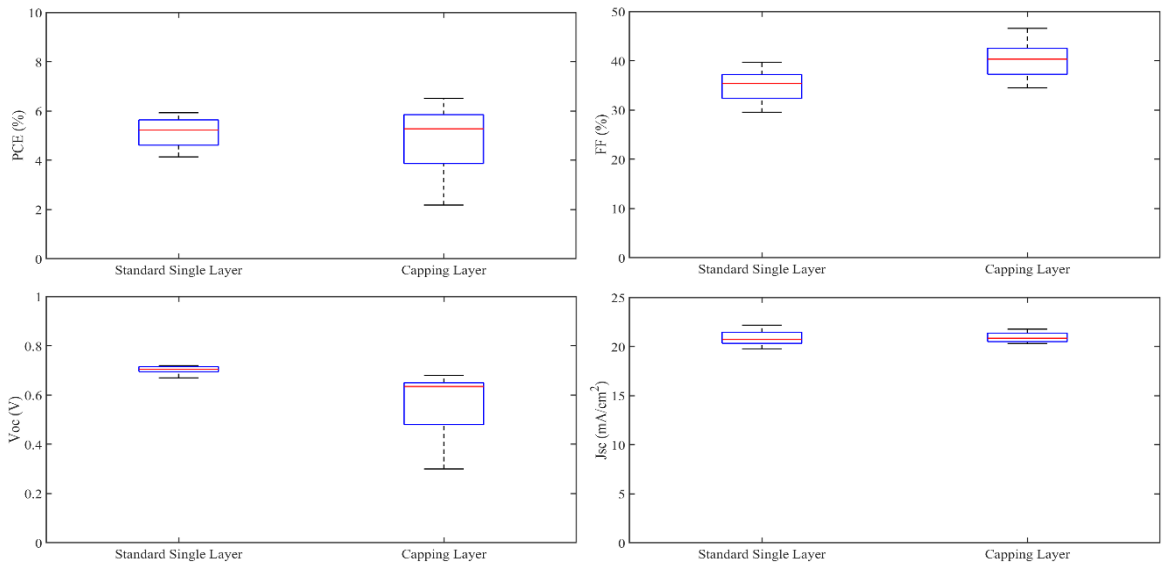

Figure 48 a (top left) PCE, b (top right) Fill Factor, c (bottom left) Voc, d (bottom right) J_{SC} data for devices with Single GEM layer and capping layer, from sets of four cells.

The data and JV curves for the standard and capping layer GEM cells are compared in table 3 and figure 49. This data reflects the overall trends for FF, V_{OC} and J_{SC} seen in the entire set of these cells, with the standard layer cell having a greater V_{OC} and the capping layer cell having a greater FF. The PCE of the capping layer cell is the greater of the two and from the increased FF this can be attributed to a more conductive electrode. This is supported by the sheet resistance being much lower for GEM layers dried at 100°C (as the capping layer is) compared to annealed layers. Increased FF has been attributed to increased conductivity and carbon perovskite interface in mCPSCs but it is unlikely to be a result of the latter in this case as the initial layers containing perovskite in both sets of cells were prepared in the same way and so should be identical [20][31].

Table 3 Cell Data for GEM single layer and capping layer champions

	PCE (%)	FF (%)	Voc (V)	Jsc (mA/cm^2)
Single Layer	5.9	38.0	0.70	22.18
Capping Layer	6.5	46.6	0.64	21.77

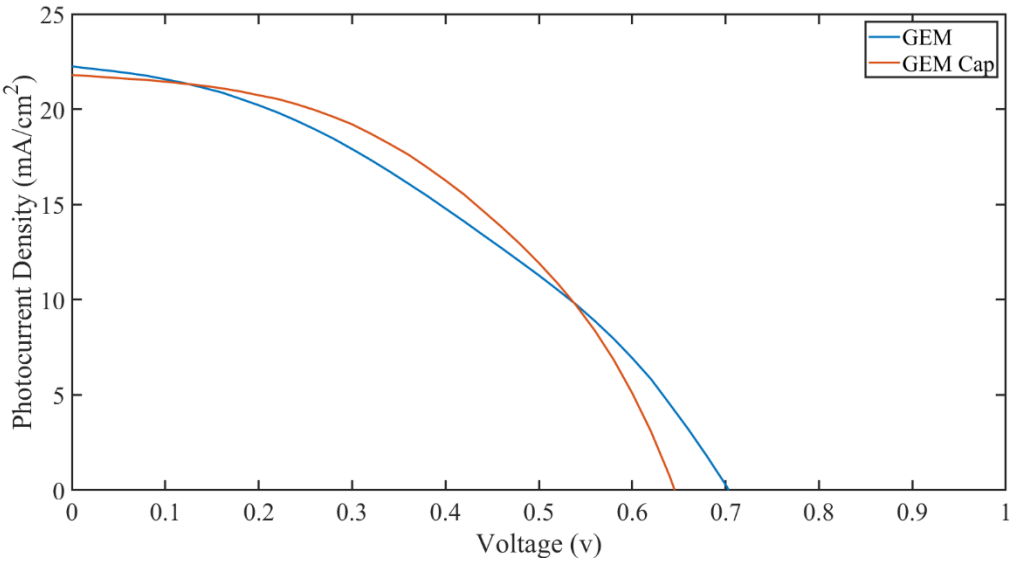

Figure 49 JV curve for GEM standard and capping layer champion cells.

These results show that it is possible to improve device performance with the use of a capping layer by increasing fill factor which is likely a result of the improved conductivity of the carbon counter electrode. However, the improvements in single devices are not significant or consistent enough to warrant the additional processing steps. The device data shows the effects of the capping layer as a counter electrode but does not show any changes brought on by the capping layer/FTO interface. As previously discussed, changes in contact resistance are negligible within single devices as contact resistances between carbon layers and FTO have been measured to be orders of magnitude lower than the sheet resistance of the carbon layer. As such, any changes in performance as a result of the carbon capping layer being used at the FTO interface would only be seen in large scale modules, where there are many of these connections in contributing to overall series resistance. The production of modules was outside the scope of this work, but it would be possible to utilize a capping layer in the same way as has been presented here with the use of mechanical scribing to remove the infiltrated carbon layer at the FTO interface before printing the second carbon layer. Scribing has been used to enhance the interconnection between cells in modules in previous work and so this could be adapted to support the use of a carbon capping layer.

4.5 Enhancing Carbon Ink with WO_3 Additive.

The previous section investigated the effect of a carbon capping layer on device performance. The capping layer acts as an improved counter electrode leaving the original carbon layer unchanged as a hole collection layer. So, whilst the carbon capping layer addresses the conductivity aspect of the carbons role it neglects hole collection. Hole collection is an

important factor in mCPSC device performance and is influenced by the work function of the carbon layer [28]. The difference between the energy levels of the carbon layer and the valence band of the perovskite is equivalent to the additional energy required for electron holes to be transferred to the carbon layer. Therefore, by tuning the work function of the carbon to be closer to the energy level of the perovskite valence band electron holes should be extracted more easily by the carbon layer, improving device performance. It has been found that the work function of carbon electrodes can be increased with the inclusion of additive materials with higher work functions acting as a "stepping stone", displayed in figure 50. These materials such as NiO, CuS, WO_3, vanadium and boron act as stepping stones due to energy levels between those of the carbon layer and perovskite valence band [28][29][51][52][53].

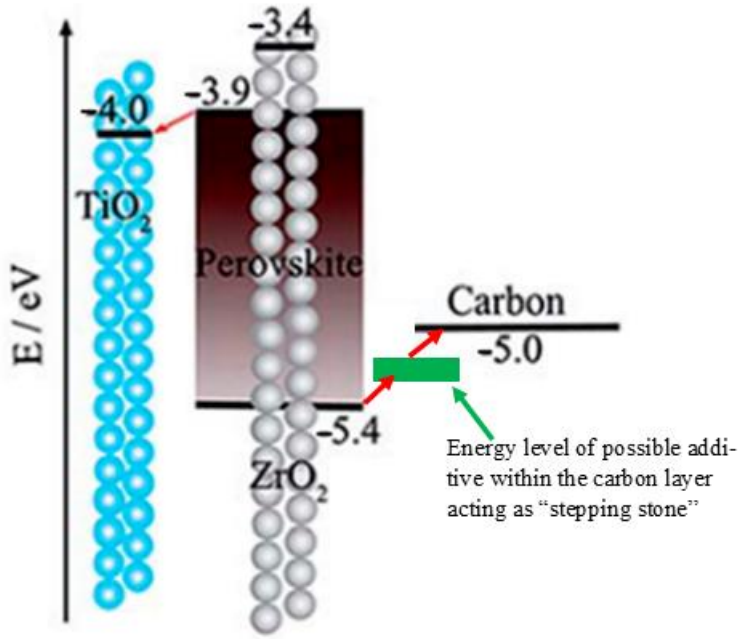

Figure 50 Energy level diagram for the mCPSC adapted from [22] to show how additives would decrease the gap in energy level between perovskite layer and carbon layer.

The effects of using a WO_3 additive in the carbon layer of the mCPSC were investigated in this study with a focus on changes in conductivity, work function and resultant device performance. Four 10g samples of GEM carbon ink were used with 0g, 0.3 g, 0.6 g and 0.9 g of WO_3 particles to evaluate how different material weights of WO_3 additives influence carbon layers. The sheet resistance of GEM/WO_3 carbon layers are presented in figure 51 and show a clear increase in sheet resistance for layers including WO_3. The sheet resistance increases with the addition of WO_3 with the 0.3 g, 0.6 g and 0.9 g samples having sheet resistances averaging around ~16 Ω/□, 18 Ω/□ and 19 Ω/□ respectively compared to the standard GEM with 0 g WO_3 sheet resistance between 11-13 Ω/□. The resistivity of these samples shown in figure 52 also shows that conductivity is impeded with the inclusion of WO_3 particles. This is likely a result of disorder within the layer caused by the inclusion of these particles which are less conductive than the carbon material within the layer [30][50].

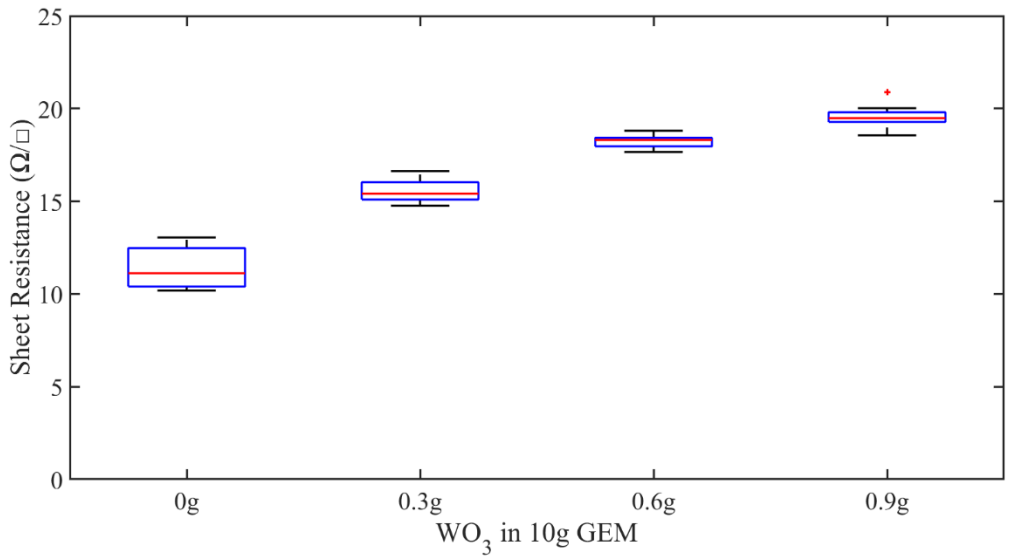

Figure 51 Sheet resistance of GEM carbon layers with varying amounts of WO_3, from sets of four cells.

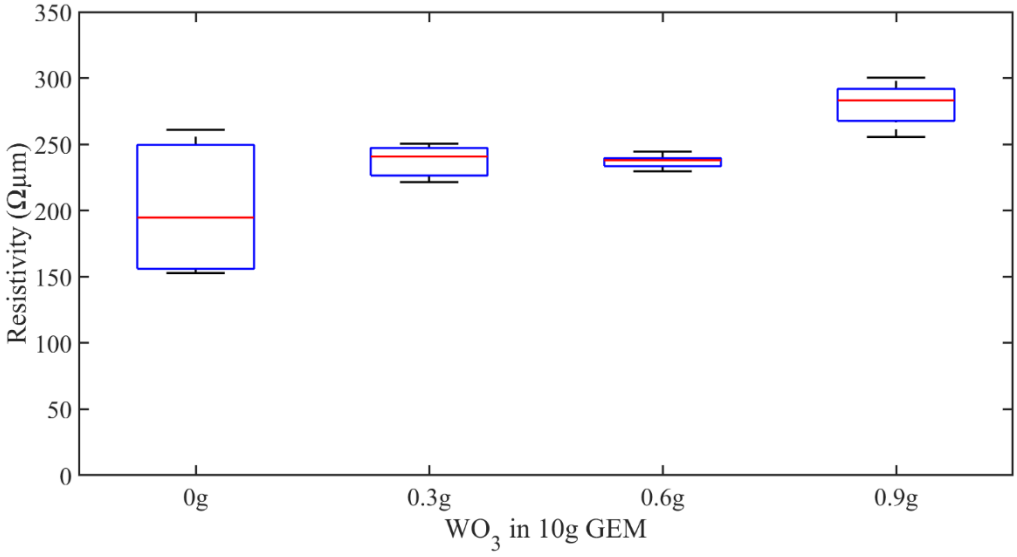

Figure 52 Resistivity of GEM carbon layers with varying amounts of WO_3, from sets of four cells.

Figure 53 shows the work function of GEM increases with the addition of WO_3 particles. There was an increase of 0.1 eV in the GEM ink with 0.3 g and 0.9 g WO_3 but the 0.6 g WO_3 appears to be the more optimum amount with a work function increase of 0.15 eV. The increase in work function indicates that these carbon layers will have energy levels closer to the valence and of the perovskite, improving hole extraction. The influence of the additives on work function is therefore clearly positive based on this data. The lower work function of the 0.9 g layers compared to the 0.6 g layers suggest that too many additive particles in the layer can hinder work function perhaps as a result of a disrupted structure within the layer. It is also possible that this is the result of unsuccessful mixing of the additive which could mean that the additive present in each layer is not proportional to the total additive in the 10 g of carbon ink, especially as the increase in work function is similar for all layers including WO_3. If this was the case, it is still clear that inclusion of these additives improves work function.

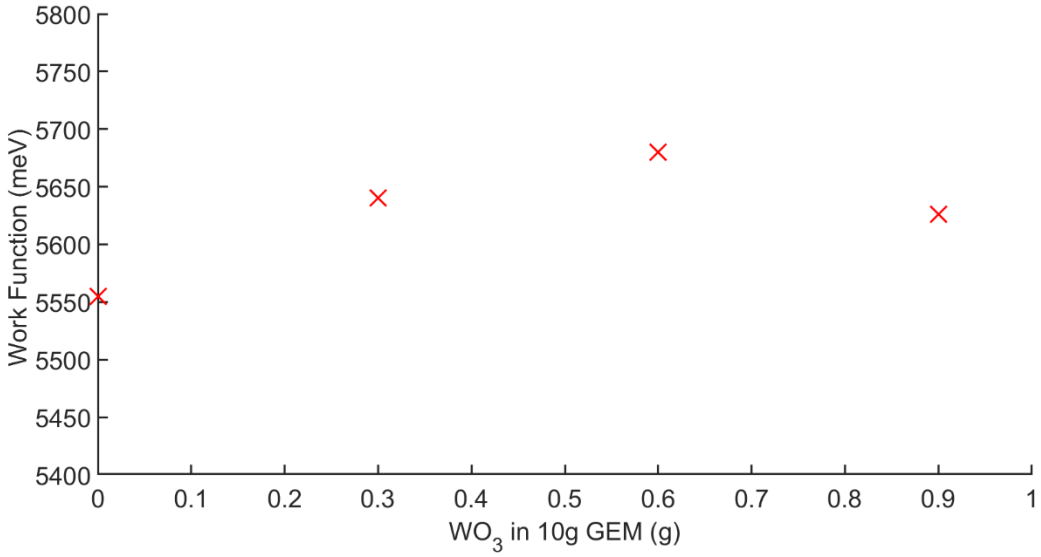

Figure 53 Work function of GEM ink samples containing WO_3, from four samples.

The sheet resistance, resistivity, and work function data show that the WO_3 reduces conductivity whilst improving work function of the carbon layer. To evaluate how these changes affect the carbon layer's role within the mCPSC, devices were fabricated with carbon layers using 0.3 g, 0.6 g and 0.9 g GEM inks and compared to standard devices without WO_3 present in the carbon layer.

The device data in figures 54a, b, c and d show that the PCE was increased for mCPSC devices with GEM carbon layers containing WO_3 compared to the standard devices. The greatest increase can be seen in the 0.6 g and 0.9 g devices where the PCE was between 5-10 % compared to the 0 g devices that had PCEs between 4-6 %. The 0.3 g a lesser increase in PCE with values between 4-9 %. The improved efficiency of the devices containing WO_3 is reflected in the FF data with the greatest increase again being seen in the 0.6 g and 0.9 g devices. These improvements are attributed to enhanced hole extraction in cells containing WO_3, which is described in previous studies as having an appropriate band alignment to provide a sort of stepping stone between the perovskite and carbon [52]. This is supported by the data in figure 53 that shows the enhanced work function of carbon layers containing WO_3. There is a

noticeable trend in figure 54c that shows an increase in J_{SC} for devices with carbon layers containing WO_3 that diminishes with increasing amounts of WO_3. This can be explained by the sheet resistance data from figure 51 that showed an increasing sheet resistance in carbon layers containing more WO_3 particles. This decreasing conductivity could be in part responsible for the 0.9 g device showing no further improvement than the 0.6 g devices but it was also seen that the 0.6 g layers had greater work function than the 0.9 g layers, and so this is likely a more optimum amount of WO_3 additive for the carbon layer.

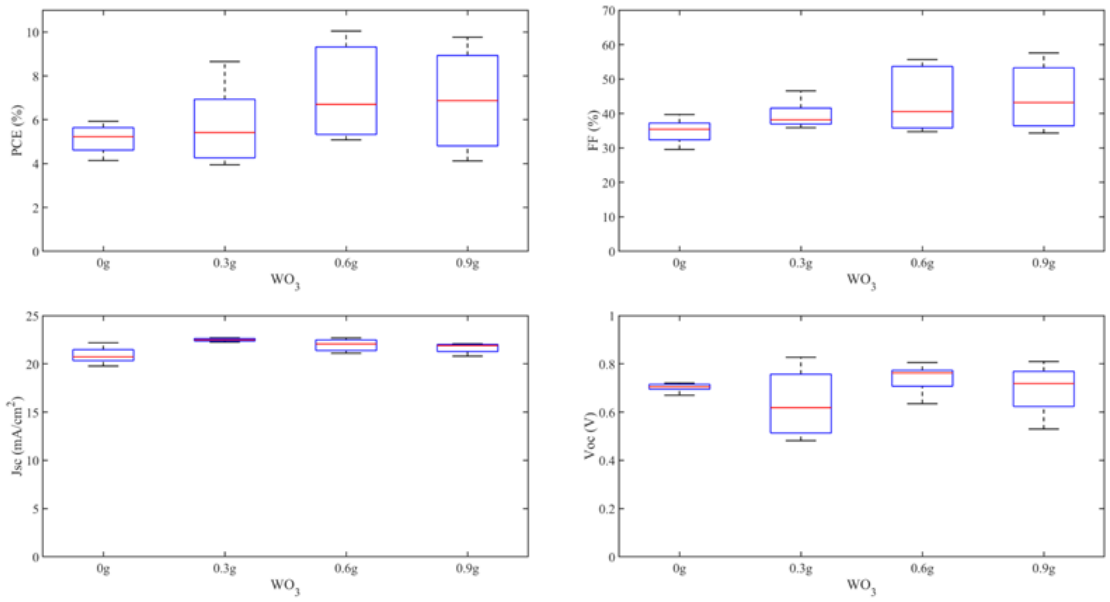

Figure 54a (top left) PCE, b (top right) Fill Factor, c (bottom left) Jsc, d (bottom right) V_{OC} data for devices with carbon layers containing WO_3.

The champion cell data and JV curves in figure 55 and table 4 show that the highest PCE device was one with a 0.6 g WO_3 in GEM carbon layer, with a PCE of 10.04 %. This is a significant increase from the 0g champion with a PCE of 5.93 %. Of the other two devices the 0.9 g device had a comparable performance with a PCE of 9.76 % and the 0.3 g was less efficient but still showed good improvement with 8.65 %. The trend seen with the champion cells match what has been seen in the overall data quite nicely with an increased PCE and FF but, it can also be seen that the J_{SC} for these devices is very similar indicating that this is not a factor in the

improved performance of devices using WO_3 in the carbon layer. The V_{OC} is more noticeably increased in the WO_3 champion cells than in the overall data shown in figure 54d which shows how the electromechanical properties of the devices with enhanced by the inclusion of WO_3. The increase seen in V_{OC} for these champion devices was not seen in all of the WO_3 devices, as shown in figure 54d. Also, despite the improvements in PCE and FF seen in the best 0.6 g and 0.9 g devices the range of results is much greater than for the 0 g devices. This suggests there is a greater level of variation in the carbon layers containing WO_3 particles further supporting the idea that a drawback of these additives is the potential for compromising the layer structure. A solution for this would be a more thorough mixing technique, such as ball milling, to further break down the WO_3 particles within the carbon ink.

Table 4 Cell data for WO_3 device champions.

	PCE (%)	FF (%)	Voc (V)	Jsc (mA/cm^2)
0g WO_3	5.9	38.0	0.70	22.18
0.3g WO_3	8.7	46.5	0.83	22.47
0.6g WO_3	10.0	55.0	0.81	22.69
0.9g WO_3	9.8	55.1	0.81	21.89

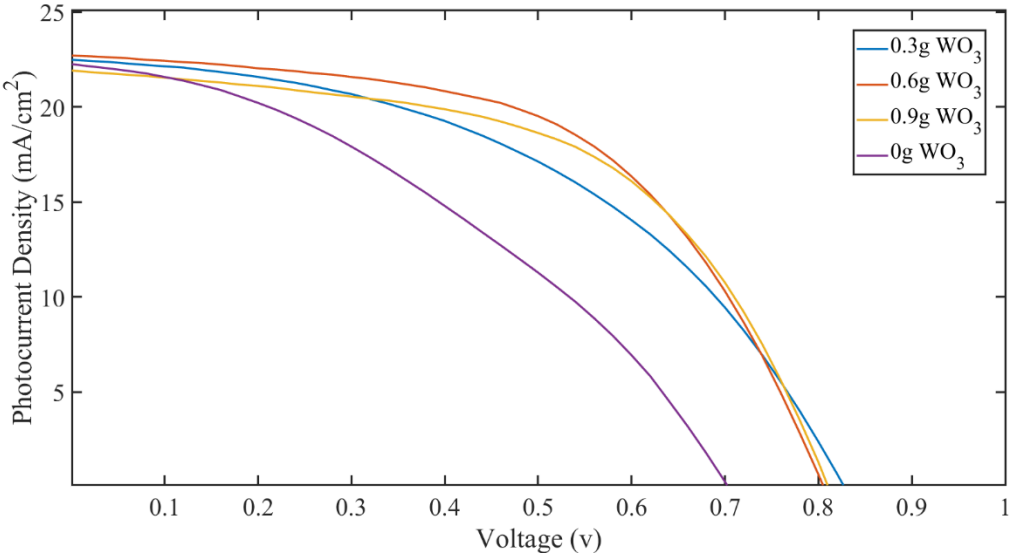

Figure 55 JV curves for WO3 champion cells

These results show that the WO_3 additives improve device performance through the increase in work function of the carbon layer. This is seen despite a decrease in the sheet resistance and resistivity of carbon layers including the WO_3 additive particles. This highlights the importance of the carbon layer as a hole extraction layer within the mCPSC and suggests there are more opportunities in improving this aspect of the carbon layer than improving conductivity. Based on the improvements made to the mCPSC device with the addition of WO_3 to the carbon layer seen in this study, the use of additives in the carbon layer would be a worthwhile avenue for further study into the improvement of the carbon layer of the mCPSC. Such further study should involve investigation into other materials such as Copper Sulfide, Boron and Vanadium oxide as well as fine tuning mixing techniques, material weight of additives included, different carbon inks and annealing temperatures.

4.6 Conclusion

In conclusion, mCPSC device performance was improved by adapting the application of the current carbon ink for carbon layers with improved conductivity and work function. Carbon layers using alternative carbon inks were found to have no improvement over the current carbon layer. Carbon inks were fabricated in-lab as an alternative to the current commercial GEM ink with the goal of establishing a new baseline from which to adapt the carbon layer. Sheet resistance and resistivity of the newly fabricated carbon inks were mostly found to be much higher than the current GEM ink. Devices including the most promising of these in-lab fabricated inks, the HT ink, had PCEs of ~2% compared the ~5% PCE of devices with GEM carbon layers. The poor device performance of the HT ink was attributed to lower conductivity negatively affecting device FF and print issues inhibiting infiltration resulting in low J_{SC} values [24][25]. These issues were likely the result of the in-lab fabricated inks having less optimum distribution of carbon material throughout the ink compared to the GEM. The speed mixing fabrication method was unable to reproduce techniques used commercially such as ball milling.

Following the poor performance of in-lab fabricated carbon inks, a range of commercially available carbon inks were compared in terms of conductivity with sheet resistance, resistivity and contact resistance measurements. The EIC03 carbon ink was found to produce carbon layers of similar conductivity to the GEM but with higher contact resistance. The other commercial inks were found to be less suitable for use in mCPSC devices due to lower conductivity. EIC03 devices were created with PCEs ~4% compared to GEM devices at ~5% PCE. The slightly lower performance of the EIC03 devices was reflected in the FF, Voc and J_{SC} with no single obvious drawback rather than small performance decrease across the board. The device performance also did not consider the lower contact resistance between EIC03 and FTO.

Finding no improvement to the carbon layer using alternative carbon inks, either fabricated in-lab or from other commercial sources, the focus of this work turned to adapting the GEM ink for carbon layer improvements. This began with a more thorough characterisation of the GEM carbon layer, looking to understand how the conditions of the mCPSC affected the carbon layer. It was found that both the annealing and infiltration process increased sheet resistance, resistivity and contact resistance whilst reducing mechanical robustness of the carbon layer. The changes to conductivity and mechanical robustness were attributed to a reduction in interparticle connections within the layer, with the contact resistance indicating that these reduced connections were also present between carbon particles and the FTO [19]. The influence of the underlying ZrO_2 substrate on the carbon layer was an increase in sheet resistance and resistivity compared to carbon layers printed straight onto glass. This increase was linked to the greater surface roughness in the carbon layers on ZrO_2 caused by the greater surface roughness of the underlying ZrO_2 compared to the smooth surface of glass.

Based on the low sheet resistance, resistivity and contact resistance observed in the carbon layers dried at 100°C compared to those annealed at 400°C it was hypothesized that the application of a dried carbon capping layer would improve device performance. This was similar to capping layers used in previous work but with a modification that replaced the carbon/FTO interface with the carbon capping layer by removing a section of the previous carbon layer. Devices create with the carbon capping layer had some increased FF indicating improved conductivity however the V_{OC} was decreased in some devices. This resulted in a range of PCE results with some showing improvement up to 6.5% and some as low as 2.5%. The low PCE devices have been affected by the reductions in V_{OC} that are likely the result of the application of the carbon capping layer interfering with the perovskite in the carbon layer below. Therefore, the capping layer showed potential for improvement but the application must be refined to avoid defects. The effect of the contact resistance between the carbon capping

layer and FTO is unlikely to have had a great impact on devices compared to the reduced resistance of the carbon layer itself. To see the effect of reduced contact resistance the capping layer should be applied to modules in future work, where contact resistance is a large contributor to series resistance [33].

Whereas the capping layer targets conductivity to increase device performance, the other main role of the carbon layer, hole collection, was targeted using WO_3 additives. Carbon layers with WO_3 particles were found to have increased work function but also decreased conductivity compared to standard GEM layer. Devices with WO_3 in the carbon layer had increased PCEs up to 10% for the best device. These devices saw improvements in FF, J_{SC} andV_{OC}due to increased work function, despite the decreased conductivity of the carbon layers. Different amounts of WO_3 additives were used with the 0.6g WO_3 in 10g GEM ink producing the highest performance carbon layers and devices. However, the GEM inks with 0.3g and 0.9g WO_3 still saw improvements. It is clear from these results that using WO_3 additives to increase carbon layer work function is a very promising avenue for increasing device performance.

4.7 Further Work Proposals

Based on the result seen in this work there a few key opportunities for further work that have been identified:

Application of carbon capping layer with carbon/FTO interface in modules. This could be achieved using laser scribes to remove the previous carbon/FTO interface before printing the carbon capping layer and would investigate the effect of the capping layer on contact resistance, series resistance and module FF.

Other materials to increase the work function of the carbon layer. Comparing the results seen here with carbon layers using other additives to increase work function such as NiO, CuS or V_2O_5. The goal would be to find the material composition that increases work function and results in the greatest device performance improvements.

The use of capping layer in tandem with WO_3 (or other) additive. This investigation would be based on isolating two roles of the carbon layer: conductive counter electrode and hole collection layer. The capping layer would be focused on improving the conductivity of the top layer allowing the original carbon layer to be developed with a focus on hole collection without considering conductivity. This could be considered taking the mCPSC into an architecture with a carbon hole transport layer and carbon counter electrode and based on the successful application of the carbon capping layer and WO_3 additives in this work could yield interesting results.

References

1. BEIS. Energy Trends December 2021. Energy Trends 2021. 2021;(December).

2. Climate Change Act 2008. Statute Law Database;

3. Sahli F, Werner J, Kamino BA, Bräuninger M, Monnard R, Paviet-Salomon B, et al. Fully textured monolithic perovskite/silicon tandem solar cells with 25.2% power conversion efficiency. Nat Mater. 2018 Sep 1;17(9):820–6.

4. Meroni SMP, Worsley C, Raptis D, Watson TM. Triple-Mesoscopic Carbon Perovskite Solar Cells: Materials, Processing and Applications. Energies 2021, Vol 14, Page 386 [Internet]. 2021 Jan 12 [cited 2021 Jan 12];14(2):386. Available from: https://www.mdpi.com/1996-1073/14/2/386

5. Green MA, Ho-Baillie A, Snaith HJ. The emergence of perovskite solar cells. Nat Photonics. 2014;8(7):506–14.

6. Ku Z, Rong Y, Xu M, Liu T, Han H. Full printable processed mesoscopic CH3 NH3 PbI 3 /TiO2 heterojunction solar cells with carbon counter electrode. Sci Rep. 2013 Nov 4;3(1):1–5.

7. Duan M, Hu Y, Mei A, Rong Y, Han H. Printable carbon-based hole-conductor-free mesoscopic perovskite solar cells: From lab to market. Vol. 7, Materials Today Energy. Elsevier Ltd; 2018. p. 221–31.

8. Etgar L, Gao P, Xue Z, Peng Q, Chandiran AK, Liu B, et al. Mesoscopic CH 3NH 3PbI 3/TiO 2 heterojunction solar cells. J Am Chem Soc [Internet]. 2012 Oct 24 [cited 2022 Feb 22];134(42):17396–9. Available from: https://pubs.acs.org/doi/abs/10.1021/ja307789s

9. Cho KT, Paek S, Grancini G, Roldán-Carmona C, Gao P, Lee Y, et al. Highly efficient perovskite solar cells with a compositionally engineered perovskite/hole transporting material interface. Energy Environ Sci [Internet]. 2017 Feb 1 [cited 2022 Feb 1];10(2):621–7. Available from: https://pubs.rsc.org/en/content/articlehtml/2017/ee/c6ee03182j

10. Ball JM, Lee MM, Hey A, Snaith HJ. Low-temperature processed meso-superstructured to thin-film perovskite solar cells. Energy Environ Sci [Internet]. 2013 Jun 22 [cited 2022 Feb 1];6(6):1739–43. Available from: https://pubs.rsc.org/en/content/articlehtml/2013/ee/c3ee40810h

11. Matteocci F, Cinà L, Di Giacomo F, Razza S, Palma AL, Guidobaldi A, et al. High efficiency photovoltaic module based on mesoscopic organometal halide perovskite. Prog Photovoltaics Res Appl [Internet]. 2016 Apr 1 [cited 2022 May 10];24(4):436–45. Available from: https://onlinelibrary.wiley.com/doi/10.1002/pip.2557

12. Maniarasu S, Korukonda TB, Manjunath V, Ramasamy E, Ramesh M, Veerappan G. Recent advancement in metal cathode and hole-conductor-free perovskite solar cells for low-cost and high stability: A route towards commercialization. Vol. 82, Renewable and Sustainable Energy Reviews. Elsevier Ltd; 2018. p. 845–57.

13. Hu R, Chu L, Zhang J, Li X, Huang W. Carbon materials for enhancing charge transport in the advancements of perovskite solar cells. Vol. 361, Journal of Power Sources. Elsevier B.V.; 2017. p. 259–75.

14. Fagiolari L, Bella F. Carbon-based materials for stable, cheaper and large-scale processable perovskite solar cells [Internet]. Vol. 12, Energy and Environmental Science. Royal Society of Chemistry; 2019 [cited 2021 Jan 14]. p. 3437–72. Available from: https://pubs.rsc.org/en/content/articlehtml/2019/ee/c9ee02115a

15. Zhou H, Shi Y, Dong Q, Zhang H, Xing Y, Wang K, et al. Hole-Conductor-Free, Metal-Electrode-Free TiO 2 /CH 3 NH 3 PbI 3 Heterojunction Solar Cells Based on a Low-Temperature Carbon Electrode. 2014 [cited 2021 Jan 14]; Available from: https://pubs.acs.org/sharingguidelines

16. Zhang F, Yang X, Wang H, Cheng M, Zhao J, Sun L. Structure Engineering of Hole–Conductor Free Perovskite-Based Solar Cells with Low-Temperature-Processed Commercial Carbon Paste As Cathode. ACS Appl Mater Interfaces [Internet]. 2014 Sep 24 [cited 2020 Nov 10];6(18):16140–6. Available from: https://pubs.acs.org/doi/10.1021/am504175x

17. Baker J, Hooper K, Meroni S, Pockett A, McGettrick J, Wei Z, et al. High throughput fabrication of mesoporous carbon perovskite solar cells. J Mater Chem A [Internet]. 2017 Sep 12 [cited 2021 Jul 3];5(35):18643–50. Available from: https://pubs.rsc.org/en/content/articlehtml/2017/ta/c7ta05674e

18. Bogachuk D, Zouhair S, Wojciechowski K, Yang B, Babu V, Wagner L, et al. Low-temperature carbon-based electrodes in perovskite solar cells. Vol. 13, Energy and Environmental Science. Royal Society of Chemistry; 2020. p. 3880–916.

19. Wissler M. Graphite and carbon powders for electrochemical applications. Vol. 156, Journal of Power Sources. Elsevier; 2006. p. 142–50.

20. Bogachuk D, Tsuji R, Martineau D, Narbey S, Herterich JP, Wagner L, et al. Comparison of highly conductive natural and synthetic graphites for electrodes in perovskite solar cells. Carbon N Y [Internet]. 2021 Jan 11 [cited 2021 Jan 20]; Available from: https://linkinghub.elsevier.com/retrieve/pii/S0008622321000300

21. Phillips C, Al-Ahmadi A, Potts SJ, Claypole T, Deganello D. The effect of graphite and carbon black ratios on conductive ink performance. J Mater Sci [Internet]. 2017 Aug 1

[cited 2021 Jul 13];52(16):9520–30. Available from: https://link.springer.com/article/10.1007/s10853-017-1114-6

22. Yang Y, Ri K, Mei A, Liu L, Hu M, Liu T, et al. The size effect of TiO2 nanoparticles on a printable mesoscopic perovskite solar cell. J Mater Chem A [Internet]. 2015 May 7 [cited 2022 Sep 20];3(17):9103–7. Available from: www.rsc.org/MaterialsA

23. Zhang L, Liu T, Liu L, Hu M, Yang Y, Mei A, et al. The effect of carbon counter electrodes on fully printable mesoscopic perovskite solar cells. J Mater Chem A [Internet]. 2015 May 7 [cited 2021 Jan 14];3(17):9165–70. Available from: www.rsc.org/MaterialsA

24. Wang H, Hu X, Chen H. The effect of carbon black in carbon counter electrode for CH3NH3PbI3/TiO2 heterojunction solar cells. RSC Adv [Internet]. 2015 Mar 27 [cited 2022 Sep 26];5(38):30192–6. Available from: www.rsc.org/advances

25. Duan M, Rong Y, Mei A, Hu Y, Sheng Y, Guan Y, et al. Efficient hole-conductor-free, fully printable mesoscopic perovskite solar cells with carbon electrode based on ultrathin graphite. Carbon N Y [Internet]. 2017;120(November):71–6. Available from: http://dx.doi.org/10.1016/j.carbon.2017.05.027

26. Li H, Cao K, Cui J, Liu S, Qiao X, Shen Y, et al. 14.7% efficient mesoscopic perovskite solar cells using single walled carbon nanotubes/carbon composite counter electrodes. Nanoscale [Internet]. 2016 Mar 28 [cited 2022 Sep 26];8(12):6379–85. Available from: www.rsc.org/nanoscale14.7%EFficientmesoscopicperovskitesolarcellsusingsinglewalledcarbonnanotubes/carboncompositecounterelectrodes†

27. Tian C, Mei A, Zhang S, Tian H, Liu S, Qin F, et al. Oxygen management in carbon electrode for high-performance printable perovskite solar cells. Nano Energy. 2018 Nov 1;53:160–7.

28. Jiang P, Xiong Y, Xu M, Mei A, Sheng Y, Hong L, et al. The Influence of the Work Function of Hybrid Carbon Electrodes on Printable Mesoscopic Perovskite Solar Cells. J Phys Chem C [Internet]. 2018 Jul 26 [cited 2021 Jul 16];122(29):16481–7. Available from: https://pubs.acs.org/doi/abs/10.1021/acs.jpcc.8b02163

29. Hu R, Zhang R, Ma Y, Liu W, Chu L, Mao W, et al. Enhanced hole transfer in hole-conductor-free perovskite solar cells via incorporating CuS into carbon electrodes. Appl Surf Sci. 2018 Dec 31;462:840–6.

30. Li W, Sasaki A, Oozu H, Aoki K, Kakushima K, Kataoka Y, et al. Electron transport mechanism of tungsten trioxide powder thin film studied by investigating effect of annealing on resistivity. Microelectron Reliab. 2015 Feb 1;55(2):407–10.

31. Jiang P, Jones TW, Duffy NW, Anderson KF, Bennett R, Grigore M, et al. Fully printable perovskite solar cells with highly-conductive, low-temperature, perovskite-compatible carbon electrode. Carbon N Y. 2018 Apr 1;129:830–6.

32. Raptis D, Stoichkov V, Meroni SMP, Pockett A, Worsley CA, Carnie M, et al. Enhancing fully printable mesoscopic perovskite solar cell performance using integrated metallic grids to improve carbon electrode conductivity. Curr Appl Phys. 2020 May 1;20(5):619–27.

33. Meroni SMP, Hooper KEA, Dunlop T, Baker JA, Worsley D, Charbonneau C, et al. Scribing method for carbon perovskite solar modules. Energies. 2020;13(7).

34. Smits FM. Measurement of Sheet Resistivities with the Four-Point Probe. Bell Syst Tech J. 1958;37(3):711–8.

35. Vinod PN. Specific contact resistance measurements of the screen-printed Ag thick film contacts in the silicon solar cells by three-point probe methodology and TLM method. J

Mater Sci Mater Electron [Internet]. 2011 Sep 26 [cited 2022 May 30];22(9):1248–57. Available from: https://link.springer.com/article/10.1007/s10854-011-0295-z

36. Reeves GK, Harrison HB. Obtaining the Specific Contact Resistance from Transmission Line Model Measurements. IEEE Electron Device Lett. 1982;3(5):111–3.

37. Schroder D. Semiconductor material and device characterisation. John Wiley & Sons, Ltd; 1998.

38. Nouchi R, Saito T, Tanigaki K. Observation of negative contact resistances in graphene field-effect transistors. J Appl Phys [Internet]. 2012 Apr 15 [cited 2022 Aug 2];111(8):084314. Available from: http://aip.scitation.org/doi/10.1063/1.4705367

39. Coatings C, Products RC, Applica- E, Tape S, Paint T, Materials R. Standard Test Methods for Measuring Adhesion by Tape Test 1. 2012;1–8.

40. Jewell EH, Hamblyn SM, Claypole TC, Gethin DT. The impact of carbon content and mesh on the characteristics of screen printed conductive structures. Circuit World [Internet]. 2013 Jan 1 [cited 2021 Jan 26];39(1):13–21. Available from: https://cronfa.swan.ac.uk/Record/cronfa14256

41. Kartikay P, Yella A, Mallick S. Binder-solvent effects on low temperature-processed carbon-based, hole-transport layer free perovskite solar cells. Mater Chem Phys. 2020 Dec 1;256:123594.

42. Potts SJ, Phillips C, Jewell E, Clifford B, Lau YC, Claypole T. High-speed imaging the effect of snap-off distance and squeegee speed on the ink transfer mechanism of screen-printed carbon pastes. J Coatings Technol Res. 2020 Mar 1;17(2):447–59.

43. Potts S-J, Phillips C, Claypole T, Jewell E. The Effect of Carbon Ink Rheology on Ink Separation Mechanisms in Screen-Printing. Coatings [Internet]. 2020 Oct 21 [cited 2021

Jul 21];10(10):1008. Available from: https://www.mdpi.com/2079-6412/10/10/1008

44. Lakhiani H, Dunlop T, De Rossi F, Dimitrov S, Kerremans R, Charbonneau C, et al. Variations of Infiltration and Electronic Contact in Mesoscopic Perovskite Solar Cells Revealed by High-Resolution Multi-Mapping Techniques. Adv Funct Mater [Internet]. 2019 Jun 21 [cited 2020 Mar 11];29(25):1900885. Available from: https://onlinelibrary.wiley.com/doi/abs/10.1002/adfm.201900885

45. Liu Z, Shi T, Tang Z, Sun B, Liao G. Using a low-temperature carbon electrode for preparing hole-conductor-free perovskite heterojunction solar cells under high relative humidity. Nanoscale [Internet]. 2016 Apr 7 [cited 2020 Dec 14];8(13):7017–23. Available from: www.rsc.org/nanoscale

46. Mishra A, Ahmad Z, Zimmermann I, Martineau D, Shakoor RA, Touati F, et al. Effect of annealing temperature on the performance of printable carbon electrodes for perovskite solar cells. Org Electron. 2019 Feb 1;65:375–80.

47. Potts SJ, Lau YC, Dunlop T, Claypole T, Phillips C. Effect of photonic flash annealing with subsequent compression rolling on the topography, microstructure and electrical performance of carbon-based inks. J Mater Sci. 2019 Jun 15;54(11):8163–76.

48. Fanjul-Bolado P, Hernández-Santos D, Lamas-Ardisana PJ, Martín-Pernía A, Costa-García A. Electrochemical characterisation of screen-printed and conventional carbon paste electrodes. Electrochim Acta. 2008 Apr 1;53(10):3635–42.

49. Lee J, Arrigan DWM, Silvester DS. Mechanical polishing as an improved surface treatment for platinum screen-printed electrodes. Sens Bio-Sensing Res. 2016 Jul 1;9:38–44.

50. Tang W, Chao Y, Weng X, Deng L, Xu K. Optical Property and the Relationship

between Resistivity and Surface Roughness of Indium Tin Oxide Thin Films. In: Physics Procedia. Elsevier B.V.; 2012. p. 680–6.

51. Zheng X, Chen H, Li Q, Yang Y, Wei Z, Bai Y, et al. Boron Doping of Multiwalled Carbon Nanotubes Significantly Enhances Hole Extraction in Carbon-Based Perovskite Solar Cells. Nano Lett [Internet]. 2017 Apr 12 [cited 2021 Jul 16];17(4):2496–505. Available from: https://pubmed.ncbi.nlm.nih.gov/28287749/

52. Zhou L, Zuo Y, Mallick TK, Sundaram S. Enhanced Efficiency of Carbon-Based Mesoscopic Perovskite Solar Cells through a Tungsten Oxide Nanoparticle Additive in the Carbon Electrode. Sci Rep [Internet]. 2019 Dec 1 [cited 2021 Oct 19];9(1):1–8. Available from: https://doi.org/10.1038/s41598-019-45374-x

53. Sun H, Hou X, Wei Q, Liu H, Yang K, Wang W, et al. Low-temperature solution-processed p-type vanadium oxide for perovskite solar cells. Chem Commun [Internet]. 2016 Jun 21 [cited 2021 Oct 19];52(52):8099–102. Available from: www.rsc.org/chemcomm